UNIVERSITY OF COPENHAGEN
FACULTY OF SCIENCE

Master Thesis

Jeppe Eriksen [MNF680]

A Field and Model Study of the Effects of Closing Haraldsborg Waterworks (Roskilde) on a Rising Water Table and Near-Surface Groundwater.

Supervisors: Jens Christian Refsgaard, Torben O. Sonnenborg & Peter Engesgaard

Date: 2/12/2019

Abstract

The purpose of this thesis is to investigate the consequences, on the near-surface groundwater, of closing Haraldsborg waterworks in Roskilde, which is a concern for residents adjacent to it. An approximately 1200 x 1200 m hydrological model, setup with the MIKESHE code, is used as a tool to isolate the effect of abstraction change from noise caused by precipitation. The model includes a geological interpretation, land use, Richard's equation and a sewer system build in MIKE11. The model is calibrated using AUTOCAL and validated on head observations in the near-surface groundwater, measured by houseowners in the area. Various scenarios are set up to examine the consequence of closing Haraldsborg waterworks and the results are according to the model minor, between 0 to 0.1 m on the near-surface groundwater. The model is also used to simulate impact of future climate; increased precipitation and evaporation and a higher sea-level, for the years 2050 and 2100 following a worst-case scenario. The change in maximum groundwater level adjacent to Haraldsborg is by 2050 between 0 to 0.4 m and by 2100 from 0.1 to over 0.6 m. The change in mean groundwater level was by the year 2100 seen to increase less than 0.3 m and by 2050 the mean level unexpectedly fell. The results are discussed emphasizing uncertainty and model improvement, and known errors are presented. Furthermore, this study includes field work; two wells established, one ERT profile, gamma ray logging and installation of divers.

Contents

List of Figures

List of Tables

1 Introduction & Study Area

In 2016 FORS, a supply company in Roskilde, announced that Haraldsborg waterworks would be closed due to pollution concentration exceeding tolerated limits. Additionally groundwater produced by Haraldsborg waterworks cost eight times more than water from an adjacent waterworks.

The decision to close the waterworks was discussed as early as 2005 and, nine years later, in 2014, the waterworks stops supplying groundwater for drinking though continuing to pump. A report was ordered to investigate the consequences of closing Haraldsborg waterworks and it was concluded that no major effect would be caused. This conclusion was built on data from a regional groundwater model created by Rambøll. Unfortunately this report did not specify the uncertainties regarding the near surface groundwater. Because of the decision to close Haraldsborg waterworks a group of local residents formed a group called "Vandgruppen" which represents the people who are uncertain about what will happen if Haraldsborg waterworks closes. Vandgruppen invited people in the affected area to join this group and suggested that house owners starts to monitor the groundwater table in their gardens. At the present day more than 40 wells (drilled by houseowners) are monitored, some more than others.

Several solutions to the expected issue have been discussed. For example that every house owner buys and install a perimeter drain, that Vandgruppen overtakes the wells and continues to pump groundwater to the fjord or that FORS keeps pumping.

The municipality of Roskilde, as the third stakeholder, sets the limitations of what is possible. Due to legislation, pumping of groundwater to Roskilde fjord is only possible at a fixed time since this is not approved by the law. According to law, groundwater should only be extracted if there is an acknowledged purpose for this.

In the recent decades increasing computational power makes the process of hydrological modelling faster and allows for more complex models. A hydrological model is a conceptualization of the natural system and can be used as a basis for water resources management and to estimate future situations and impacts of changing conditions, such as e.g. climate change. Distributed hydrological models is setup using thousands of grid points which covers the variability of the natural system as well as possible using parameters that during the modelling process is prone to calibration [Refsgaard, 1997].

Hydrological models are also used to investigate the impacts of e.g. deforestation, changes in irrigation, pollution transport, changes in land use etc.

The purpose of this thesis is to use hydrological modelling to assess the impact on the near-surface groundwater in the area adjacent to Haraldsborg waterworks if it stops extracting groundwater from the limestone aquifer. Furthermore, the hydrological model will be used to estimate the impact of increased precipitation and increased sea level caused be climate change. In addition results from fieldwork is presented.

The location of the study area in Haraldsborg, Roskilde, is seen in figure 1, page 3.

This thesis is constructed with a presentation of theory regarding the constructed field work, hydrological modelling and urban hydrology. Hereafter follows a chapter, which describes the methods used to complete the field work and how the hydrological model is setup. The hydrological model is setup first as a reference model which then adds separately distinct improvements of complexity, these are as follows

- Land use: This model's surface is divided into areas of grass and areas of urban structures, whereas the reference model only simulates grass.
- Geology: This model includes interpreted geological layers compared to a sandbox in the reference model.
- Richards eq.: This model uses Richards eq. instead of a two-layer solution which is used in the reference model.
- Drainage system: This model includes additional river branches which functions as drainage whereas the reference model uses only one river branch.

A fully distributed model is then constructed by assembling all the above mentioned. This model is partly inverse calibrated and partly manually calibrated. The manual calibration is performed on the Van Genuchten parameter and the hydraulic conductivity in the unsaturated zone and the hydraulic conductivity and the anisotropy factor in the uppermost saturated zone layer. Several scenarios are set up to investigate the effects of closing Haraldsborg waterworks. These are

Scenario 1 Simulates a stop of abstraction using observations.

Scenario 2 Simulates a stop of abstraction using simulated values from a regional groundwater model.

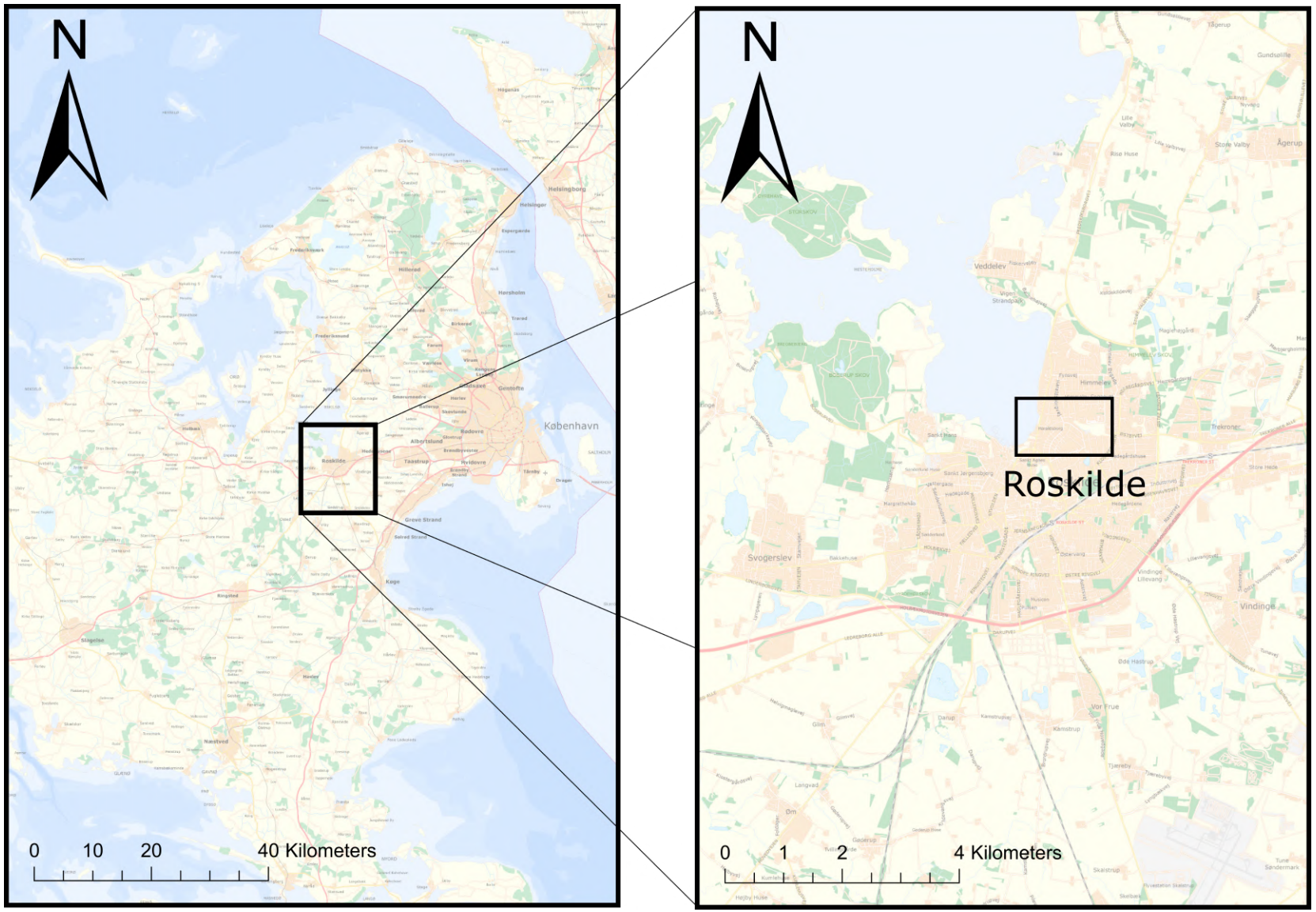

Figure 1: Map of Sealand to the left and a closer look at Roskilde with the model area in the black box to the right.

Scenario 3 Specific storage is increased by a factor of 10 throughout all layers.

Scenario 4 An approximately 10-15 m thick sand layer is changed to a clay layer.

Two scenarios are setup to examine the consequences of climate change. One scenario project the current situation to the year 2050 and the other to the year 2100. Lastly the effect, on near surface groundwater of urbanisation, is studied. This includes two scenarios. One excludes the sewer/drainage system and the other one reclasses urban structures to grass.

The results are discussed and lastly a conlusion is presented. Furthermore the appendix include extra figures and timeseries for each established well, that include observations, for the calibration and validation period.

2 Theory

In this section the governing theory regarding the conducted field work, multielectrode tomography profiling, gamma ray logging, hydrogeology in urban settings and lastly the equations regarding the MIKESHE code will be explained.

2.1 Gamma Ray Wireline Logging

Uranium, thorium and potassium are all radioactive elements and are a natural component of many geological layers. Each of the three elements are found in distinctive concentrations in various geological layers with the highest amount recorded in shales, if only investigating sedimentary rocks [Rider, 2011]. For this reason, the gamma ray log is referred to as the shale log. Sand with a high amount of quartz minerals, which are not radioactive, will show only small gamma ray counts. This makes the gamma ray log ideal to identify and locate sand layers among clay layers. Pitfalls exist though and some sand types have a high concentration of radioactive elements. Mica sands and sometimes marine sands with a relatively large content of radioactive glauconite are examples of sand with a higher radioactive content [Rider, 2011].

2.2 Electrical Resistivity Tomography

Electrical Resistivity Tomography (ERT) surveying is a non-invasive method for investigating the electrical resistivity of the underground. ERT surveying uses the physical properties that different materials conduct electrical currents differently [Kearey et al., 2013]. The fraction of pore water in a geological material will often be the controlling physical property since the free ions of water conducts the electrical current. A higher content of water equals a lower resistivity. Clay minerals also have a lowering effect on the electrical resistivity since clay minerals are ionic charged [Fitts, 2002]. The electrical current is sent through a current electrode in the ground and received by another current electrode. The potential drop is then measured in potential electrodes as seen in figure 2, page 6.

2.3 Urban Hydrology

The definition of an urban area is vague [McGrane, 2016]. Often this definition is based on the population size and density and the presence of structures like roads, buildings and drainage- and sewer systems. Salvadore et al. [2015] set up some key

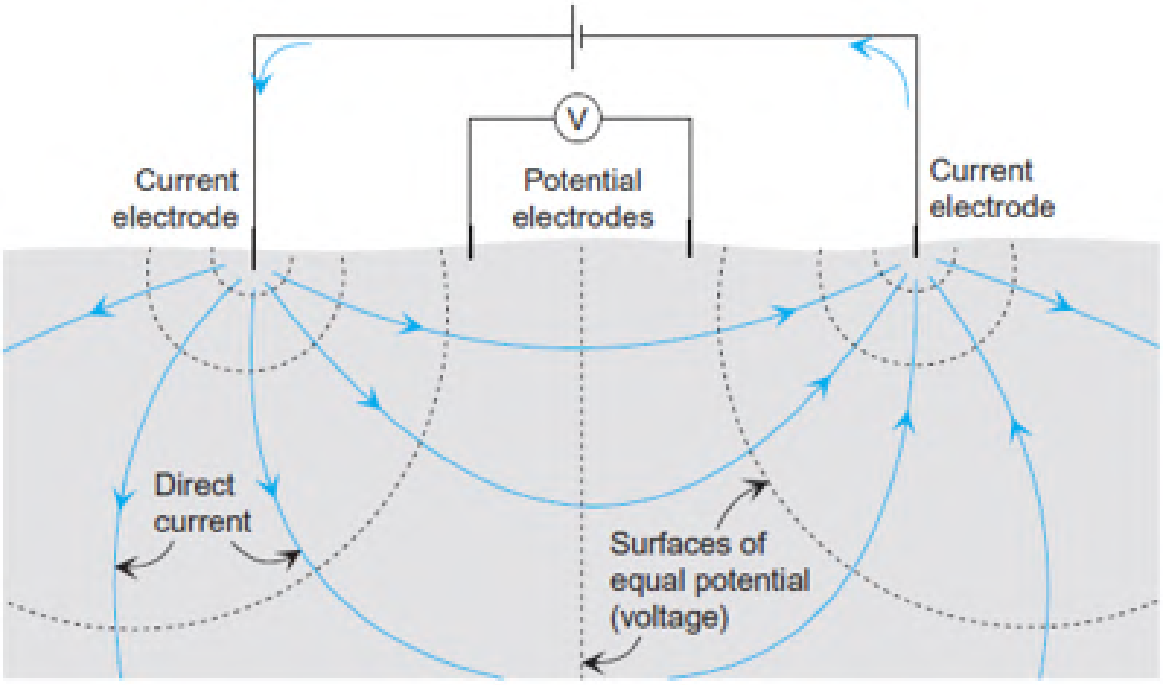

Figure 2: A theoretical setup with ERT. An electrical current is send through the left current electrode and then travels to the right current electrode. The resistivity is calculated using the potential drop measured at the potential electrodes. Figure is from Kearey et al. [2013].

factors to whether an area is considered urban or rural. An urban area includes many houses, high population density, pollution of water sources, modification of rivers and wastewater treatment. The urban area differs from the rural in many complex ways, which is explained in the following.

The effect of urbanization on recharge is still actively discussed [Fletcher et al., 2013]. Salvadore et al. [2015] mention three ways that urbanization may affect precipitation:

1. An urban area will function as a heat island (UHI – Urban Heat Island).
2. Surface changes might influence the wind patterns.
3. Pollution particles effect the nucleation of rain droplets.

Salvadore et al. [2015] cites several studies that postulates that urbanization will increase the precipitation by 5 - 15 % but warns that these numbers have a high degree of uncertainty.

Evapotranspiration (ET) is, in urban areas, effected in two ways [Fletcher et al., 2013]. When plants are removed the transpiration is lowered and when impervious surfaces are constructed more water moves with overland flow constraining the infiltration. These two effects work in separate ways and for this reason the effect of urbanization can either increase or decrease the base flow [Fletcher et al., 2013].

Paved areas might affect the flow in two ways. It might lead the water to a storm water sewer, hence constraining recharge, or it might lead surface water to pervious areas hence allowing recharge [Mitchell et al., 2001]. Ramier et al. [2011] studied how rain behaved on an impervious area finding that up to 30-40 % of the water would either recharge or evaporate, leaving 60 – 70 % of the water to actual runoff.

Salvadore et al. [2015] reports that the depression storage is highly adjusted in paved areas, with values between 0.2 - 3.2 mm, whereas rural areas have a detention storage of between 0.5 - 15 mm.

Urban areas have complex drainage and wastewater subsurface pipe systems. The European drainage system is built to withstand 10-50 years precipitation events [Salvadore et al., 2015]. Lerner [1990] recognized almost 30 years ago that subsurface pipes will either drain the groundwater or leak to the groundwater depending on where the pipe is located compared to the groundwater table, the age, condition and material of the pipes [Mitchell et al., 2001]. Salvadore et al. [2015] gives as an example that an estimated 70 % of the wastewater going to the wastewater treatment plant is clean

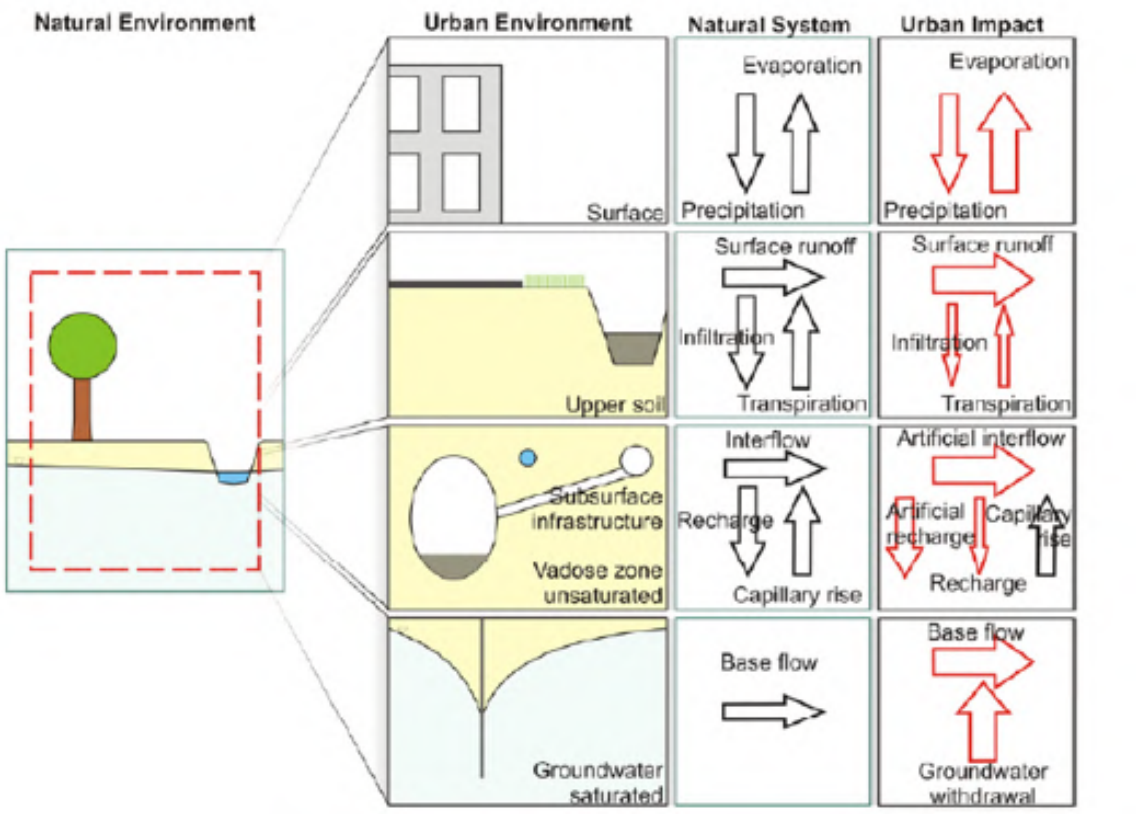

Figure 3: Difference between the natural system and the impact of urbanization and the hydrological cycle. The figure is from Schirmer et al. [2013]

water drained by the wastewater pipe system.

The effect of underground structures in urban areas was shown to have no or very little effect on the groundwater table in areas with a low hydraulic gradient (close to 0.1 %) Attard et al. [2016]. This research was performed on a structure significantly larger (100x50x15 m) than an ordinary single-family home.

Governmental interference and legislation can also cause effects on the groundwater in urban areas as well as the collective behaviour of residents in an urban area [Salvadore et al., 2015].

In figure 3, page 8, the overall effect of urbanization on the hydrological cycle is illustrated.

2.4 Climate Change and Urban Flooding

Climate change will cause an increase in sea level and in precipitation which will impact the urban drainage [Refsgaard et al., 2013] and coastal areas will be put under pressure [Arnbjerg-Nielsen and Fleischer, 2009].

The effect of climate driven increases in precipitation in winter periods can be a higher groundwater table which might cause flooded basements, water on surface and/or increases in subsurface drainage [Sonnenborg and Jacob, 2016]. Rising sea level causes the fresh water/saline water interface to move inland. The effect of a rising sea level is theoretically largest when the inland gradient is small which is not the case in the studied area [Taylor et al., 2013].

Urban flooding often happens due to storm events when the drainage system is incapable of redirecting the recharge. In the future, storm events will be more severe and occur more frequently [Arnbjerg-Nielsen and Fleischer, 2009].

Urban flooding can cause direct damage on human structures including flooded basements. The damage can also be of monetary and indirect in form of traffic disruptions etc. Furthermore, flooding can have social consequences e.g. if house prices decrease due to abundant flooding [Mark et al., 2004].

2.5 Hydrological Modelling

Hydrological modelling in MIKESHE is a complex conceptualization of the natural groundwater-surface water interaction. In figure 4, page 10, the interaction of different components in a fully distributed hydrological model is seen. In the following section a description of the primary components of the model is presented.

Overland Flow

The overland flow component of a hydrological model is simulating how overland lateral flow in ponded areas moves from cell to cell, according to topography, until it reaches its destination. The controlling parameters of the OL (overland) component are Manning's number, M, and the detention storage. The Manning number describes the roughness of the surface and spans from 10 to 100, where smooth surfaces have a high Manning number and very rough surfaces have low Manning number [DHI, 2017a]. Detention storage describes how much water (in mm) is needed before overland flow is possible. As an example, a detention storage of 4 mm require more than 4 mm of ponded water

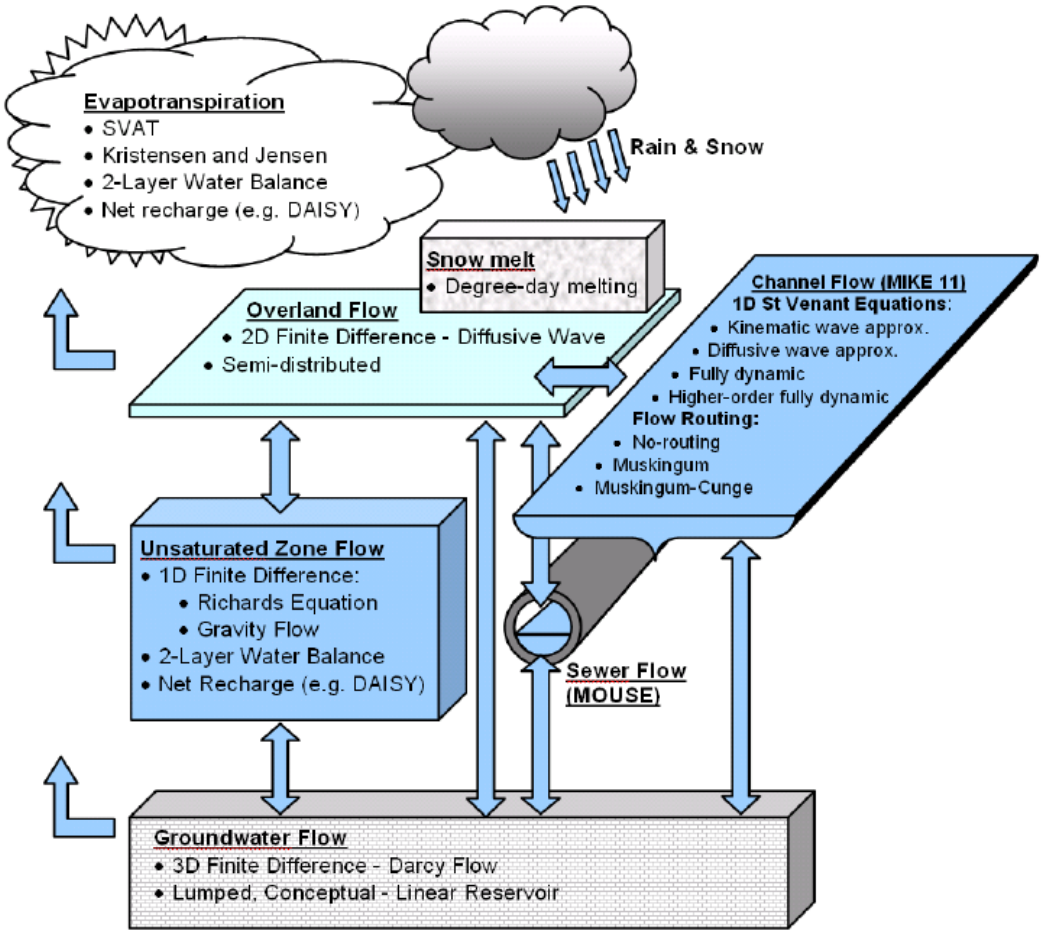

Figure 4: Different components in MIKESHE's code DHI [2017a].

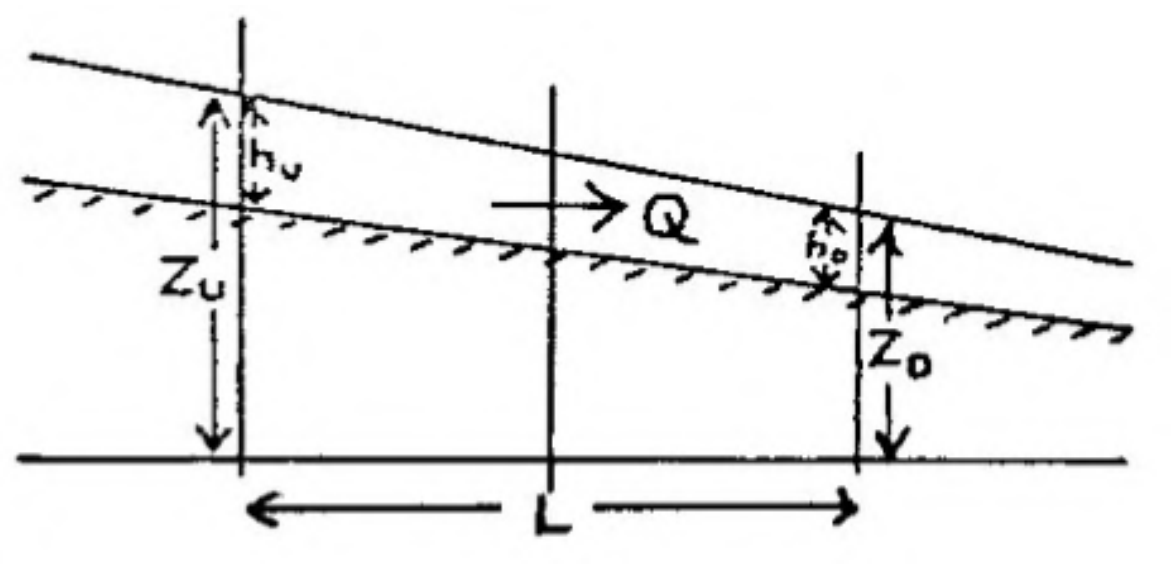

Figure 5: Overland flow between two cells DHI [2017b] .

before overland flow occurs.

It is recognized by DHI [2017a] that the overland flow component can be very time consuming. This is because MIKESHE lowers the length of each timestep when a rapid flow occurs in order to constrain the overland flow to only move one cell at the time.

As a means, to a significantly lower computational time, MIKESHE is equipped with a function called ponded drainage. This function works by shortcutting how the water is moving from the ponded area to local depressions or rivers. If ponded water is present at a cell the drainage is calculated based in a specific order; first rainfall enters the cell, secondly, OL drainage is calculated, thirdly, ET (evapotranspiration) is removed, fourthly infiltration is calculated and after these steps, the calculation of lateral overland flow completed [DHI, 2017a].

Overland flow is calculated between cells using equation

$$Q = \frac{M\Delta X}{\Delta X^{1/2}}(Z_U - Z_D)^{1/2} \cdot H_U^{5/3}$$

Where M represents Manning's number, Z_u and Z_d are the higher and lower water column, and h is the depth of water available for flow, see figure 5, page 11, [DHI, 2017b].

Unsaturated Zone Flow

The unsaturated zone (UZ) is often described as heterogeneous and with little or no

horizontal flow except on e.g. hill slopes [DHI, 2017a]. Therefore, with aforementioned assumption, MIKESHE only calculates the vertical flow in the UZ. The UZ receives water from recharge and loses water primarily from evapotranspiration and loss to the saturated zone (SZ). MIKESHE provides three solutions for the unsaturated zone but only two is mentioned here; a 2-layer solution and Richards equation solution.

The 2-layer solution is the simpler of the two, dividing the UZ in two layers with the upper layer being the depth where ET occurs [DHI, 2017a]. The second layer begins where ET is no longer possible and to the groundwater table. Parameters controlling the UZ are water content at saturation, water content at field capacity, which describes how much water is left after lateral movement and infiltration cease, water content at wilting point, which describes the minimum amount of water content before plants starts to die, and lastly the saturated hydraulic conductivity. These parameters are dependent on soil type and will vary between those. This solution is meant to produce an average of the UZ, with respect to how much water evaporates and how much infiltrates [DHI, 2017a].

Richards equation is more complex than the 2-layer solution thus more computationally challenging but also the most accurate for the unsaturated zone [DHI, 2017b]. The controlling parameters in Richards solution is the gradient of the hydraulic head and the pressure relative to the atmospheric pressure [DHI, 2017a]. With this solution capillary- and adsorptive forces retain water in the unsaturated zone thus making available for evaporation and transpiration. The relationship between these two parameters is known as the soil moisture retention curve [DHI, 2017a]. When the soil is close to saturation, the hydraulic conductivity is the controlling parameter but when the soil dries, more air fills the pores, letting the capillary forces and the adsorption dominate the flow.

Richards solution is calculated using

$$\frac{\delta\theta}{\delta t} = \frac{\delta}{\delta z} \cdot (K(\theta)\frac{\delta\psi}{\delta z}) + \frac{\delta K(\theta)}{\delta z} - S(z)$$

Where θ is the soil moisture, $K(\theta)$ is the unsaturated hydraulic conductivity, z is the gravitational component, ψ is a pressure component and S is the root extraction sink term [DHI, 2017b].

Saturated Zone

The flow in the saturated zone (SZ) is controlled by the gradient, $\frac{\delta h}{\delta_{x,y,z}}$, between cells and by the hydraulic conductivity (K) according to Darcys' equation. The 3d flow equation used by MIKESHE is

$$\frac{\delta}{\delta x}(K_{xx}\frac{\delta h}{\delta x}) + \frac{\delta}{\delta y}(K_{yy}\frac{\delta h}{\delta y}) + \frac{\delta}{\delta z}(K_{zz}\frac{\delta h}{\delta z}) - Q = S\frac{\delta h}{\delta t}$$

where S is the specific storage coefficient [DHI, 2017b]. The saturated zone interacts with all other components of the groundwater model [DHI, 2017a].

Channel Flow/MIKE11

The last component used is the channel flow or river component set up in MIKE11. The main parameters controlling the flow in the river is the topographical gradient and the bed resistance. The bed resistance, Manning (M), is equivalent to the description of the overland flow and ranges between the same values [DHI, 2017d]. Another parameter to mention regarding MIKE11 is the groundwater leakage coefficient. Groundwater leakage to the river is calculated as

$$Q_{Leakage} = C_L \cdot P \cdot D \cdot \Delta x$$

Where C_L is the leakage coefficient, P is the wet parameter, D is the water depth and Δx is grid spacing [DHI, 2017d].

3 Data Description

3.1 Observations

Since 1/1-2018, 48 observation wells have been established in the model area by residents, most of them are seen in figure 6, page 15. During the last year, 2018, the precise location and elevation of the top of the wells was measured with a Trimble GPS with a maximum precision of 0.015 m vertically and 0.008 m horizontally. Wells established later in time, are not presented on this map, since the map in figure 6 is based on the GPS coordinates. Records of head elevation is done by residents who measures the distance from the top of the wells to the top of the groundwater table with different methods and varying temporal resolution. Some observations are performed with ruler, some with floating devices and in one instance with a laserpointer. One resident had a specific technique using a ruler and potato flour. Several houseowners created two or three wells in their gardens. If used during this thesis a well will be named fx Baldersvej 10(2), which means that this well is established on Baldersvej 2 and it is the second well establish on this premises.

Additionally, four divers have been installed at the two waterworks properties. One in each extraction well and one in the 6 m (DGU: 206.2574) and the 12 m (DGU: 206.2575) well that was established at Valhalvej 55.

Four preexisting divers are located at the waterworks two properties, two on each, located between 2 and 5 meters in depth (DGU: 206.2567, 206.2568, 206.2569, 206.2570). This data is supplied by FORS A/S.

3.2 Topography

The topography map from GEOSCENE3D is displayed in figure 7, page 16. The highest areas are located at the northeastern and southwestern corners of the model area, reaching heights of more than 36 m.a.s.l. Moving from east to west the topography decreases to 0 m.a.s.l. at the fjord. There is a valley-like depression in the middle of the model area, where the topography is a few meters higher than sea level.

3.3 Climate

Precipitation data is provided by DMI, that has a measuring station in the model area, called Nymarken. The precipitation is corrected for wetting loss and wind effect

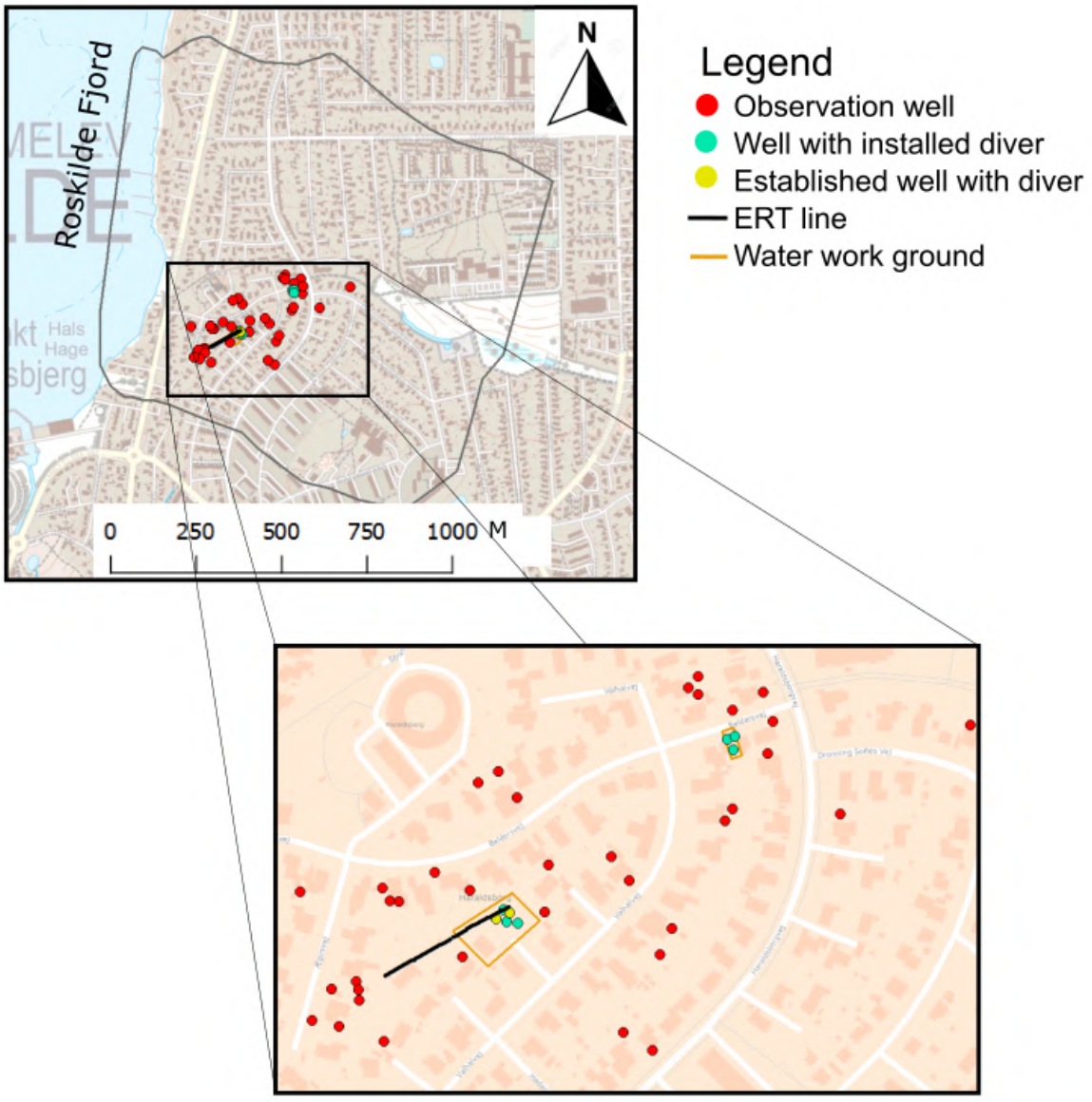

Figure 6: An overview of the model area in Roskilde with the location of wells and fieldwork.

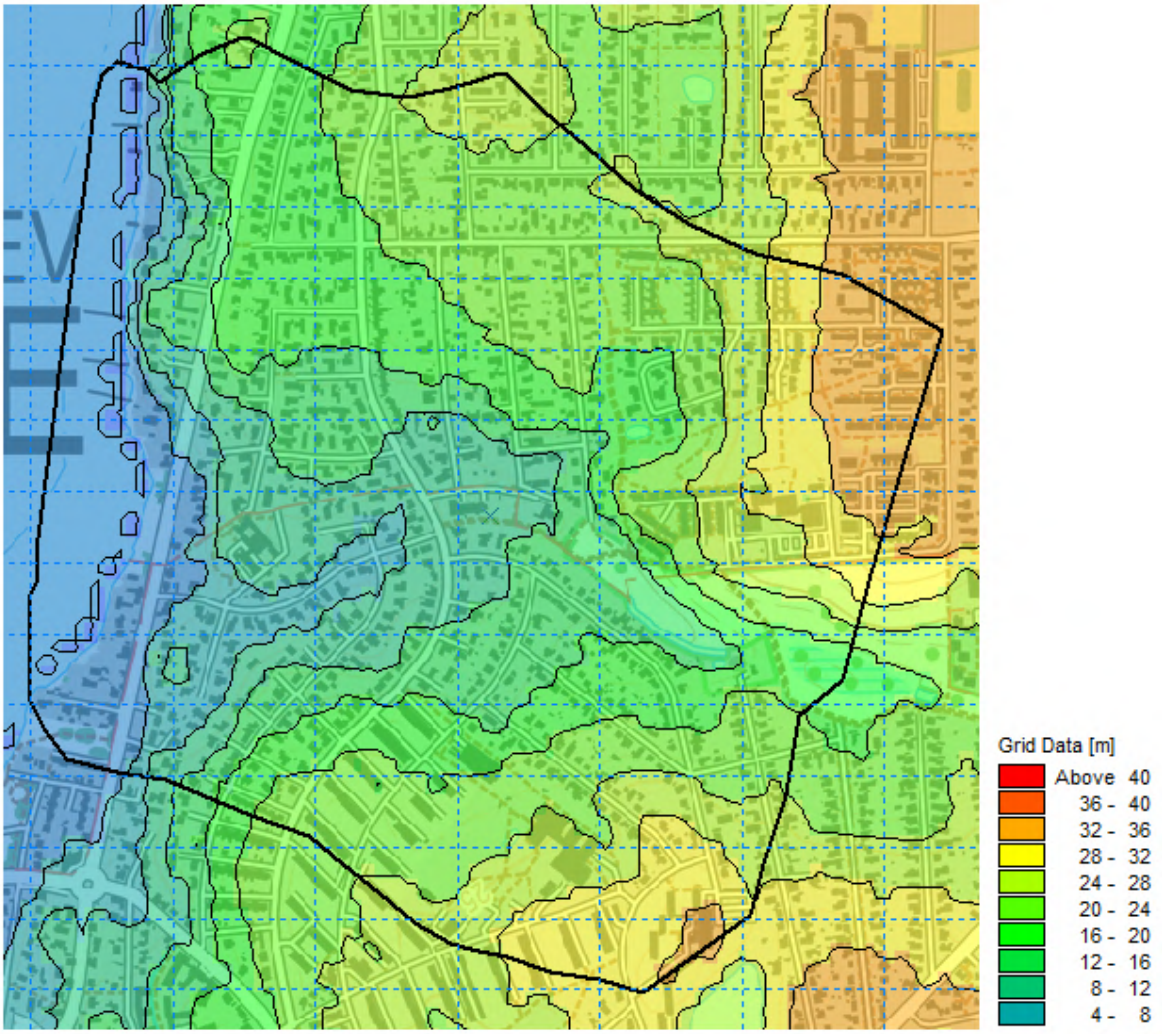

Figure 7: Topography of the area. Highest areas are shown in red and orange colors and lowest in blue.

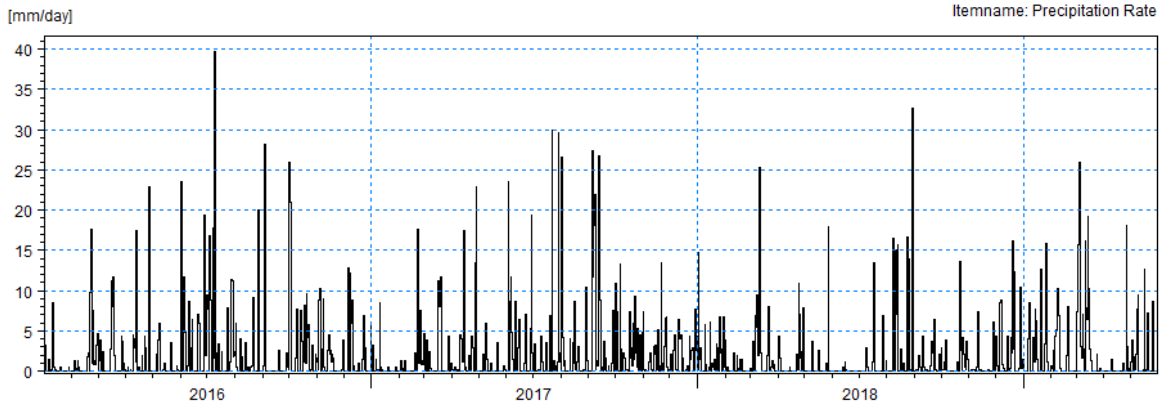

Figure 8: Daily precipitation from 1/1-2016 to 31/5-2019, in mm/day

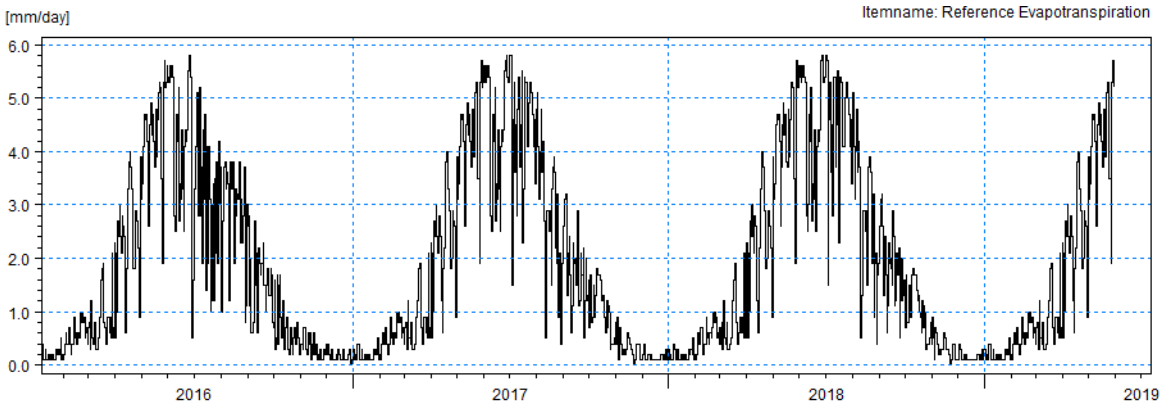

Figure 9: Daily evapotranspiration from 1/1-2016 to 31/5-2019, in mm/day. Notice that some data is repeated from a previous year.

according to Allerup et al. [1998] using the "moderat læ" correction. NOVANA provides evaporation and transpiration data from their 20x20 km climate grid. This data is not updated as often as DMI's rain gauge measurements and therefore some of the used ET data is repeated from previous years. The resolution of the climatic data is daily and precipitation for 2016 and onward is presented in figure 8, page 17. Evapotranspiration is presented in figure 9, page 17.

3.4 Paved Areas

A map of the distribution of paved areas, rooftops, roads, gardens and wetlands is available from www.kortforsyningen.dk (imperviousness). For simplicity the map is divided into two distinct categories - one being paved areas and the other being grass. The parameter values for paved areas is a leaf area index of 0.5 and a root depth of

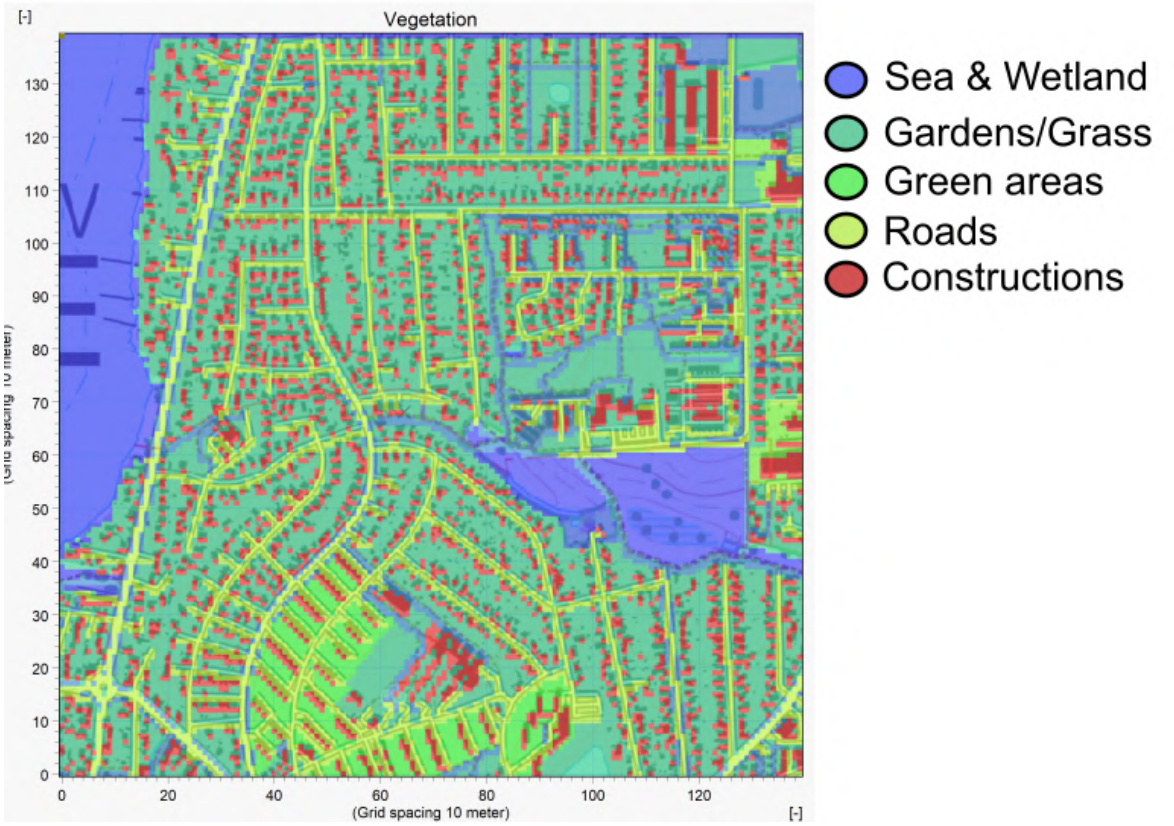

Figure 10: Surface classification within the model domain shown with black line.

150 mm. For gardens a leaf area index of 4 and root depth of 600 mm is selected. The map is seen in figure 10 with yellow representing roads, purple representing rooftops, turquoise gardens, blue wetlands and sea.

3.5 Richards Equation Soil Types

The model area is divided into three distinct soil types, as seen in figure 11, page 19. Dark blue corresponds to freshwater peat and sand, light blue corresponds to moraine clay and purple corresponds to deluvial sand. Further details for each soil type can be found in Waagepetersen et al. [2008]. The unsaturated zone is divided into 3 horizons, named a,b and c. The a horizon is located from the surface to 0.3 m below the surface, with a discretization of 6 cells with each cell being 0.05 m thick. The b horizon is placed from 0.3 m to 0.8 m below the surface and has a discretization of 5 cells with each cell being 0.1 m. The c horizon is located at 0.8 m to 100 m below the surface. This horizon is split into 3 different discretizations; from 0.8 to 2 m 6 cells is created with each cell being 0.2 m. From 2 to 10 m each cell is 0.5 m thick, making a total

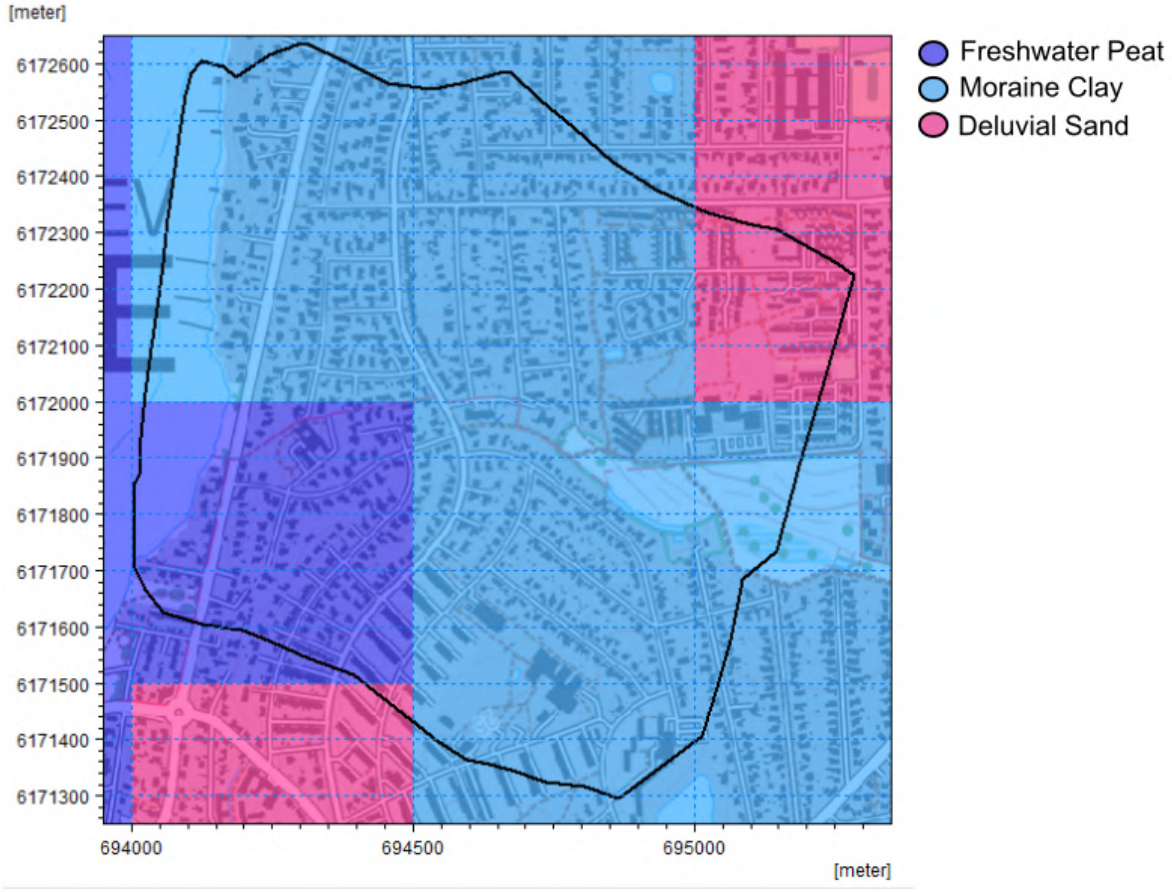

Figure 11: Soil type division in the model. Each color represents a specific soil type.

of 16 cells. From 10 to 100 m 90 cells are created, with a thickness of 1 m. Hydraulic conductivities and the van Genuchten parameter (n) of each soil type and horizon is specified in table 1, page 1. More parameters exists for each soil type, these can be seen in the appendix.

3.6 Drainage/Sewer System

A GIS map of the sewer and drainage system placement in Roskilde was distributed by FORS A/S and is seen in figure 12, page 21. The red dots shows the observation wells and the blue lines shows where subsurface pipes are located. From the provided data, type of material, age and redevelopment status was investigated. Approximately 26 km of subsurface pipes exist inside the model domain. The material of these 26 km pipe is primarily concrete, 72 %, and PWC, 10 %. The majority, 88 %, of the pipes are not redeveloped and 9 % have been treated with CIPP lining, which is a development

999	a	b	c
Ks(m/s)	$7.5 \cdot 10^{-7}$	$9.4 \cdot 10^{-7}$	$1.6 \cdot 10^{-6}$
n	1.312	1.261	1.294
5067	a	b	c
Ks(m/s)	$3.8 \cdot 10^{-7}$	$1.3 \cdot 10^{-7}$	$2.5 \cdot 10^{-7}$
n	1.23	1.217	1.192
5077	a	b	c
Ks(m/s)	$2.0 \cdot 10^{-7}$	$4.2 \cdot 10^{-7}$	$3.3 \cdot 10^{-7}$
n	1.205	1.227	1.2

Table 1: Parameters, used in the Richards Equation model setup.

of the pipes to reduce leakage. Approximately 2/3 of the pipes are old concrete pipes (from 1960s) with no improvements since the establishment. These pipes are used to form the base of the drainage system.

In the model the drainage system is build using MIKE11 and not the actual drainage component in MIKESHE. The reasoning behind this is to keep the drainage component empty, so it can be used to build perimeter drains.

The river build in MIKE11 is seen in figure 13, page 22. This is created based on the analysis of the sewer system, but with modifications. Modifications are necessary since all segments must be connected to allow flow. One stream excisted some 50 years ago. It is now piped and flows in the drainage system, see figure 17, page 29. An additional part of the drainage system is build using the drainage component of MIKESHE. This specific part is one line between Haraldsborgvej and Valhalvej.

3.7 Limestone Hydraulic Head Maps

Two maps exists with simulated hydraulic head in the limestone, both created by Rambøll. The map in figure 14, page 23, shows how the hydraulic gradient is in a no-pumping situation. The highest hydraulic head is seen in the southeastern part, with a value of more than 20 m, decreasing to less than 10 m in the northwestern part. In figure 15, page 24, the simulated cone of depression caused by groundwater abstraction from Haraldsborg waterworks is shown. The unit shows how much the head in the limestone would increase if the waterwork stops pumping.

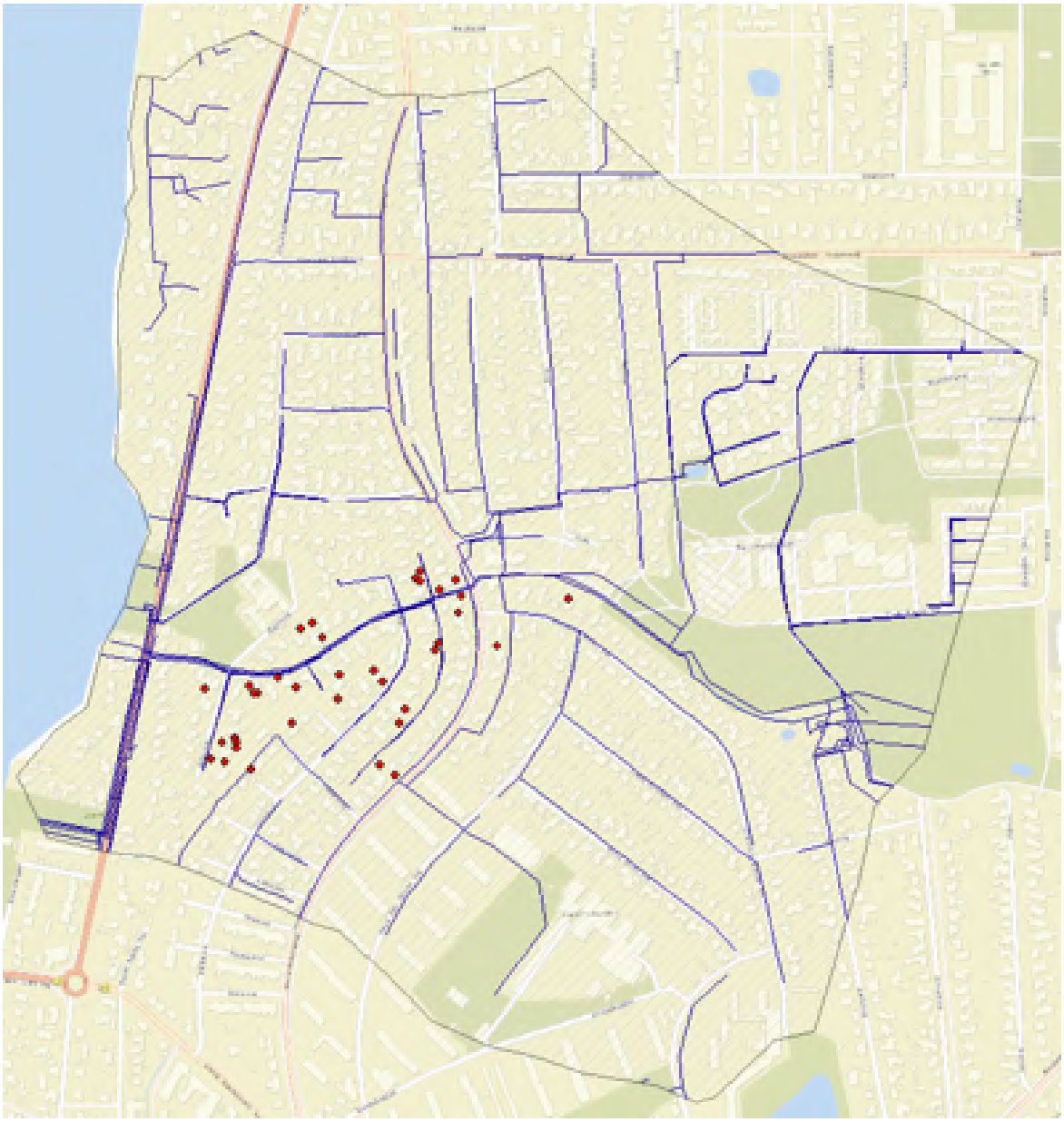

Figure 12: Overview of subsurface pipes in the model area.

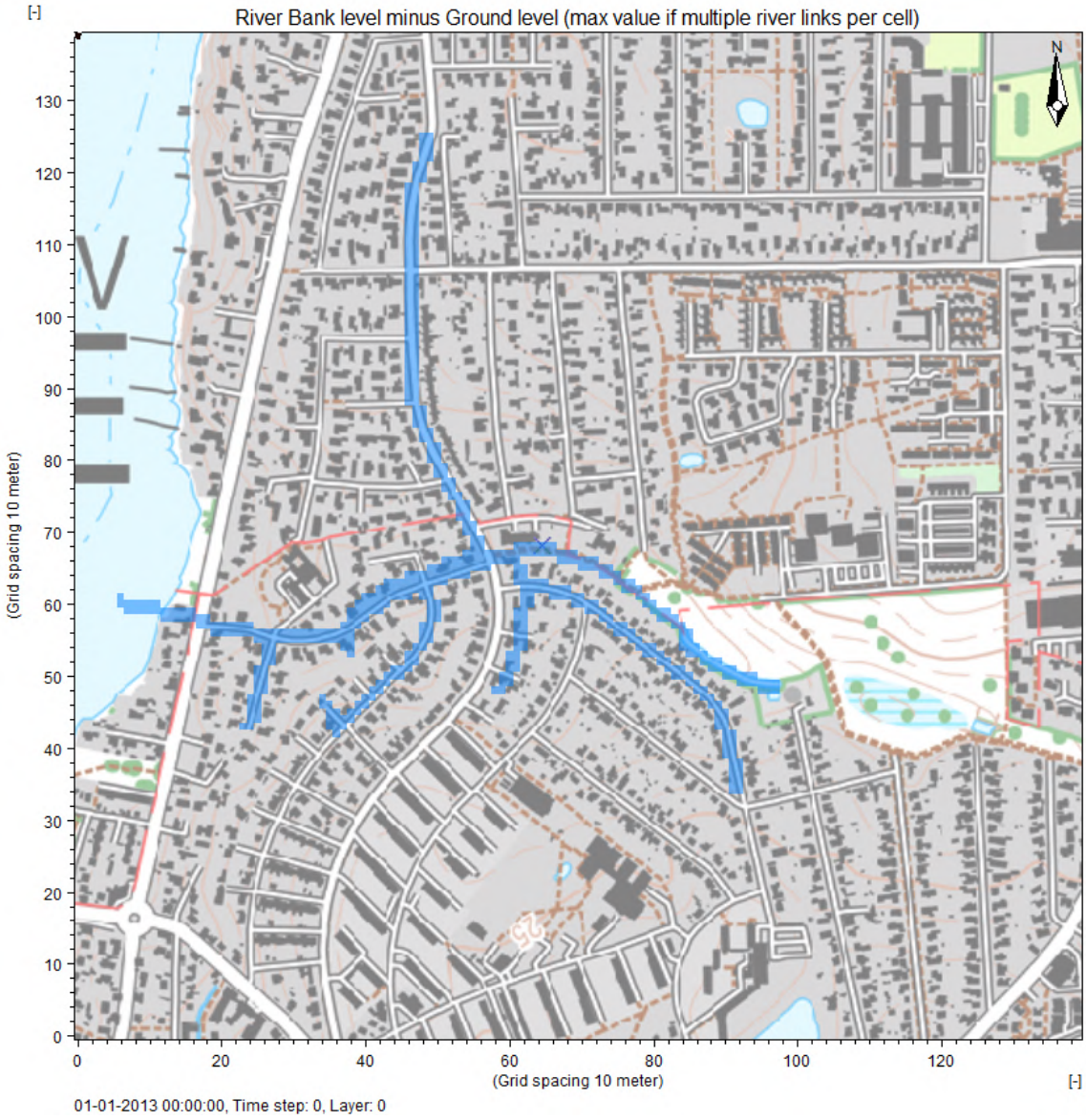

Figure 13: The MIKE11 build drainage system is seen with blue lines.

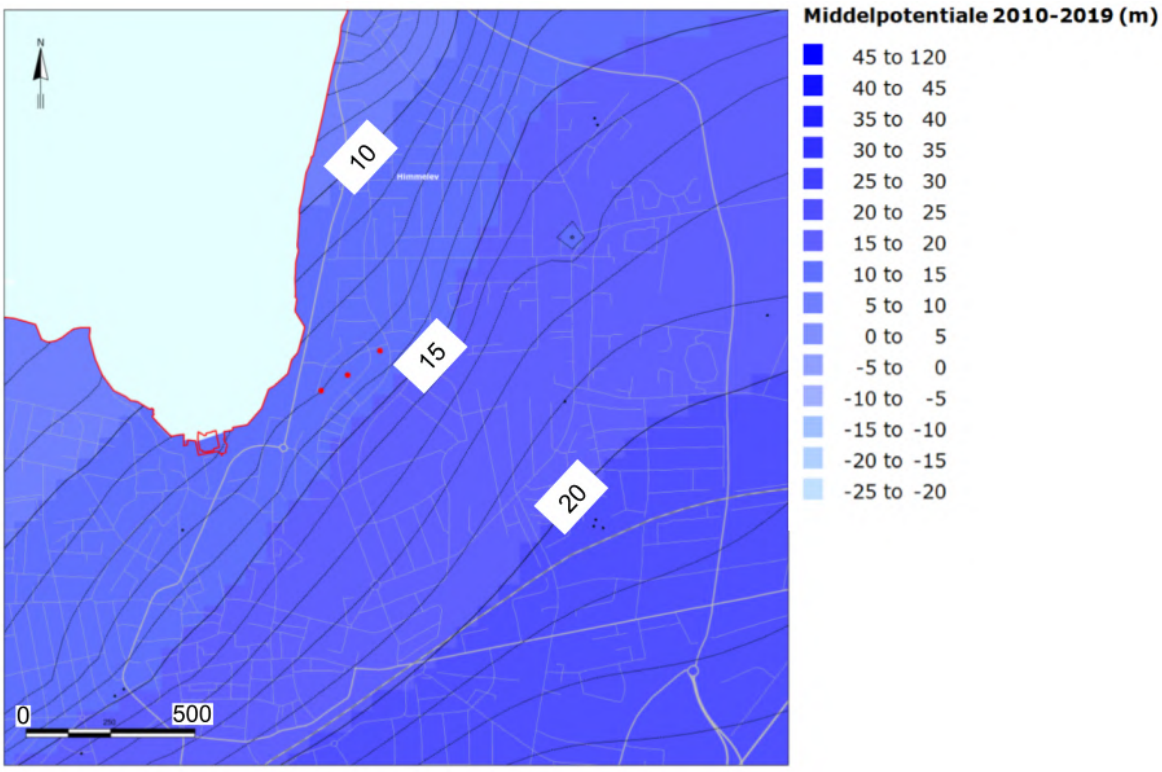

Figure 14: Simulated limestone hydraulic head gradient in no-pumping conditions. The pressure decreases from 22-23 m in southeast and reaches less than 10 m in the nortwestern area [Rambøll, 2017].

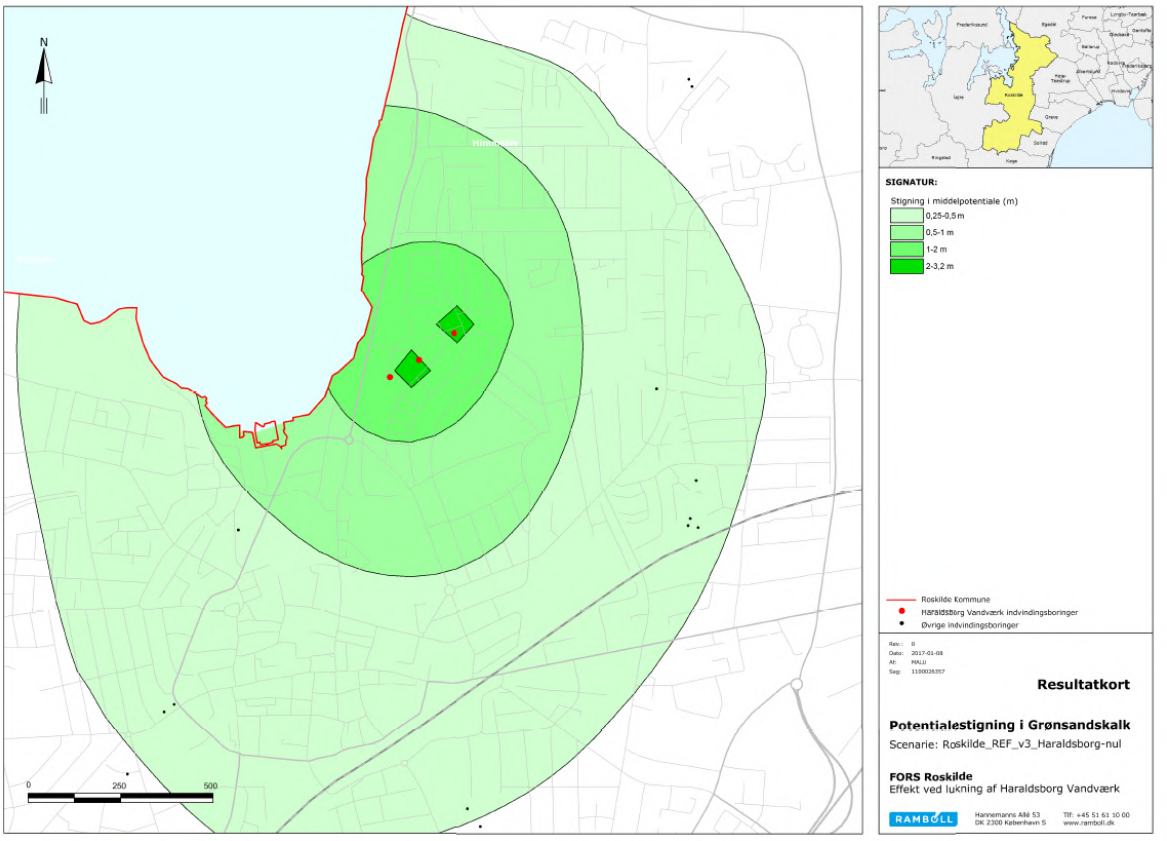

Figure 15: The simulated effect of pumping from Haraldsborg waterworks [Rambøll, 2017].

4 Methods

Methods for the executed field work and hydrological modelling will be presented in this chapter. Figure 6, page 15, gives an overview of the geographical location where the field work took place. The red dots are wells monitored by residents in Himmelev, Roskilde. The two yellow dots are wells established using a drilling rig. The blue and yellow dots are wells, monitored using divers. The installation of divers only took place on the waterworks premises seen with a golden outline. The black line in figure 6 represent the ERT line.

The field work conducted during this study was used to clarify the position of a sandlayer beneath Haraldsborg waterworks but also to install divers in different depths to observe the propagation of changed pressure in the limestone.

4.1 Gamma Ray Logging

GEUS' wireline logging equipment was used to record the gamma ray count in the 12 m borehole (DGU: 206.2575) on the perimeter of Haraldsborg waterwork. The equipment consists of a tripod from where an approximately one meter long measuring pipe was lowered down into the borehole. The pipe was lowered to the bottom and then recorded the gamma ray count as it was pulled upwards.

4.2 Electrical Resistivity Tomography

96 spears were put along a line through three gardens in Roskilde on Valhalvej 53, 49 and 47b, as seen in figure 16B, page 26. The spears were put into the ground with a 1 meter spacing, allowing for a relatively high resolution and with the possibility to measure resistivities from the sand lense or sand layer that was searched for. With a one meter spacing between each spear the vertical resolution reached approximately 15 m (approximately 1/5 of the total length of the line of 95 m). The ERT line was placed to be as far from electrical wires in the ground as possible since these might interfere with the signal. In figure 16A, page 26, the electrical wires in the ground are seen with red lines and the ERT profile is shown with a black line. The map of buried electrical wires is from the LER database (www.ler.dk). In figure 16B the same ERT line is shown. On this figure it is seen how the outline stretches through multiple gardens. After the collection of data the inversion was done using the RES2DINVX32 software to produce the 2D resistivity maps.

Figure 16: A: Electrical wires in the subsurface. B: Placement of the ERT-line

4.3 Geological Model

The geological model is based on hard data, in the form of drilling logs from the JUPITER database and from GEO's database, GEOATLAS LIVE, along with drilling logs constructed during field work. This was supplimented with soft data from geophysical exploration field work (this being an electrical resistivity tomography and gamma ray logging from borehole). In addition, several geotechnical reports have been received with geological information primarily from the upper few meters.

The geological model is build in GeoScene3d software, which uses an inverse distance weighted interpolation wizard.

4.4 Hydrological Model Setup

Setting up the hydrological model is done in steps starting with a reference model, which includes only the basics. After this, 4 models of various complexity is constructed. Each model is a copy of the reference model and uses only the level of complexity as described, in other words, the landuse model changes only the landuse component but not the geology, drainage system or the UZ solution. The models are as follows

- Reference model
- Landuse model, which include urban structures like roads and rooftops.
- Geological model, which include the interpreted geology.
- Richard's equation model, which includes a more sophisticated solution for the UZ.
- Drainage model, which include a drainage network.

The initial time steps of the reference model is set to 1.5, 3, 12 and 24 hours for the initial time step, overland time step, unsaturated zone time step and saturated zone time step, respectively. These values are put as high as possible to reduce calculation time but not higher than 24 hours since a daily output is used to monitor groundwater levels. Control parameters for overland, unsaturated- and saturated zone in MIKESHE are left as default.

The model domain is seen in figure 6, page 15. The model covers an area of almost $1200 \cdot 10^3 m^2$ of which $90 \cdot 10^3 m^2$ are situated in the fjord. 140 cells in the x and y

direction, with a cell size of 10 m, cover the model domain. The horizontal discretization of 10 m is selected to enable multiple head observations in several gardens. 4 vertical layers are created in the reference model with each layer having a total of 12043 cells. The thickness of each vertical layer varyies throughout the model.

The northern and southern boundaries are placed according to a topographical high, with the assumption that no flow occurs below these [Sonnenborg and Henriksen, 2005]. The western boundary is located in Roskilde fjord. This allows for a constant potential head of 0 m and an inner boundary condition with a constant potential head of 0 m at the upper few meters of the model area in the fjord [Sonnenborg et al., 2003]. The western boundary is placed arbitrarily, though with respect for two concerns; it should be so far away that an eventual influence on the head simulations in the area of concern is minimal and it should also be relatively close to the same area in order to constrain computational time. After attempts with a linear pressure decrease throughout the geological column below the boundary, it was decided to make no flow boundary conditions since no effects were observed following head simulations in the area of concern.

An inner boundary condition exists in the bottom layer representing the hydraulic head simulated by Rambøll, see figure 14, page 23.

Vegatation throughout the basemodel is assumed to be grass, with a leaf area index (LAI) of 4 and a root depth of 600 mm.

One simple river with only one segment stretches from the eastern part of the profile and reaches the fjord in the western part, see figure 17, page 29. This river is placed according to the position of a piped river in the area.

The Manning number of the overland flow is 10 and the detention storage is set to 4 mm. Time constants for the ponded drainage component is set to 0.001 s^{-1} with a runoff coefficient of 1. Drain codes are added that routes overland flow in the eastern part of the model area into the river and in the western part overland flow is routed to the sea. The division is made according to the topography and is seen in figure 17.

The two-layer solution is used for the unsaturated zone. The unsaturated zone is constructed of 1 soil type representing sandy clay (JB5) with an evapotranspiration depth of 0.04 m. The remaining parameters for this soil type is seen in figure 18, 29.

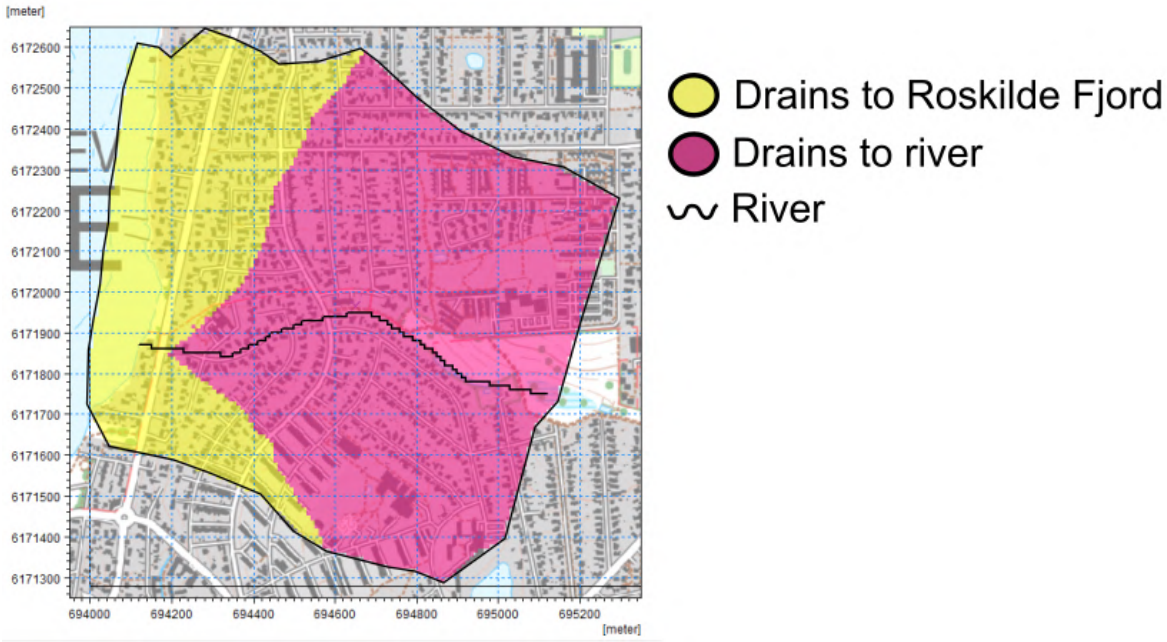

Figure 17: Overland ponded drainage function drains according to color. Pink color drains to the river and yellow color drains to the sea.

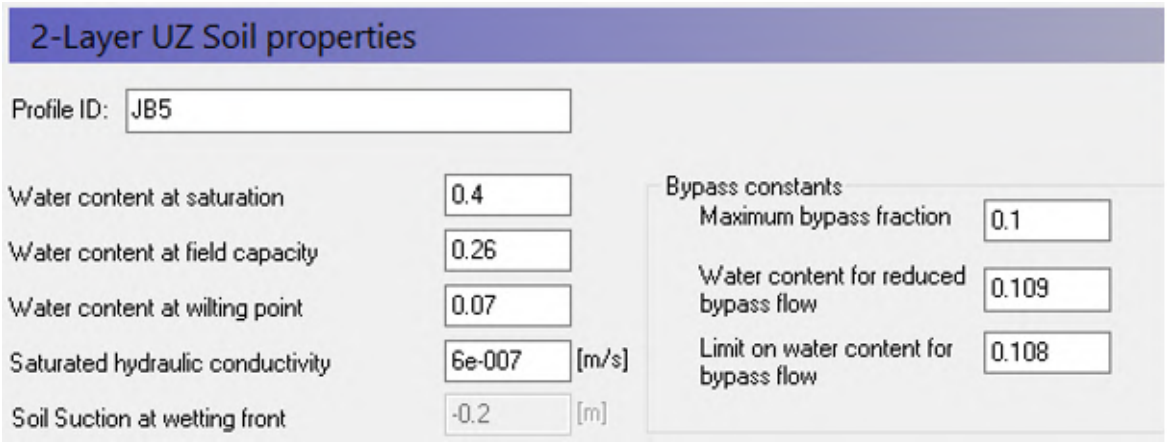

Figure 18: Parameter values for the unsaturated zone.

4.5 Sensitivity Analysis, Calibration and Validation

4.5.1 Sensitivity Analysis

A sensitivity analysis was performed using MIKE ZERO's Autocal software to identify the parameters most important for the parameter-optimization. Autocal finds the most sensitive parameters in a defined parameter space, which means that a certain parameter might be insensitive in a given parameter space but highly sensitive in another [DHI, 2017c].

51 parameters were selected and for each of those an initial value and a lower and upper band level was defined. These parameter values are based on Henriksen et al. [2003] and Danielsen [2018]. The bands for Manning's number in MIKE11 are chosen as an order of magnitude in both directions from the initial value. This arbitrary bandwith is due to high uncertainty regarding this specific parameter.

The sensitivity analysis uses 38 observation wells from the area of interest and 1 observation well from the northern boundary of the defined catchment as the RMSE target (Root mean square error). Autocal defines the sensitivity of a parameter as

$$S_i = \frac{\delta F}{\delta \theta_i}$$

where F is the output measure and θ is the model parameter under consideration.

To compare coefficients of different parameters and scale, a scaled sensitivity is calculated using

$$S_{i,scale} = S_i(\theta_{i,upper} - \theta_{i,lower})$$

where $\theta_{i,upper} - \theta_{i,lower}$ is the upper and lower boundary for a parameter. This transformation allows a direct comparison of parameters sensitivity [DHI, 2017c]. The most sensitive parameters can be seen in figure 19, page 31. From figure 19 it is seen that the most sensitive parameters are related to the conductivities in the unsaturated zone and the conductivities in the saturated zone.

4.5.2 Inverse Calibration

MIKESHE's calibration engine Autocal was used to calibrate the model. Several setups, including different paramater sets and varying parameter bands was tested before the final calibration was carried out. The first attempts included UZ parameters, SZ parameters and the river leakage coefficient. These calibrations never managed to produce an acceptable objective function and often the calibrations barely converged. The

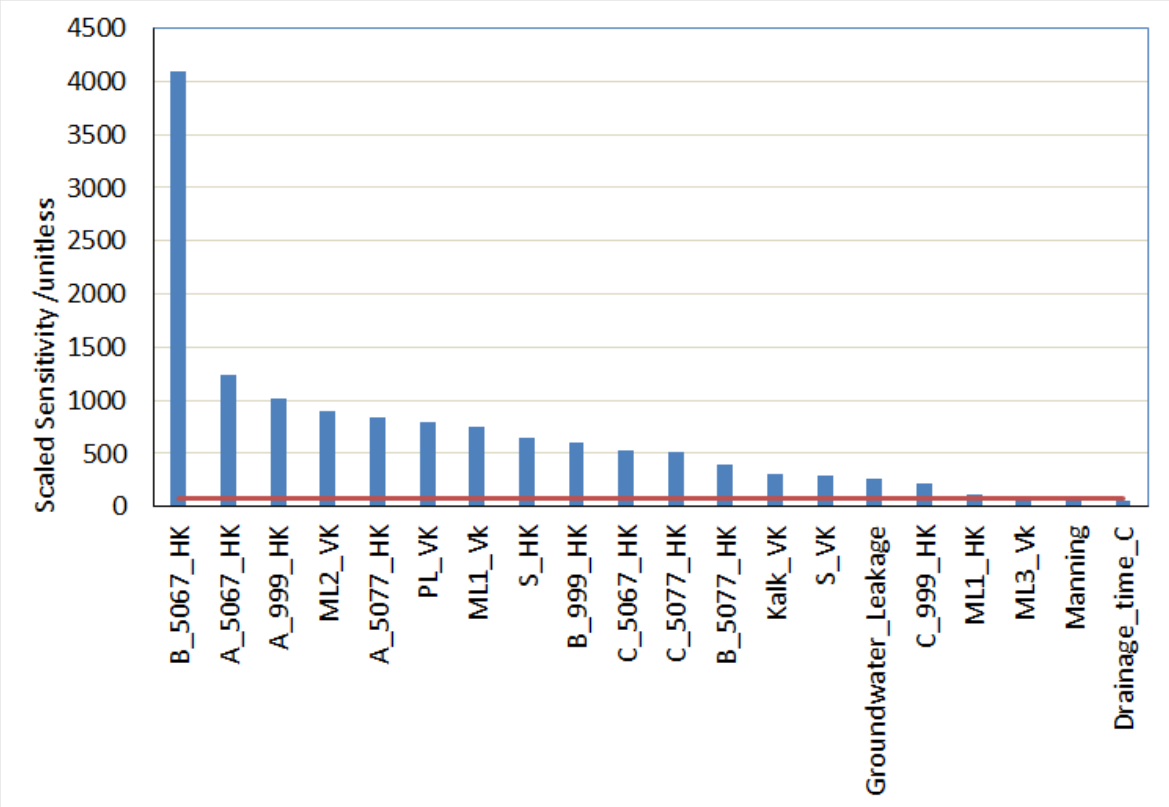

Figure 19: The scaled sensitivity coefficients are seen on this figure with the most sensitive parameters at the left side decreasing to the right.

conceptualization of the model was changed at this point to make the calibration work. The change included a new upper layer of 4 m in thickness representing a fractured moraine clay and/or fillings. At the same time the width of the river branches were increased from less than 1 meter in thickness to 3-4 m to avoid simulation crashes due to numerical problems. An additionally river segment was added using the drainage component of MIKESHE. The western boundary condition was moved a few cells into the fjord and the inner boundary condition with a potential head was created.

The sensitivity analysis was not performed again, so the same parameters were used for calibration.

Different methods to perform the inverted calibration was also attempted, including the shuffled complex evolution and the population simplex evolution.

Due to the issues regarding the inverse calibration, a manual calibration was performed to investigate the effects of different parameters and to find a reasonable value for parameters that did not converge during the inverse calibration. The results from the manual calibration is found in the next section.

The calibration is set up using 4 free parameters which are the horizontal hydrological conductivity of the new upper layer, the moraine clay deposits, the sand layer and the marl layer - expecting an anisotropy of 10.

Observed hydraulic heads on 32 wells from the period 1/1-2018 to 31/5-2019, serves as the calibration targets.

Parameter sampling is done using Latin Hypercube to reduce the needed model simulations [Refsgaard et al., 2007].

The final calibration used the population simplex evolution algorithm, which is explained below.

Population Simplex Evolution (PSE) The PSE is a global minimum algoritm that works in 4 steps.

1. An initial sample of 35 parameter sets is created. Each parameter set is within the defined parameter space

2. 35 simplexes are created with the size of each simplex being 3. A simplex can be understood as a connection of three parameter sets. Then the simplex is evolved according to the algorithm. This evolution is either a reflection, contraction or a random parameter set depending on the effect on the objective function.

3. A new population is created with respect to the previous step.

4. The algorithm repeats step 2-3 until a stopping criterion is met, which could be a maximum number of simulations, number of loops of convergence or to little change in the objective function.

The simplex evolution is visualized in figure 20, page 34 . This figure shows a two dimensional parameter space with a global minimum. The black dots represent parameter sets and the dashed lines represents simplexes. The simplex including a green dot is evolved using reflection and this leads to a better objective function. The simplex with a red dot shows a contraction where the point moves to the middle of the simplex, creating a poorer objective function. The blue dot is a mutation where the algorithm choses a random parameter set which would improve the objective function. Figure 20 is only for vizualisation.

The calibration output is seen in figure 21, page 35, which presents the 10 best simulations. The dottet lines is the upper and lower defined parameter boundaries. In the upper 4 m layer and in the moraine clay the best simulations lie close to the lower boundary. In the sand and marl the dots are spread videly across the parameter band. This means that for the upper layer and for the moraine clay, a better RMSE value is obtained using relatively low hydraulic conductivities, while for the sand and marl the hydraulic conductivity is less important for a better RMSE. Figure 54, page 89 in appendix shows all simulations during inverse calibration. In this figure it seems, that only the upper 4 m layer is converging. Values for each calibrated parameter is seen in table 2.

Parameters/values	New Value (m/s)	Initial Value (m/s)
Fractured Clay	$2.72 \cdot 10^{-6}$	$6.00 \cdot 10^{-6}$
Moraine Clay	$8.89 \cdot 10^{-9}$	$3.22 \cdot 10^{-8}$
Sand	$7.44 \cdot 10^{-6}$	$3.22 \cdot 10^{-6}$
Marl	$2.04 \cdot 10^{-6}$	$7.13 \cdot 10^{-6}$

Table 2: Parameter values before and after the final calibration.

A model simulation with the new parameter values was compared to the model using the initial parameter values and by examining the simulated heads it was decided that despite the RMSE value was slightly lower, the fits during the peaks looked better with

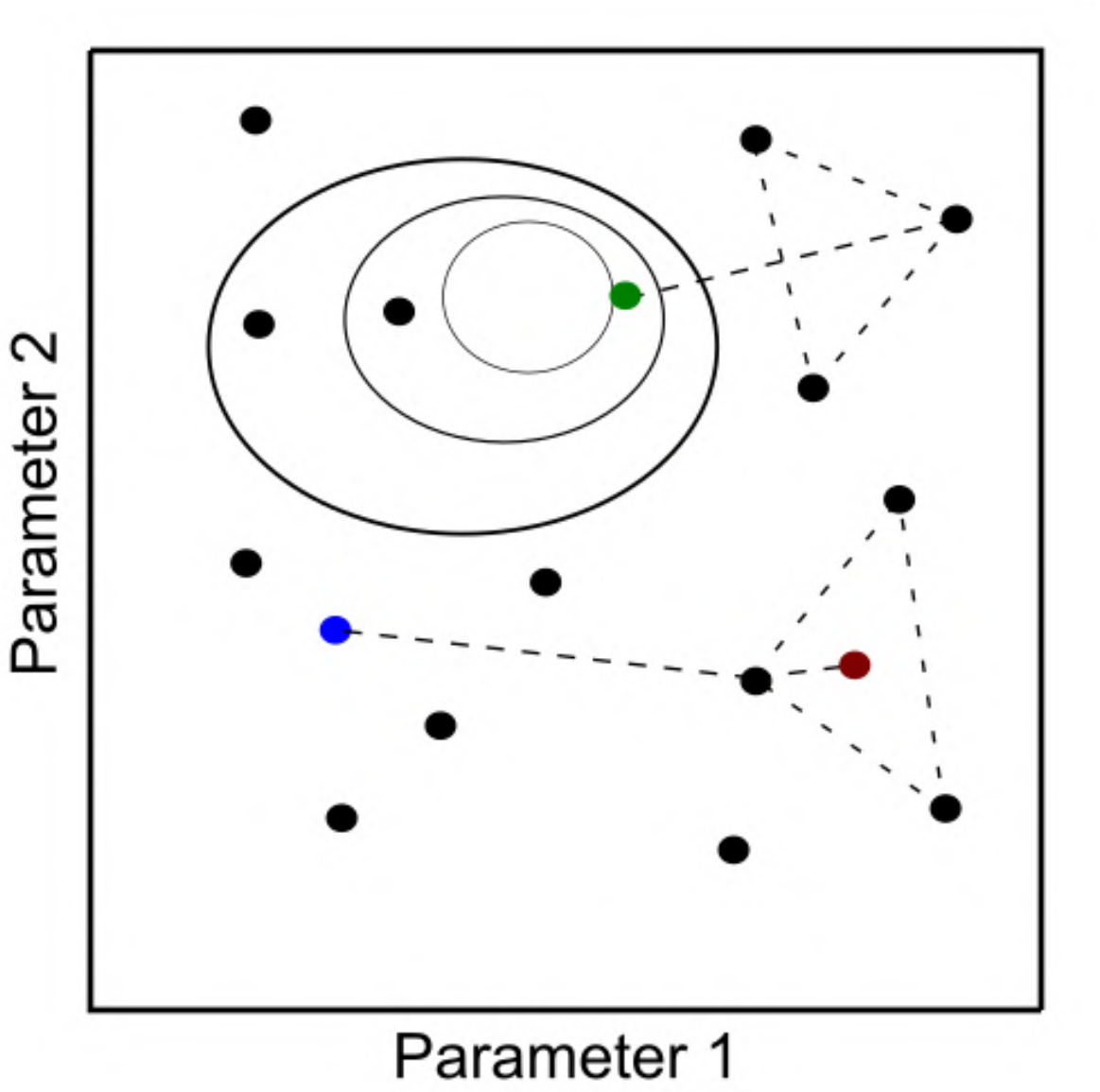

Figure 20: Different evolving methods for the PSE algorithm. The global minimum is inside the inner oval. Simplexes can evolve with reflection (green dot), by contraction (red dot) or by mutation (blue dot)

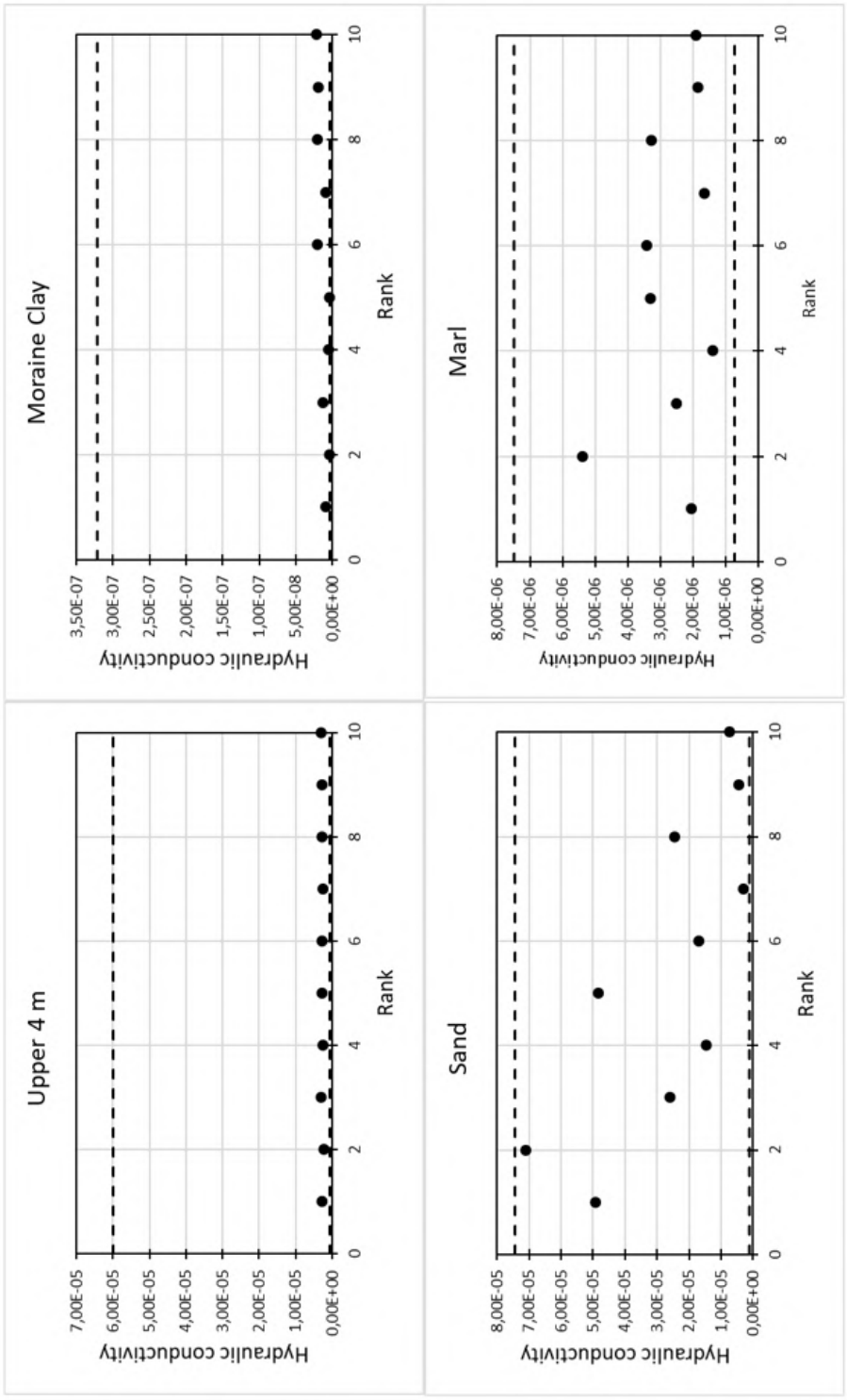

Figure 21: Each black dot represents a simulation. The y-axis is the parameter value and the x-axis is the rank according to objective function value.

the initial values. This decision is purely qualitative, based on comparison of graphs, see figure 49-53, from page 84 to 88 in appendix.

4.5.3 Manual Calibration

After several attempts to use Autocal it was decided to improve the model by manually calibrating some parameters. These parameters are in the unsaturated zone the Van Genuchten parameter (n) and the hydraulic conductivity. Parameters in the saturated zone used for manual calibration is the hydraulic conductivity of the upper 4 m layer and the moraine clay. Furthermore, the anisotropy factor is included in the manual calibration. In the following section, selected results from the manual calibration is presented. The manual calibration is based on comparison of more than one location, but only one location is presented per parameter.

UZ parameters

The Van Genuchten parameter (n) and the UZ hydraulic conductivity was the first targets of calibration. The n parameter was mistakenly left out of the sensitivity analysis. The Van Genuchten parameter describes the retention curve in the unsaturated zone. A lower n means a steeper retention curve where a higher n yields a more flat curve and hold porewater more efficient.

From figure 22, page 37, the result of a varying retention curve is seen. The lowest tested value of n = 1.1 shows the most pronounced amplitude which decreases as n is increased. The amplitude of n = 1.1 fits the observations better than n = 1.5 and n = 2.0.

Figure 23, page 38, shows the effect of an increase and a decrease of the hydraulic conductivity in the UZ. The model using a low K was stopped early due to the conclusion that a lower K value produces a poorer comparison to the observations. A higher K value fits the gradient in time and the amplitude better than the low K value. The initial K value seems to have an equally good gradient but catches the amplitude better than the high K, hence the initial K value is left as default.

SZ parameters

In the SZ, the K value of the top layer and the moraine clay and the anisotropy factor was calibrated manually.

In figure 24, page 39 the result from increasing and decreasing the K value of the upper layer is shown. It is demonstrated that a lower K value is a better fit than a

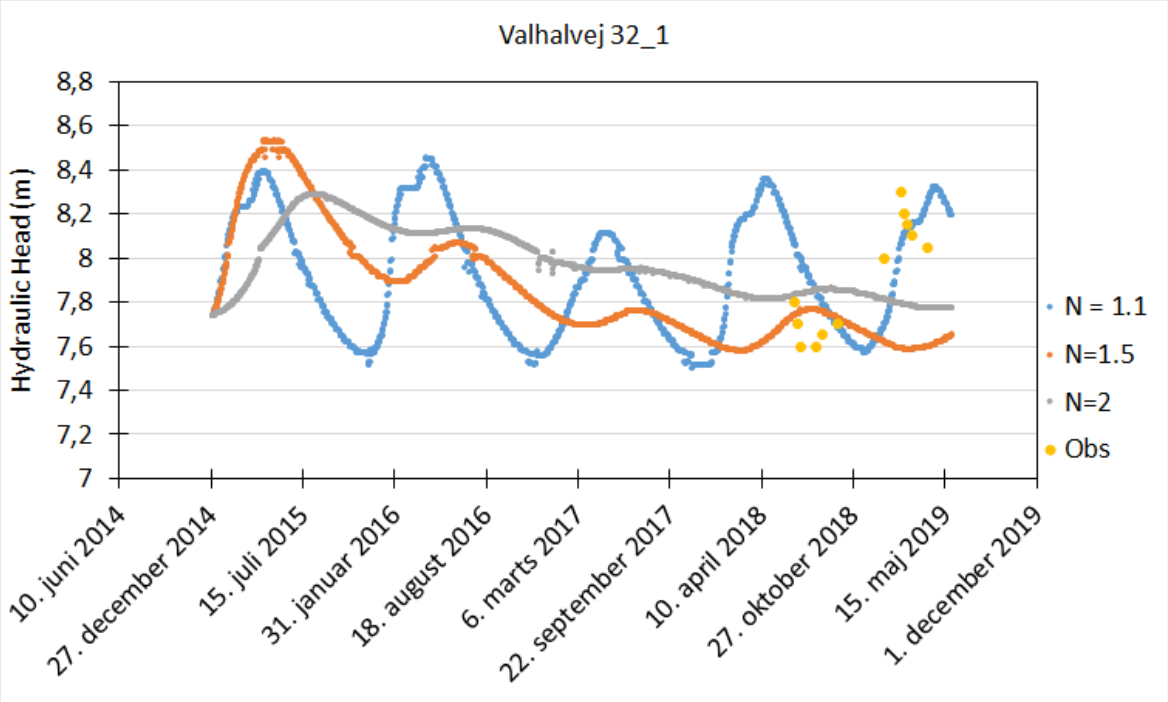

Figure 22: Three model simulations with varying n parameter is seen in this figure. The blue line shows the simulated head elevation with n = 1.1, orange line with 1.5, grey line with 2 and the yellow dots are observations from Valhalvej 32.

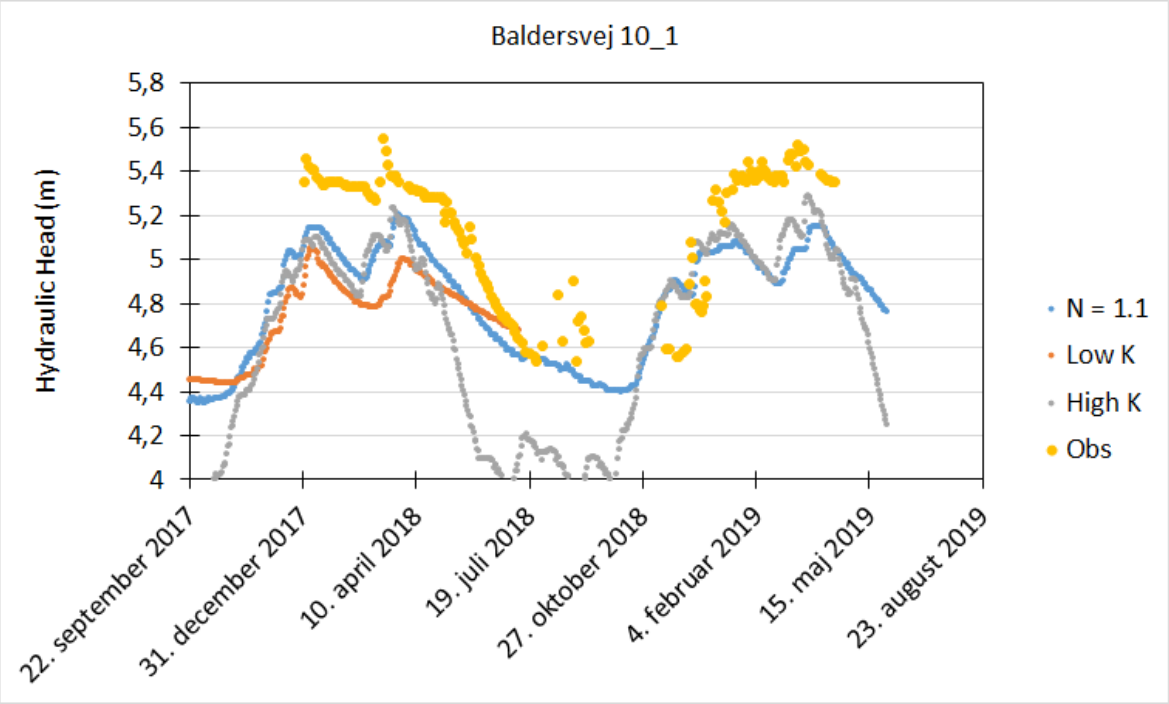

Figure 23: The blue line is the simulated head on Baldersvej 10 with the same settings as the blue line in figure 22. The grey line represents an increase of the hydraulic conductivity in the upper 4 m with a factor of 10. The orange line represents a decrease with a factor of 10. The yellow dots represents observations from Baldersvej 10.

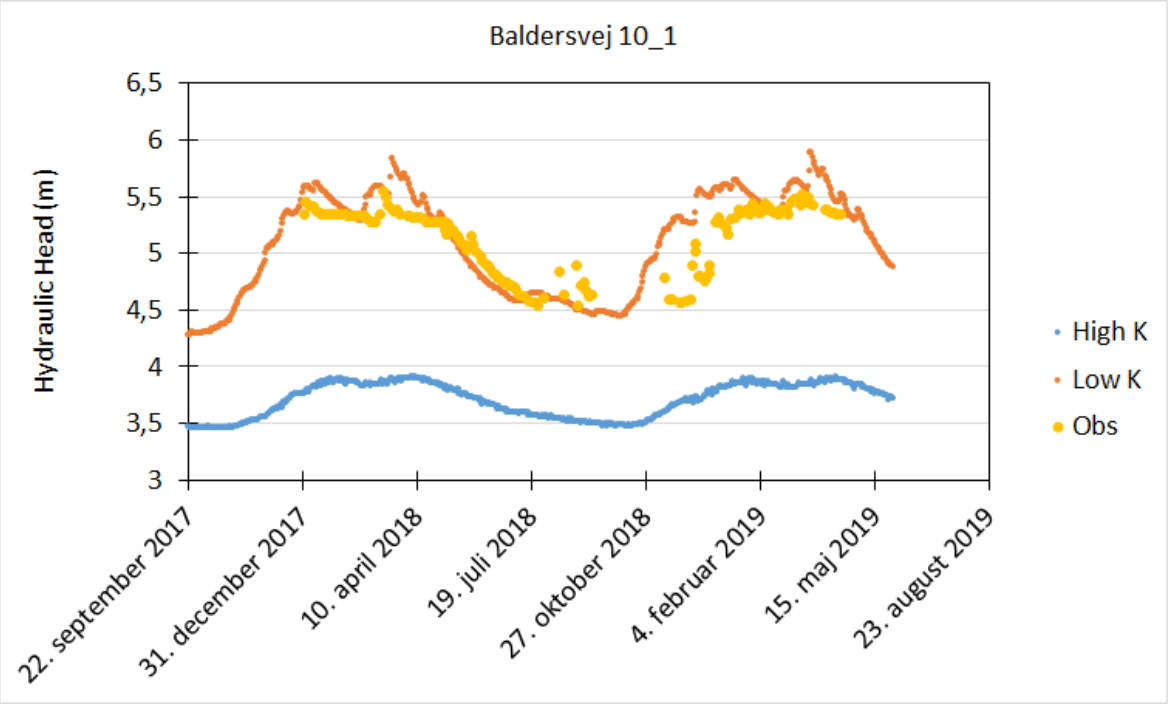

Figure 24: High and low hydraulic conductivity in the upper 4 m layer.

higher.

Figure 25, page 40 shows an example with increased anisotropy. It is seen that an anisotropy of 10, shown with blue dots, do not differ much from an anisotropy of 50. Both the anisotropy of 50 and 10 shows a better fit on the observations compared to the anisotropy of 100. The anisotropy is left at 10.

4.5.4 Validation

The validation of the model is done using a split sample method where data from before 31/05-19 is used for the calibration and data from after the same date is used to validate. Validating the model should be done by comparing the model output to a predefined performence criteria. A performence criteria was not defined in this study. The performance criteria should be decided by the water manager [Sonnenborg and Henriksen, 2005]. Of the 37 wells used for calibration, 12 are selected for validation based on RMSE, though the lack of the performance criterion makes the validation impossible.

The validation is done with respect to the number of data points in the timeseries. Some wells do not have any data for the validation period, others are deemed dry and

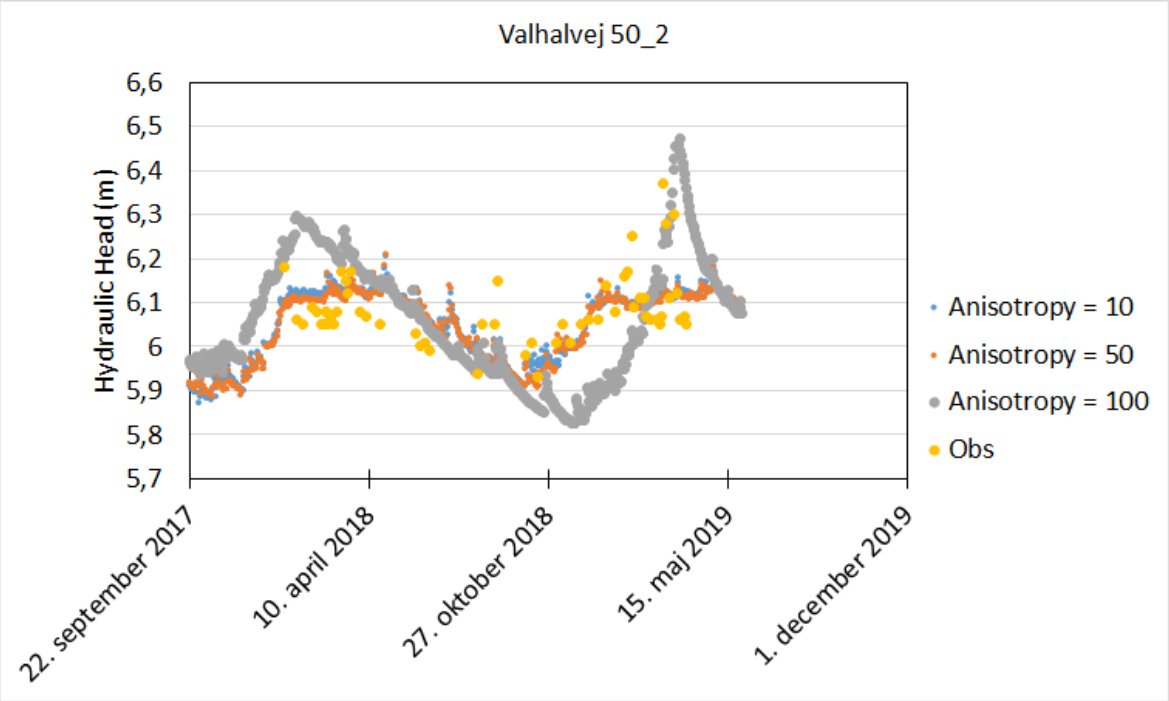

Figure 25: Manual calibration of the anisotropy.

RMSE (m)	Maksimum	Minimum	Mean
Calibration Period	0.73	0.15	0.45
Validation Period	0.81	0.11	0.45

Table 3: RMSE values for the calibration and validation periods.

a few have only one or two points and are excluded. The remaining ones are Valhalvej 32(1), 32(2), 65(1) 65(2), Baldersvej 14(1), 10(1), 10(2) and Ægirsvej 2, 5(1), 5(2), 7(1) and 7(2).

During the validation period, the highest RMSE value is 0.81 m and the lowest is 0.11 m, with an average RMSE of 0.45 m, see table 3. The RMSE values obtained during the calibration period is seen on table 3 aswell. The average RMSE, for the calibration period, is the same while the minimum is 0.04 m higher and the maksimum is 0.08 m lower. The average RMSE is not weighted to adjust for number of observations.

5 Results

5.1 Established Wells

Two wells were established during this study. The first well reached 6 m.b.s. and the second 12 m.b.s. Three attempts were used to establish the wells but due to rocks one attempt were given up, and the 6 m well had to be stopped after 6 m. The overall lithology found in all wells were moraine clay with content of silt, sand and gravel. The upper part was redeposited moraine clay (fillings) and an old surface with old topsoil were found beneath the fillings. Both wells are descriped in details in GEUS JUPITER database. The 6 m.b.s with DGU: 206.2574 and the 12 m.b.s with DGU 2016.2575.

5.2 Gamma Ray Logging

The result from the gamma ray logging is seen figure 46, page 81, in the appendix. Measured gammy ray lies within a range between 50 API to 90 API throughout the entire measured length, except for a length of 0.1 m just above 4 m.b.s, where the value is 40 API. Values of 40 API to 90 API can correspond to either clay or sand. The logged well was drilled during this study, hence the majority of lithology is already known to be moraine clay. The 0.10 m section of lower API value might be a sand lens, that was not resolved during the well drilling. It might also be clay with a slightly different composition than the remaining clay.

5.3 Electrical Resistivity Tomography

The resulting 2D map from the ERT fieldwork can be seen in figure 26, page 42. The top profile is the actual measured resistivty and the bottom profile is the inverted profile. The middle profile is how the top profile should look to obtain an RMS value of 0. After 3 iterations the resisitvity profile looks very chaotic and disturbed. The same occurs in a minor degree after two iterations, hence the profile created after 1 iteration is presented here. The profiles after 2 and 3 iterations are presented in the appendix. Note that the RMSE is 11.2 %.

The profile goes from east to west and the depth reaches 15 m in the middle. The measured resistivities ranges from 15 $ohm \cdot m$ in the blue areas to above 350 $ohm \cdot m$ in the purple areas. The high resistivity is only measured in the top 2 m and mainly in the most eastern and middle part of the profile. This is the area on the waterworks

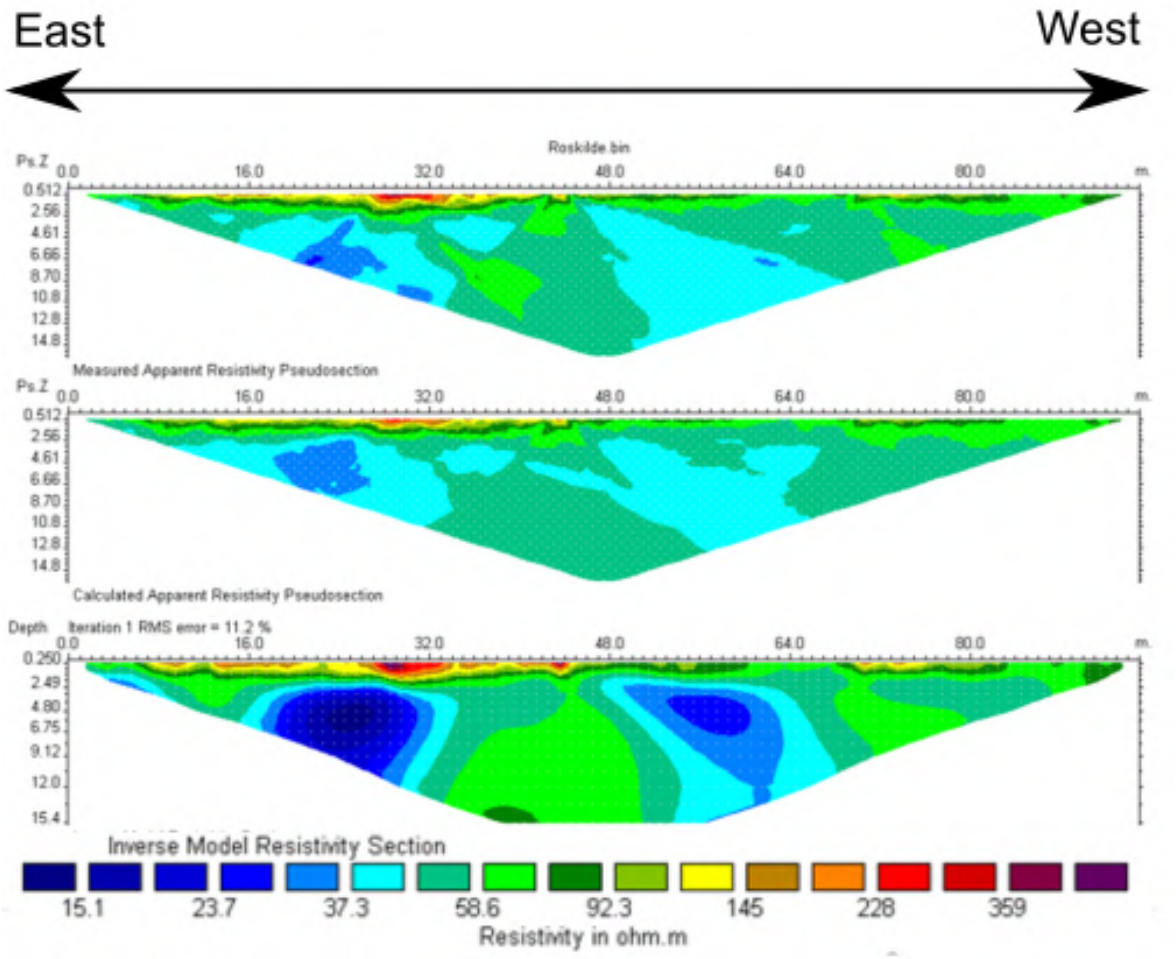

Figure 26: 2D map of the electrical resistivity below the waterworks ground. Blue colors show areas of lower resistivity and red colors higher resistity. The green color covers intermediate resistivities.

premises where foundations and/or subsurface watertanks exists. The majority of the profiles' resistivity values lies between 20 $ohm \cdot m$ to 60 $ohm \cdot m$. These low values are likely to stem from to clay deposits. These values confirm what was seen in the boreholes from the waterworks premises where nothing but moraine clays were found.

5.4 Geological Model

Quaternary meltwater and moraine deposits are dominating the upper 20-30 m of the model area with moraine clay being the most abundant lithology. In the eastern part of the model area, the quaternary deposits reaches thicknesses of more than 40 m. In several wells, samples of sand have been described in 10-15 meters below surface and

some sand samples are described near the pre-quaternary deposits. The sand observed in the top is interpreted as being lenses of sand, while the lower sand is interpreted as being a sand layer due to its higher propagation and thickness.

A thick layer of up to 40 m of Selandian deposits are found under the quaternary geology. The Selandian deposits are divided in two formations which are the Lellinge greensand Fm. and the Kerteminde Marl Fm.. The Lellinge Greensand Fm. consists of greensand clay, greensand chalk and greensand [Ditlefsen et al., 2008]. Lellinge greensand is found in the southeastern and northwestern part of the model area, with a thickness of more than 30 m. Lellinge greensand consist of either chalk sand or quartz sand with glauconite [Ditlefsen et al., 2008]. Ditlefsen et al. [2008] reports that the Lellinge greensand Fm. is often a continous layer and can reach a thickness of 160 m and Heilman-Clausen [1995] reports that in the area around Roskilde and Holbæk it often reaches a thickness of 30 m. A few wells from JUPITER have sand just above the limestone that is not categorized chronostratigraphically, which could then be either glacial sand or greensand.

The other Selandian Formation is the Kerteminde Marl Fm., which consists of clay with a high content of carbonate [Ditlefsen et al., 2008]. Kerteminde Marl is found in many wells with a thickness between a few metres and up to around 40 m. At some wells the Kerteminde Marl is not present and instead sand is found on top of the limestone.

Danien limestone (Kalksandskalk, Københavnerkalken and Slamkalk) is found at the bottom of multiple boreholes, often at depths of 60 – 70 m below the surface. In one specific area the limestone is found approximately 30 m below the surface.

The geological model is visualized in two transects at figure 28, page 45, and figure 29, page 46. The transects' geographical location is seen in figure 27. The sand layers are shown with red for the upper lenses and orange for the widely distributed lower greensand. The orange layer also cover some glacial sand but it is merged with the greensand to form one hydrostratigraphical unit. The moraine deposits are shown with brown and gray colors, and are divided into 3 separate units in order to properly divide the sand units. The light blue color represents the Selandian Kerteminde Marl and the green layer is the limestone. The purple layer is interpreted as anthropogenic filling but is later recategorized to moraine clay for simplicity.

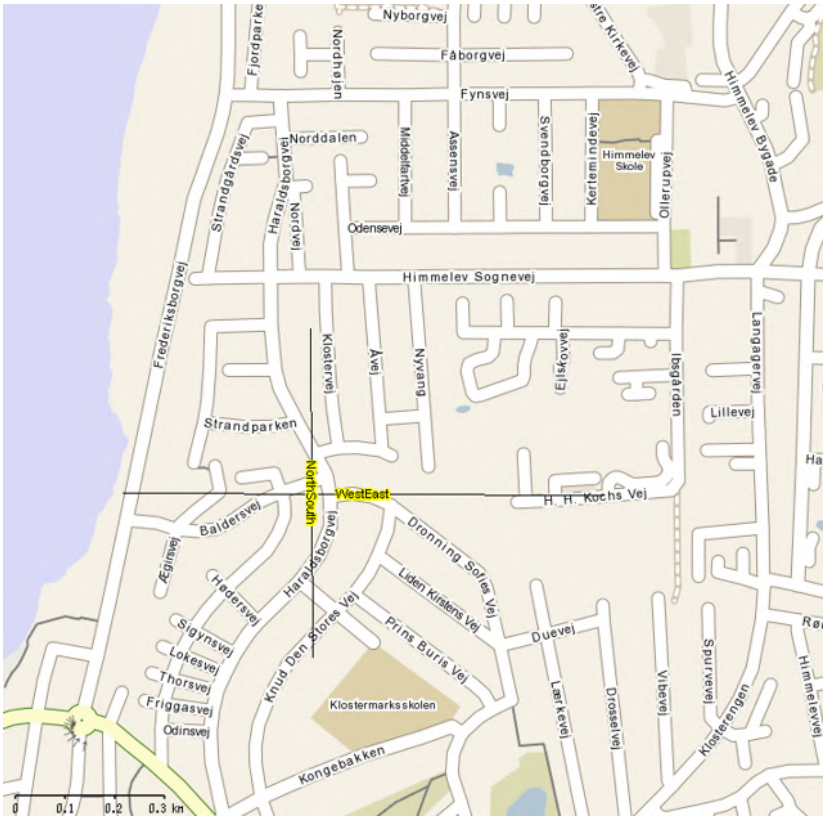

Figure 27: Map of the central part of the model area from GEOSCENE3d. Two transects are shown with black lines.

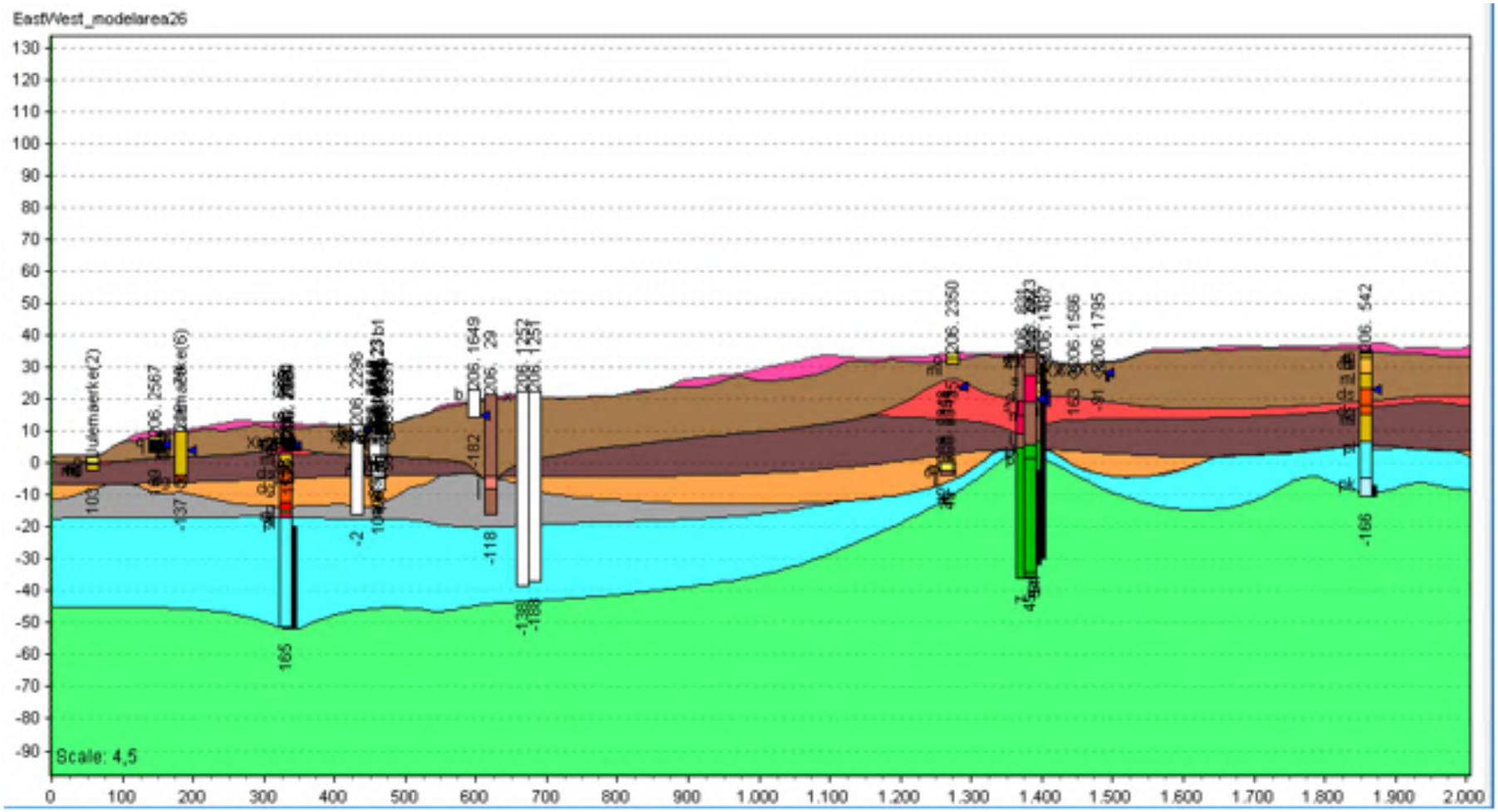

Figure 28: Eastwest transect of the geology. Red and orange colors are sand, dark brown, light brown and grey are clay, light blue is marl and green is limestone.

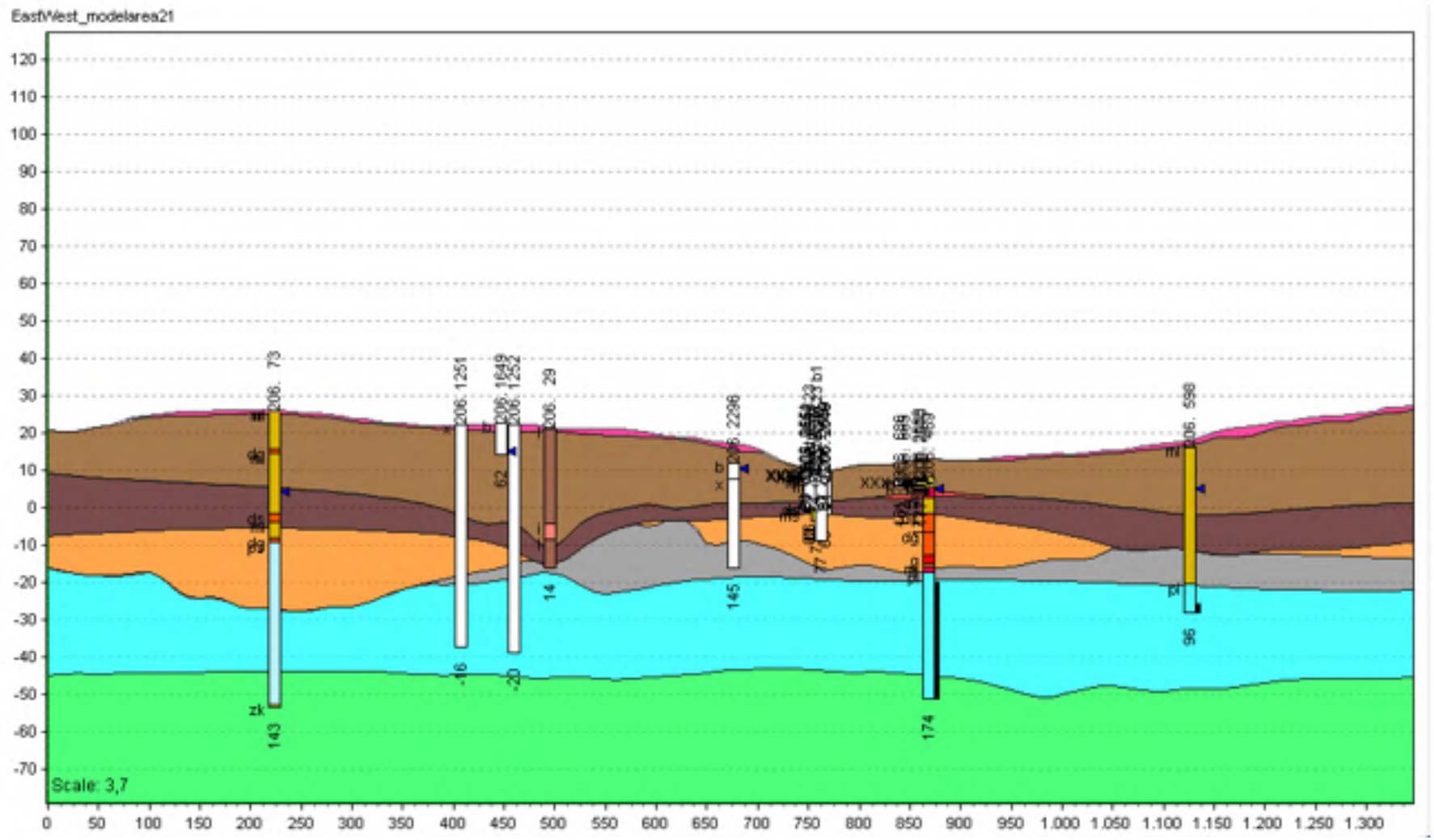

Figure 29: Northsouth transect of the geology. North is right and South is left.th Red and orange colors are sand, dark brown, light brown and grey are clay, light blue is marl and green is limestone.

5.5 Timeseries From Divers

Time series from divers are recorded from the two waterwork premises. In both instances, the divers have recorded in 2 and 5 m.b.s, respectively, and in the limestone aquifer. Additional on Valhalvej 55 two divers have been recording in the 6 m and 12 m borehole that was created during this project.

The purpose of recording the groundwater levels was to examine how a change in pumping condition, and thus abstraction, rate would propagate through the geological layers.

Figure 30, page 49, shows how the hydraulic head in the limestone aquifer reacts to changing pumping rates. DGU 206.468 is on Valhalvej and DGU 206.469 is on Baldersvej. The first change in abstraction occurs on 1st of february 2019, when the pumps were increased to their maximum capacity. This change generates a drop of between 1 to 1.5 m, from 4.9 m to between 3.2 m and 3.8 m, during a 10 day period. The 4th of june 2019 the pumps were turned off for 3 months until the 7th of september 2019. Turning off the pumps yielded a rise in the hydraulic head. DGU 260.468 increased from 4.4 m to 6.4 m and DGU 206.469 from 3.4 m to 6.7 m. This increase occured in approximately 8 days. The 7th of september 2019 the pumps were turned back on to their full capacity. The hydraulic head levels reached approximately the same levels as before the pumps were stopped. The spike around the 12th of october is assumed to be related to a temporal stop of the pumps.

Figure 31, page 50, shows the recorded hydraulic head 6 m below the surface on Valhalvej 55. The head observations show fluctuations in the order of 0.3 to 0.4 m with few larger fluctuations. The hydraulic head seems to be controlled by seasonal variabilities, with lower head in the summer and higher head in the autumn and winter. The head increases from the 12th of june to the 17th of june by 0.5 m. This increase corresponds with the closing of the pumps. It also corresponds with an episode of 46 mm of rain in just 4 days. The hydraulic head is declining in general when the pump is stopped and it increases when the pump is on. The opposite would be assumed if the pressure in the limestone was the controlling factor.

Figure 32, page 51, shows the hydraulic head in 2 m and 5 m below surface. The areas where the curve is straight is assumed to be caused by groundwater levels being below the diver position. Both curves follow the same overall pattern. The highest hydraulic head is recorded during the winter and then decreasing levels into the summer period. The fluctuations are almost twice the magnitude in the 2 m well compared to the 5 m well. The recession of both curves starts closely after the pumps are adjusted

to maximum capacity and continues until the middle of august. There is a peak in the 5 m well just as the pumps are turned of around the 14th of june. This peak is similar to the one in the 6 m well. The hydraulic head in these wells appear to be controlled by seasonal variability.

The data from the three remaining divers are avalable in the appendix. The 2 m well on Baldersvej seems to be dry throughout the studied period. The 5 m well seems to be controlled by seaseonal variablity like as the 5 m well on Valhalvej. The 12 m well on Valhalvej behaves in a suspect way. The hydraulic head increases from 3.4 m to 5.5 m in approximately 4 months before it stabalizes. It is deemed unthrustworthy because, compared to the data discussed above, the flow is initially downward until at one point it changes direction. Perhaps the filter got stuck when establishing the well since it appears to be disconnected from the actual hydraulic head. All 3 are found in the appendix, figure 55 to 57, page 90 to 91.

A specialized diver recording the barometer effect was installed on Valhalvej 55. On figure 58, page 92, in the appendix a short timeseries of the 6 m well on Valhalvej 55 with the barometer effect is shown. The barometer effect does not seem to correlate with the hydraulic head. Rosbjerg and Sonnenborg [1999] states that an increase in air pressure is divided between an increase in the water pressure and an increase in the effective soil matrice. One explanation why the barometer effect is hard to distinguish could be due to the geology primarily being clay, which has a relatively high specific storage meaning that the increase in air pressure primarily effects the grain structure.

5.6 Adding Complexity to The Model

Four degrees of complexity is added to the reference model described in section 4.4. These are landuse/paved area, Richards equation, geology and a drainage system. In this section the water budget for the reference model is compared to water budgets from each specific layer of complexity added to the model. Each water budget is extracted from a two year period from October 2017 to october 2019. In this period 1517 mm of recharge is recorded which is the same for all models.

Besides the recharge, water enters the model from the fixed head western boundary. The amount, in mm, is seen in figure 33, page 52. The blue column is the reference model and from this the other model setups can be compared, to visualize their effect. The landuse model and the drain model are similar to the reference model and lie within 5-6 mm from it. The model simulating UZ flow with Richards equation is 15 mm above and the geological model is 45 mm below. These differences are caused

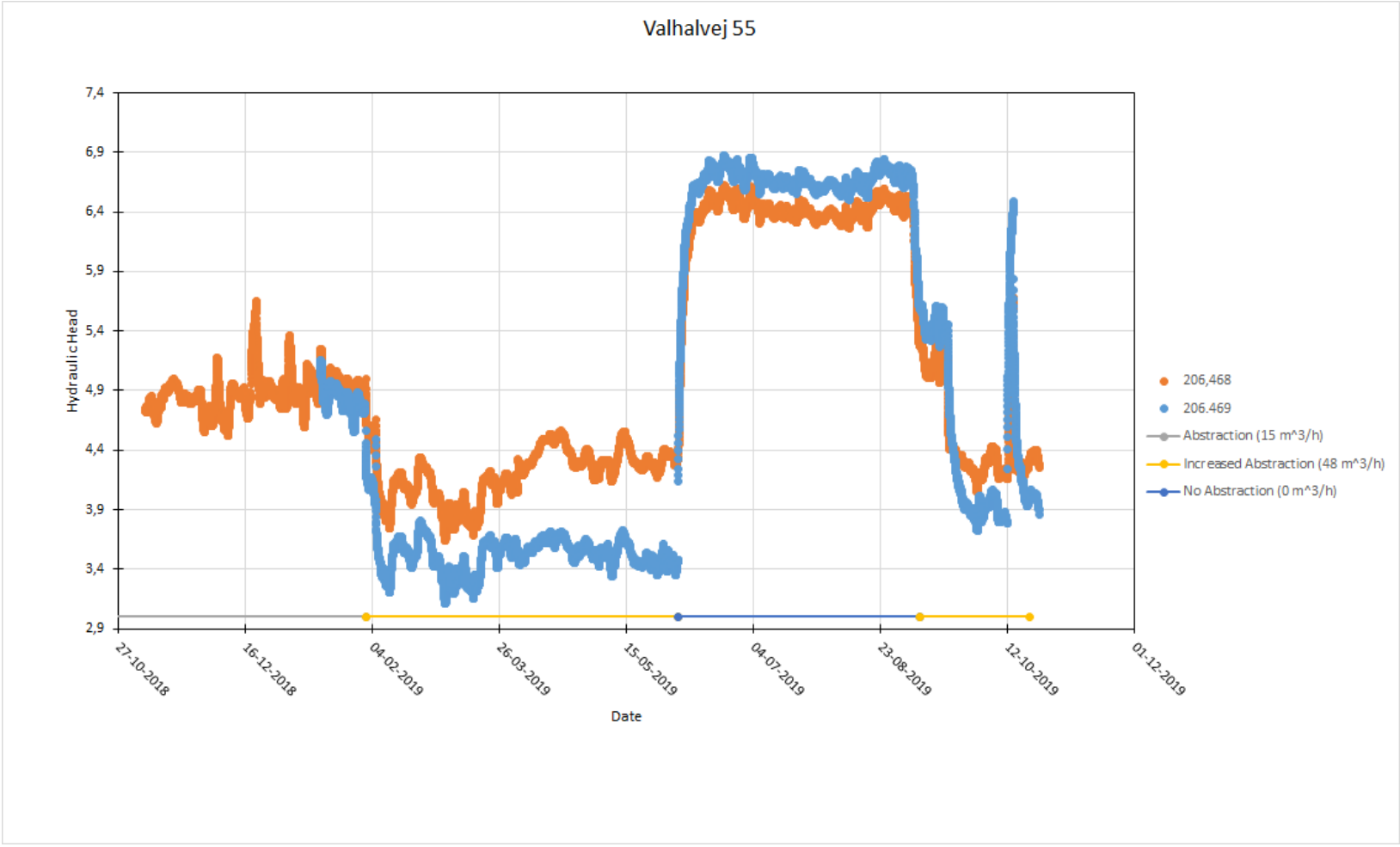

Figure 30: Hydraulic head in the limestone is affected by changes in the abstraction rate. The vertical line at 3 m represents varying pumping conditions. Grey line is a pumping rate of 15 m^3/h, yellow is pumping at maksimum capacity at 48 m^3/h and the blue line represent a no pumping situation.

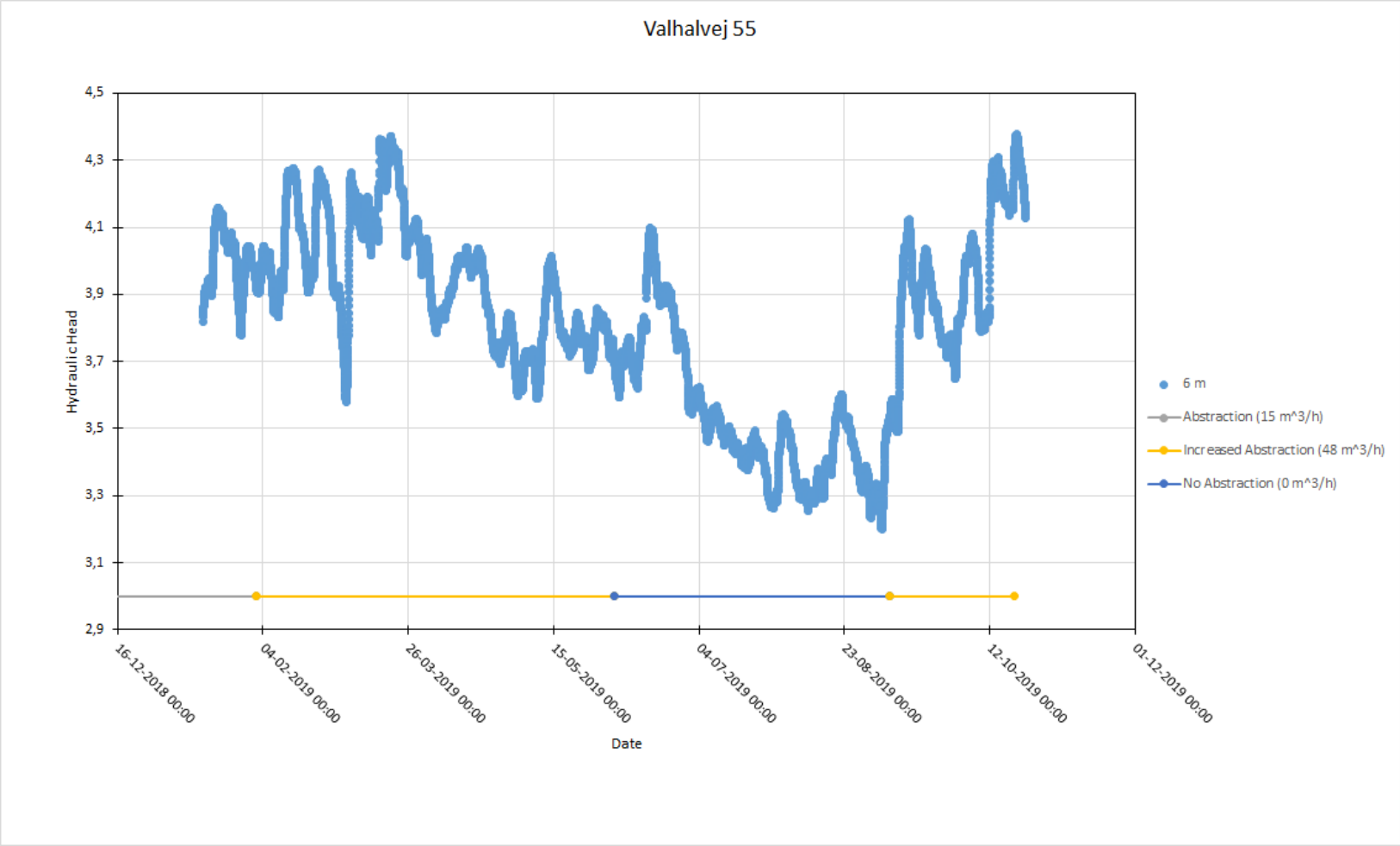

Figure 31: The hydraulic head 6 m below the surface on Haraldsborgvej 55.

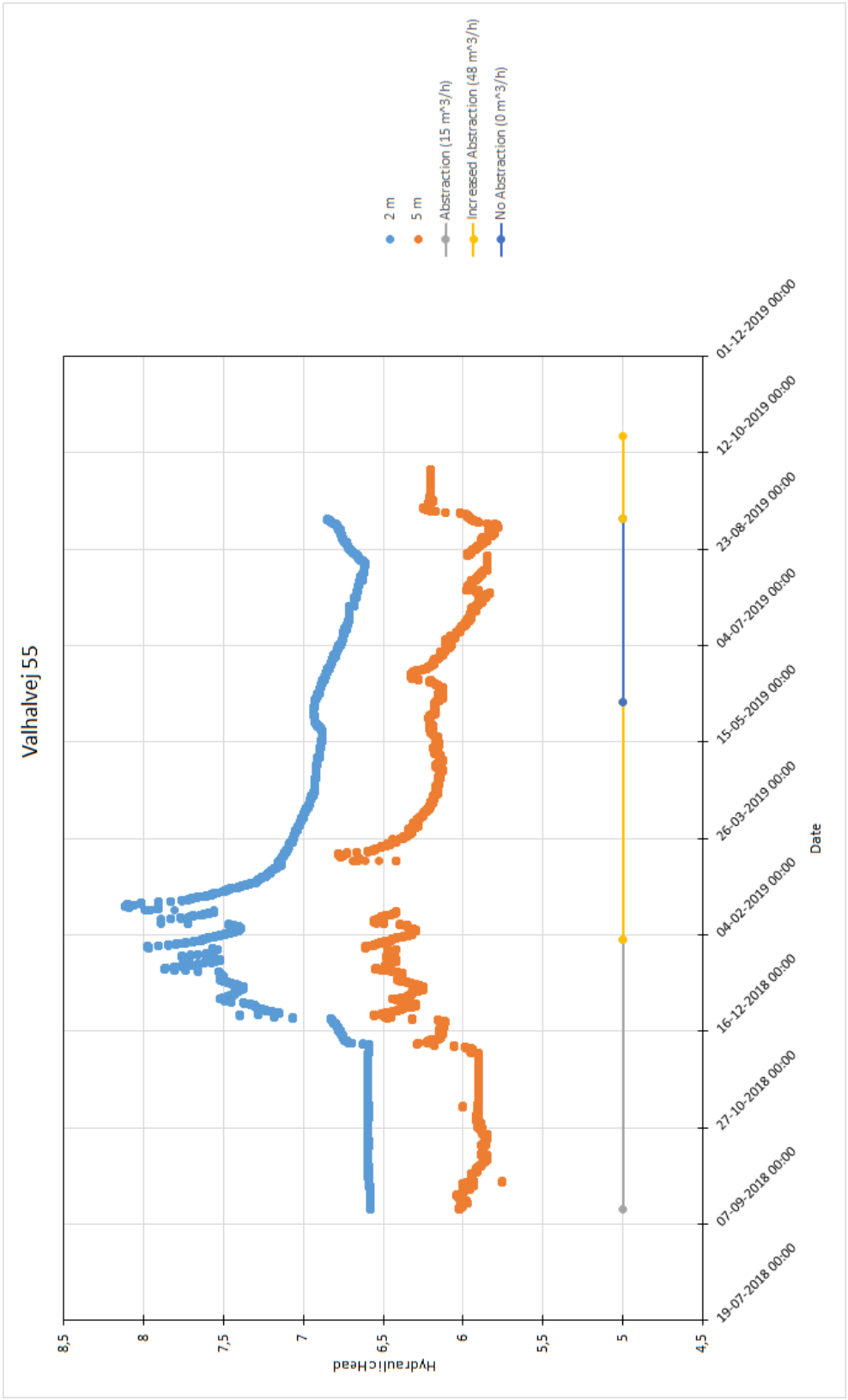

Figure 32: Hydraulic head 2 m.b.s and 5 m.b.s on Haraldsborgvej 55.

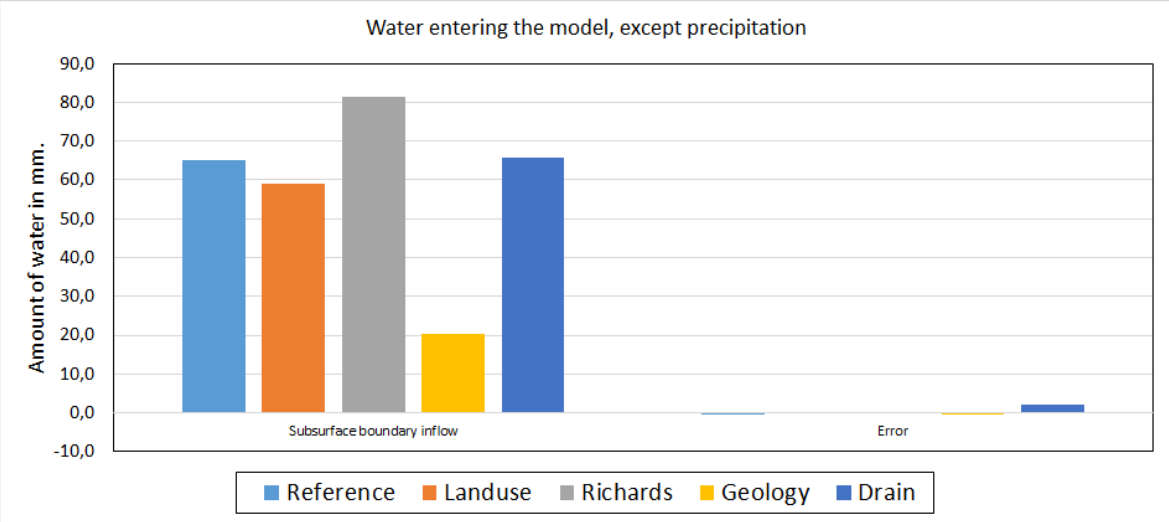

Figure 33: Water entering the models.

because the Richards Eq. model evaporates more, hence lowering the overall groundwater table and allowing a higher inflow from the boundary. The opposite is true when adding the geology to the model. Here, the overall groundwater table rises, because of the large amount of clay, constraining the inflow from the boundary. Figure 33 also contains the error for each model. The highest value is on the drain model where the error is 2 mm. This is well below 1 % of the recharge.

Figure 34, page 53 shows how water is removed from the model. The evapotranspiration is by far the largest sink, which removes approximately half of the precipitation. Simulating flow in the unsaturated zone with Richards eq. increases the ET by 170 mm. Adding landuse lowers the ET by 60 mm. The overland drain to the river is similar to the reference model in each of the other models, except the one adding geology, here the drain increases with 100 mm. Overland drain - overland out is around 200 mm for each model except the drainage model which is around 100 mm. The subsurface storage is around 70 mm for the reference, landuse and drainage model while it is decreased to 50 mm for the Richards equation and geology model. 230 mm leaves the models as subsurface boundary outflow except the geology model which only gives 4 mm. Only the drain model loses water through SZ drain, since this is the only model that actually has a SZ drain. The baseflow to river is 26 mm in the reference model. This value is almost 100 mm in the geology model and 40 mm in the drain model.

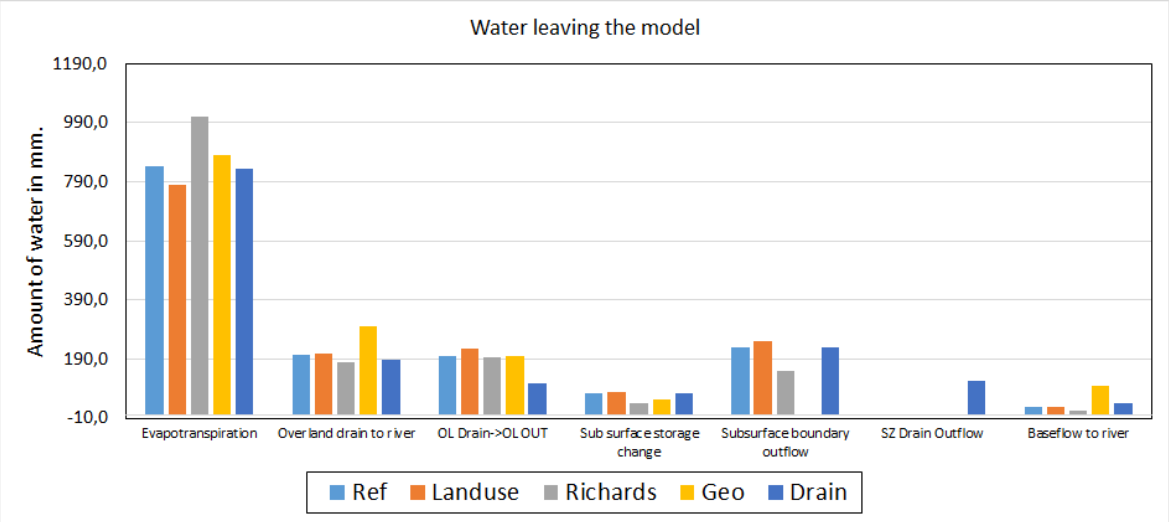

Figure 34: Water leaving the models.

5.7 Closing Haraldsborg Waterworks Scenarios

Two scenarios, 1 and 2, are set up to investigate the effect of closing Haraldsborg waterworks. Both scenarios are compared to a reference model, which in the following is the model using the calibrated parameters. The reference model is set up to represent an abstraction rate of 130000 m^3/y or 15 m^3/h. While scenario 1 and 2 simulates no abstraction. Both scenarios are based on the gradient from figure 14, page 23, while scenario 1 is adjusted to the measured head in the limestone, scenario 2 uses the predicted cone of depression (figure 15, page 24) to estimate the head increase in the limestone. Scenario 1 uses a head increase of 1.5 m just below Haraldsborg waterworks and scenario 2 uses one of 2.6 m higher than the reference model.

Figure 35, page 54, A and B, shows two maps of the change in the maximum level of the phreatic surface, for scenario 1 (A) and scenario 2 (B). Both maps rarely show increases of more than 0.1 m in the maximum simulated groundwater level. The area surrounding Ægirsvej seems to be a bit more affected than the other areas, this is also very low in elevation, compared to the other places. Scenario 2 do have a higher number of points where the maximum groundwater level exceeds 0.1 m, but the overall pattern (or lack of thereof) is similar to scenario 1.

Figure 36, page 56, and 37, page 57, show the change in head, as a function of time. The figures start 30 m below surface and continues up to 12 m.b.s, 6 m.b.s and 3 m.b.s., respectively.

Figure 36 shows the difference in head between both scenarios and the reference

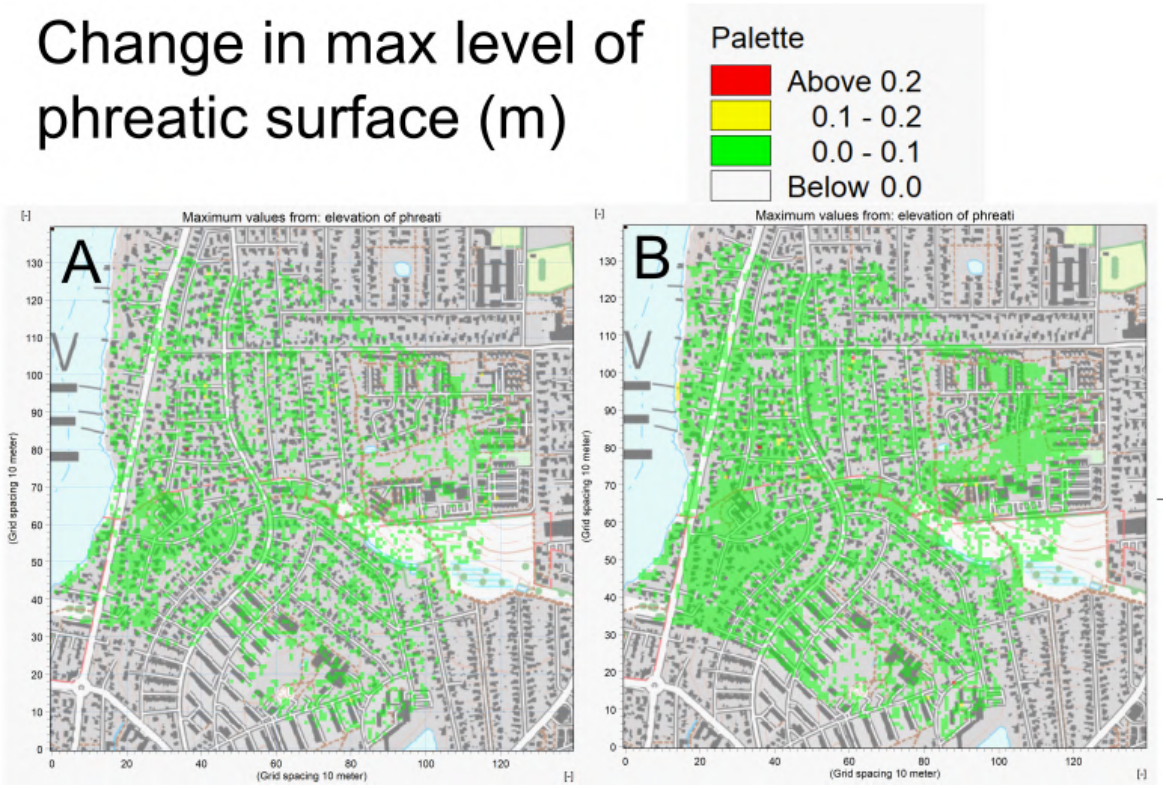

Figure 35: The change in maximum level of the phreatic surface (Scenario model - reference model). A is scenario 1 and B is Scenario 2.

model. At 30 m.b.s the full impact (90 % of the highest change in head) is seen in scenario 1 after 6 days, and scenario 2 after 8 days, at 12 m the full impact occurs after 24 days and 33 days, respectively, and at 6 m it occurs after 27 days and 35 days, respectively.

The inner boundary condition in the limestone is placed approximately 56 m below surface, where the pressure is increased by 1.6 m in scenario 1 and 2.6 m in scenario 2. At 30 m.b.s the change in head is decreased to 1.6 m and 0.65 m. At 12 m.b.s scenario 1 has a change in head of 0.8 m and scenario 2 of 0.6 m. At 6 m below surface the change in head is less than 0.2 m for both scenarios and in 3 m.b.s no clear change in head can be seen.

Timeseries of hydraulic head in 3 m, 6 m and 12 m are seen in figure 38, page 58. The y-axis is the hydraulic head (m) and the x-axis is the date. These figures include scenario 4, which is similar to scenario 1 except that the sand layer is changed to represent clay. The top graph shows 12 m.b.s, the middle from 6 m.b.s and the bottom from 3 m.b.s. At 12 m.b.s each scenario clearly differ from the reference model. As seen in figure 38 scenario 2 lies approximately 0.6 m higher than the reference model in the peaks. Scenario 1 is roughly 0.15 m higher than the reference model and scanario 4 is inbetween scenario 1 and 2. At 6 m.b.s the scenarios are harder to distinguise, yet it is possible to see that all scenarios reaches higher levels than the reference model. The highest difference between the scenarios and the reference model is now approximately 0.10 m. At 3 m.b.s the models are impossible to distinguish from the reference model, except for a few points that might differ with a few cm.

A last scenario (scenario 3) which increasing the specific storage from $10^{-4}m^{-1}$ to $10^{-3}m^{-1}$ was tested to examin the effect of the propagation of the pressure change in the limestone boundary. The result from scenario 3 is plotted with the result from scenario 1, as a change in head compared to the reference model, see figure 39, page 60. In 36 m.b.s scenario 3 drops 0.15 m in the first time step, probably because the matrix now has a higher specific storage, the pressure in the matrix increases causing the groundwater pressure to decrease. From 36 m.b.s to 12 m.b.s it is evident that increasing the specific storage delays the propagation, since the grey curve is under the blue. Table 4 shows the difference between scenario 1 and 3 before they reach 90 % of their maximum head change. At 36 m.b.s the effect of changing the abstraction rate peaks approximately after 5 days for both scenarios. At 24 m.b.s, scenario 3 is delayed 15 days and at 12 m.b.s the delay is 33 days. At 6 m no delay is observed. This might be due to adjustments in specific storage influencing how the model responds

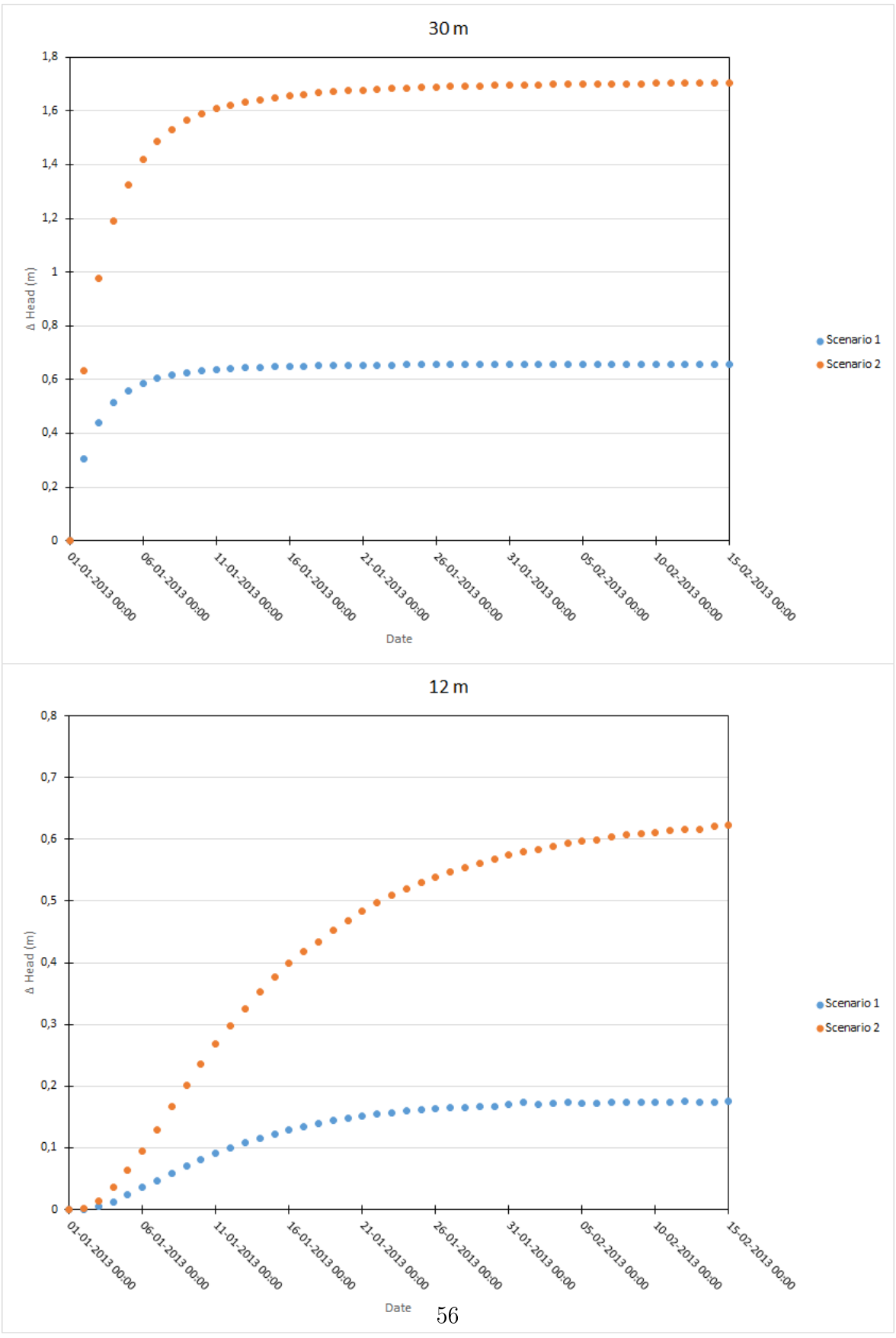

Figure 36: Pressure change in 30 m and 12 m below surface after applying stop of abstraction.

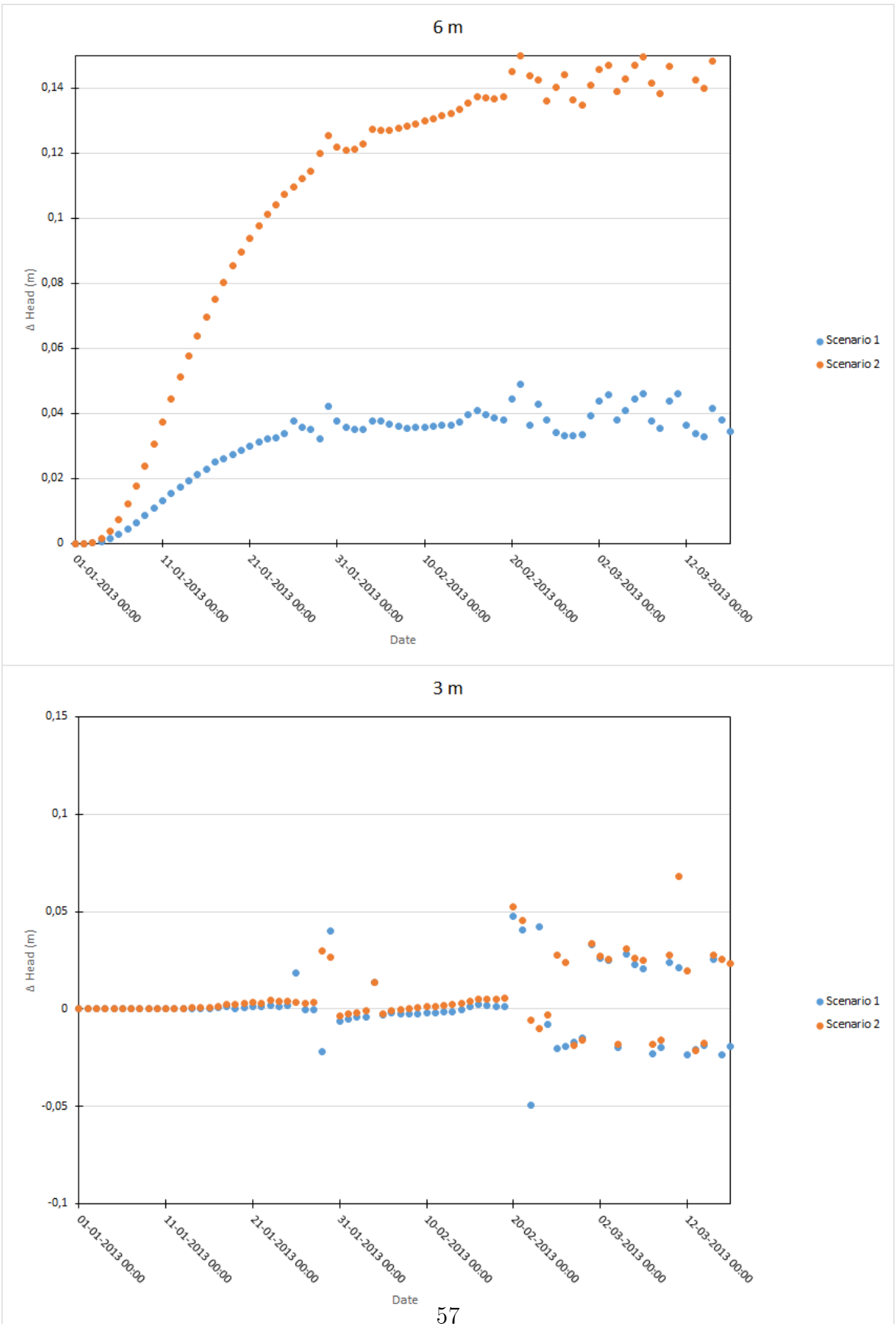

Figure 37: Pressure change in 12 m and 3 m below surface after applying stop of abstraction.

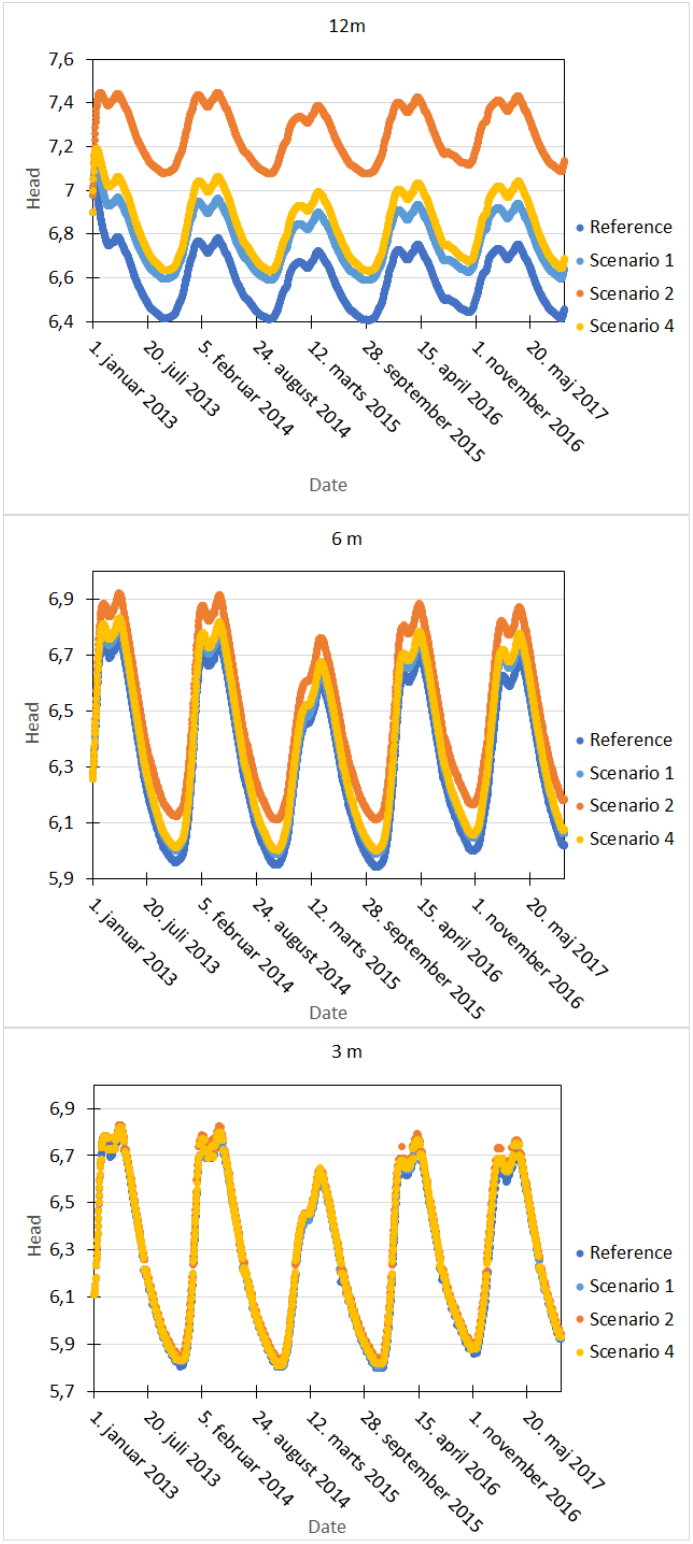

Figure 38: Timeseries of hydraulic head in 12, 6 and 3 m below surface on Valhalvej 55.

Days until abstraction change reaches depth	Scenario 1 (days)	Scenario 3 (days)	Delay (days)
36 m	5	5	0
24 m	9	24	15
12 m	21	54	33
6 m	27	N/A	N/A

Table 4: Comparison of the time it takes, after applying no pumping, between scenario 1 and 2.

to seasonal variability. For this reason the geometry of the curve is altered and out of sync.

5.8 Climate Scenarios

The climate scenarios are based on the Representative Concentration Pathway (RCP) 8.5 following the IPSL-CM5A climate model, which represents an increase to 8.5 W/m^2 of radiative forcing by the year 2100, and an increase in precipitation by 215 mm [Pasten-Zapata et al., 2019]. Two other scenarios are constructed to investigate the effects of climate change by 2050. The coefficients used for these scenarios were received by Pasten-Zapata (pers. comm.), and can be seen in table 5. To simulate the expected

Coefficents		Jan	Feb	Mar	Apr	Maj	Jun	Jul	Aug	Sep	Oct	Nov	Dec
2050	Precipitation	29	34	18	30	-1	22	22	7	-27	0	9	15
	Evaporation	25	24	17	13	10	8	9	13	14	15	18	18
2100	Precipitation	48	72	43	25	18	14	5	-6	2	17	38	35
	Evaporation	39	41	25	18	17	15	15	22	22	22	28	36

Table 5: Percent change in precipitation and evaporation for 2050 and 2100.

climate, a monthly coefficient is multiplied to the recharge and the evaporation. The sea level is also assumed to rise, therefore the boundary condition at Roskilde Fjord is changed from a fixed head of 0 m to a fixed head of 1 m. The climate scenarios are done stepwise to separate the change from sea level rise and climatic changes. The comparison is done with a model that do not simulate pumping from the limestone aquifer (scenario 1).

Table 6 shows the change in precipitation and evaporation after multiplying the coefficients to the data. By the year 2050, precipitation increases 8 % and evapotranspiration increases 12 % and by the year 2100 the change is 20 % and 19 % respectively.

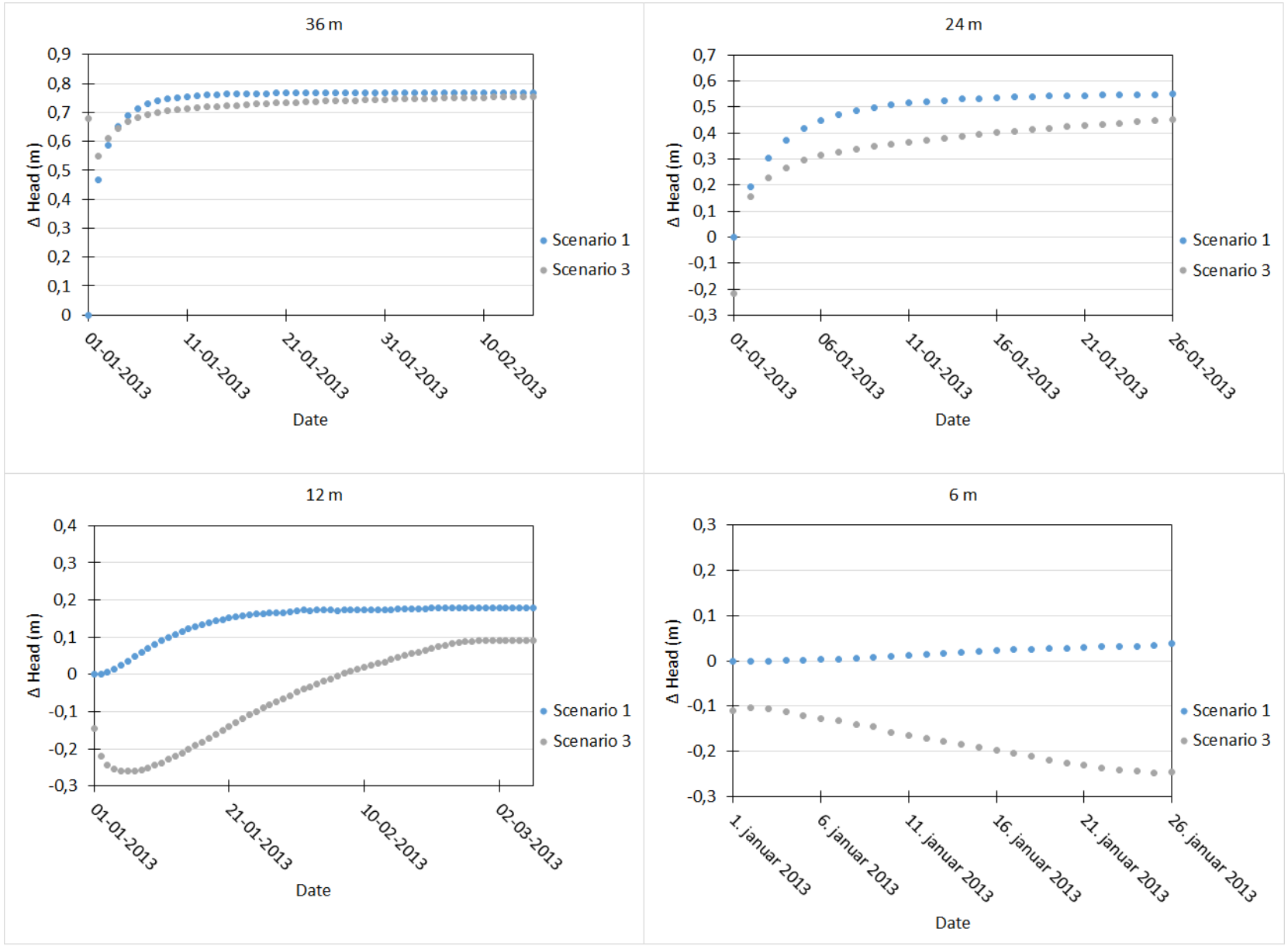

Figure 39: Scenario 1 and 3 minus the reference model is seen in different depths below surface. Scenario 3 is equal scenario 1 except the specific storage is increased with a factor of 10.

The calculation is based on climate data from 1/7-2016 to 20/10-2019.

Change in %	2050	2100
Precipitation	+8	+20
Evaporation	+12	+19

Table 6: Increase in climate data for the period 1/7-2016 to 20/10-2019.

In figure 40, page 63, three maps show the change in mean phreatic surface by the year 2100. Figure 40A shows the impact of increased sealevel, 40B of increased recharge and evaporation and 40C is the combination of both. The mean impact of sea level change is only seen adjacent to the fjord, where the phreatic surface lies between 0.05 m and 0.30 m higher than the reference model, 20 to 40 m inland. The climate impact in figure 40B shows areas inland where the mean phreatic surface is raised with 0.05 to 0.30 m. The areas with the highest change are also the areas of relatively high elevation, which might be caused since the phreatic surface in these areas lies below the drainage system. Another explanation is, that at high elevation the groundwater table lies deeper than at low elevation which means that the groundwater table can rise relatively more until it reaches a drain or a high conductivity layer. Figure 40C is similar to 40B, since 40A do not have much impact inland.

The mean value for the change in mean groundwater level is 0.08 m throughout the entire area (minus the fjord), by the year 2100. A map of the change in mean groundwater level, in the area surounding Haraldsborg, is found in the appendix, figure 59, page 93.

Figure 41, page 64, is set up the same way as figure 40, except this shows the maximum change in phreatic surface by the year 2100, and the legend is modified. At 40A it is observed that the maximum elevation of the phreatic surface is barely changed by changing the sea level. A much larger impact is seen when applying the climatic projection to the model. The climate simulation shows that the area around Haraldsborg waterworks will experience an increase in maximum groundwater level of more 0.6 m. The biggest change is found in the northeastern part of the area, where the change in some cells exceeds 1.5 m. In the area adjacent to Haraldsborg waterworks the change in maximum groundwater exceeds 1.2 m in a few cells. a map of the area is in the appendix, figure 60, page 94.

To further test the low impact of raising the sea level in the model, another test was made, which increasing the pressure in the limestone aquifer with 1 m. This change had no or little impact on the resulting map.

Figure 42, page 65, shows the change in maximum recorded level of phreatic surface of the 2050 climate model and the reference model. The figure shows that in some areas adjacent to the observation wells, the model with the projected climate data suggest increases in groundwater levels of more than 0.2 m and in a few places more than 0.4 m. A map of the change in mean levels is added in the appendix in figure 61, page 95.

5.9 Effect of Urbanization

To investigate the effect of urbanization, a model is run without the drainage system and then compared to the reference model. In figure 43, page 66, the resulting map is seen with the change in mean values. This shows how much higher the groundwater table would be without the drainage system. The biggest change is marked with red colors (over 2 m) and changes of less than 0.1 m are not drawn. Most of the affected area is visualized with green or light green colors, which represents a change in mean of between 0.1 m to 1.0 m. The yellow, orange and reddish areas show where changes of more than 1 m occurs. These areas corresponds, as expected, with the location of the MIKE11 build drainage system.

The effect of changing paved areas to grass was also simulated and is seen on figure 44, page 67. The values on this figure are negative, which indicate that the urban structures actually raised the groundwater level, which is the opposite of the expected. This result is reviewed in the discussion section.

During the setup of the model, tests, with and without basements were done in adjacent cells to see if these urban structures somehow interfered with the flow. The basements were constructed as lenses with a very low hydraulic conductivity. At this point no effect were observed in the simulations and it was decided not to add the basements in the model. This was tested again with the calibrated model, to see if the result would be similar. In the calibrated model, tests were made on Haraldsborgvej and Ægirsvej, corresponding to high and low elevation, on the upstream and downstream side of the houses and at different depths 1.5 and 4.2 m.b.s. After the calibration no effects of basements was seen. Graphs from this test are added in the appendix from figure 64 - 63, page 97 to 98.

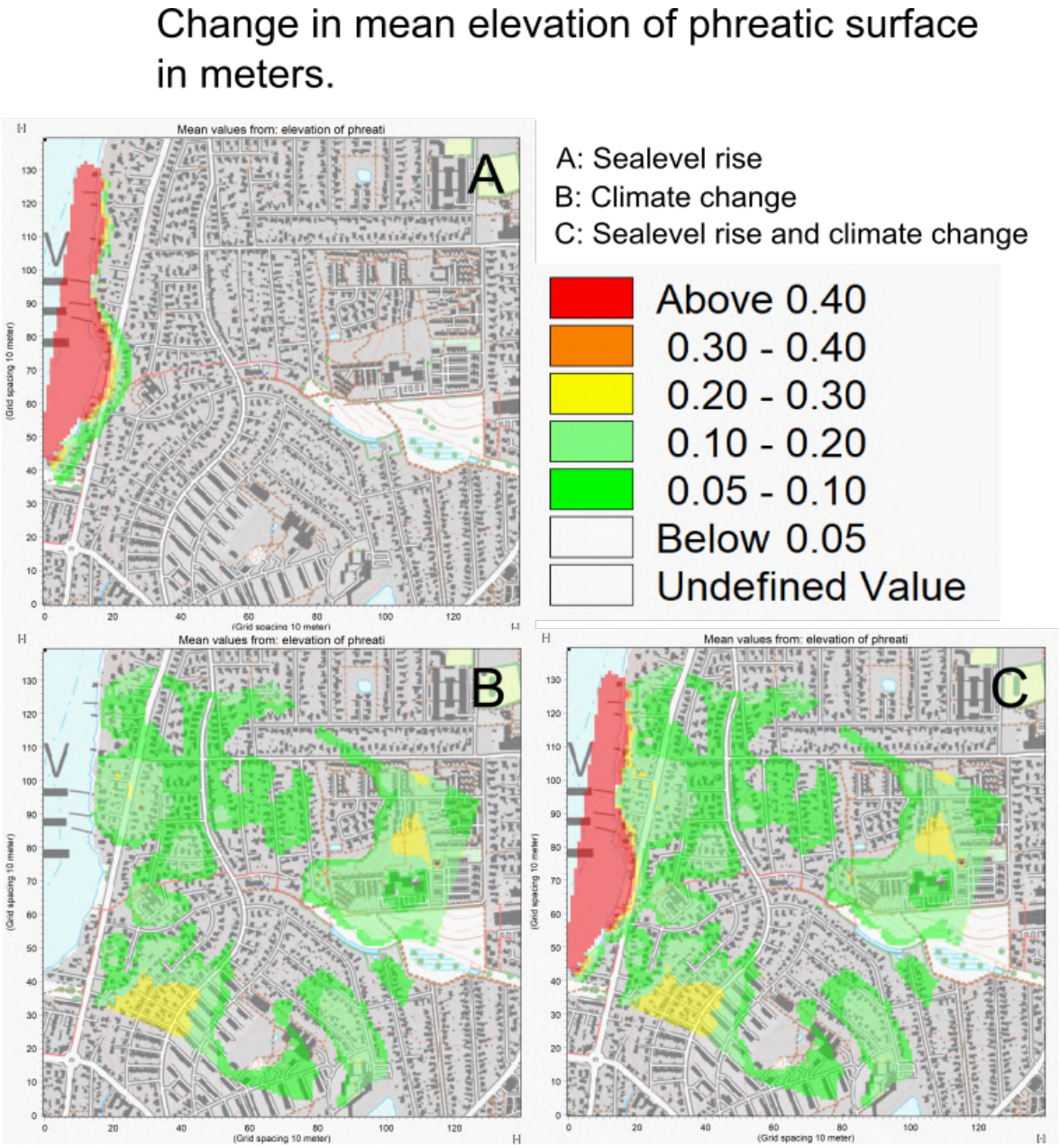

Figure 40: Mean impact of sea level rise by (A), climate change (B) and the combination of both (C) in the year 2100.

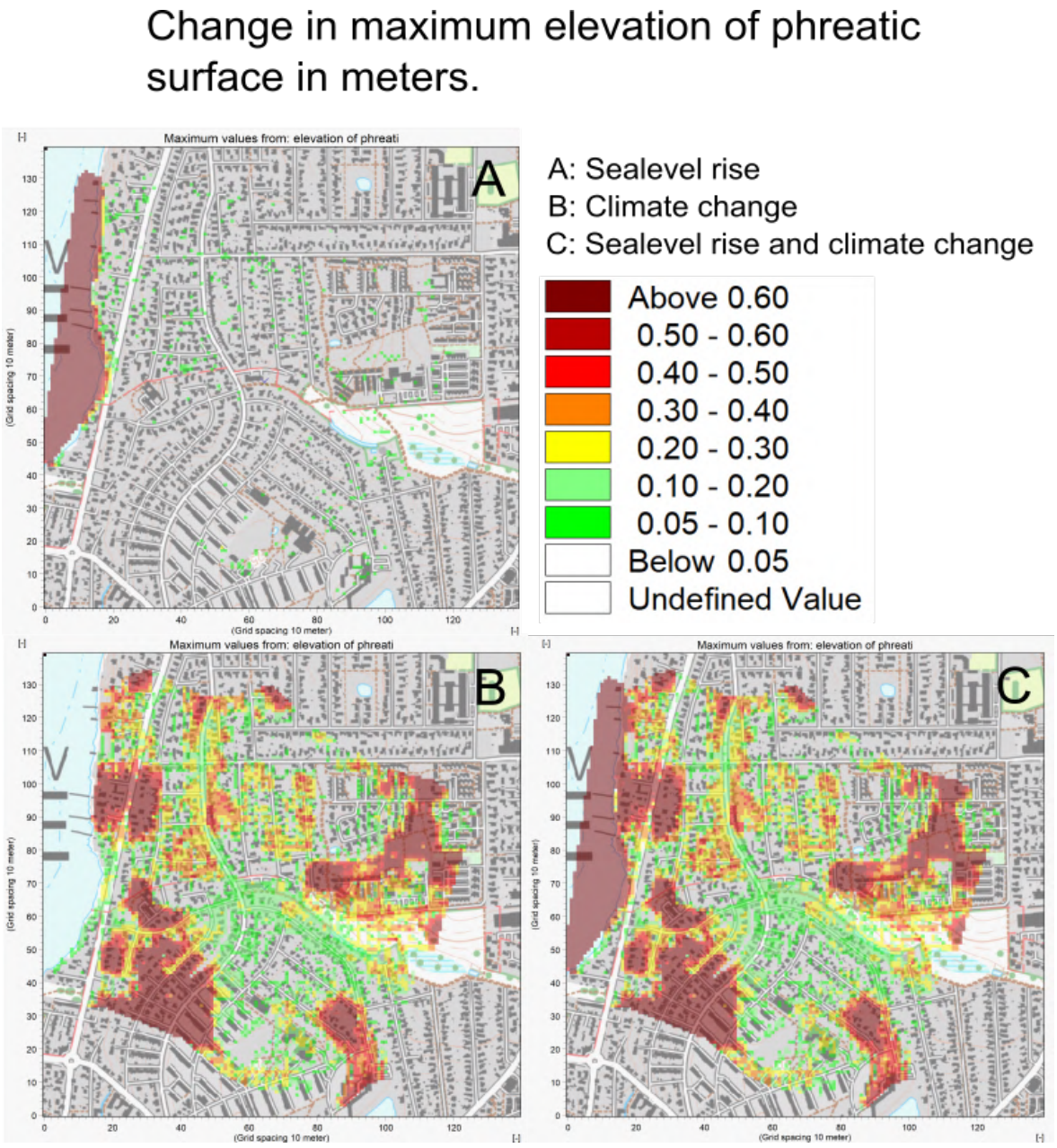

Figure 41: Max impact of sea level rise (A), climate change (B) and the combination of both (C) in the year 2100.

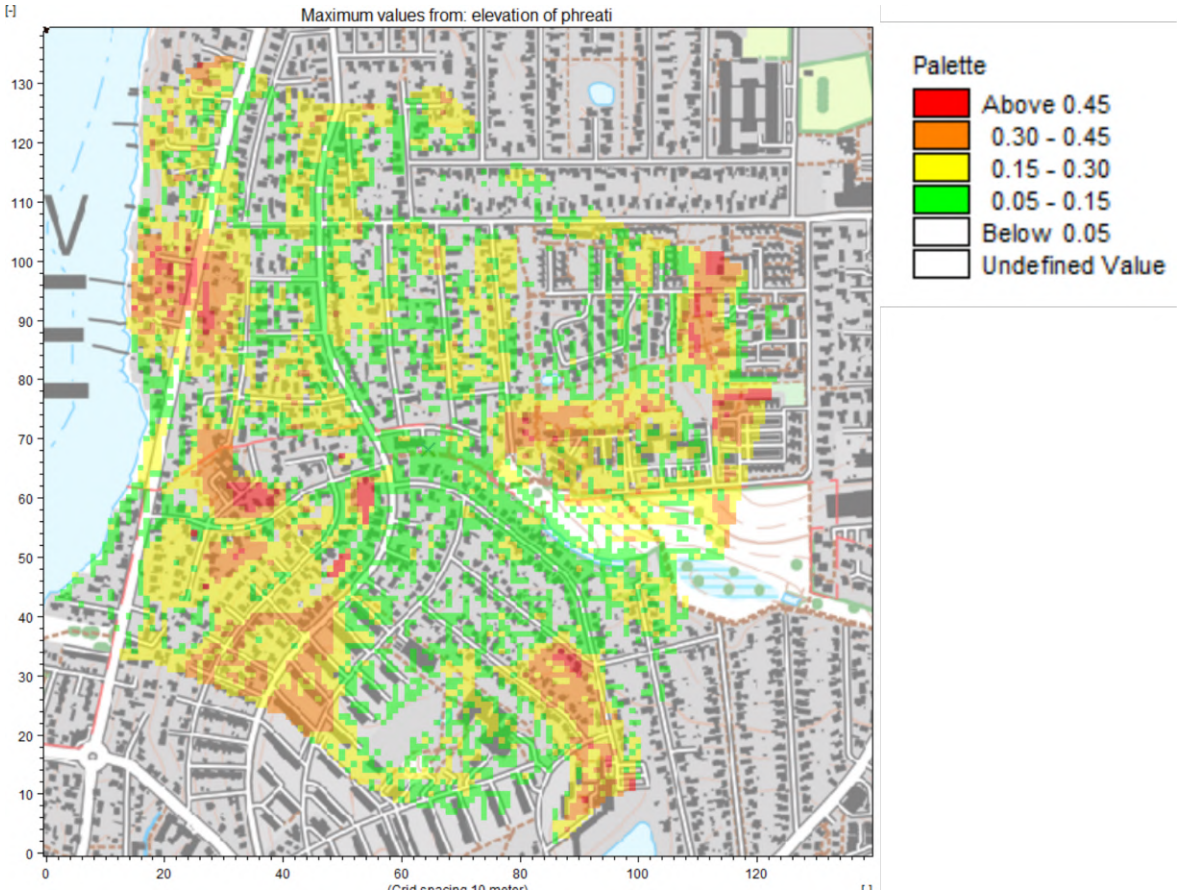

Figure 42: Change in maximum recorded level of the phreatic surface projected to the year 2050, compared to the period from 2013-2019

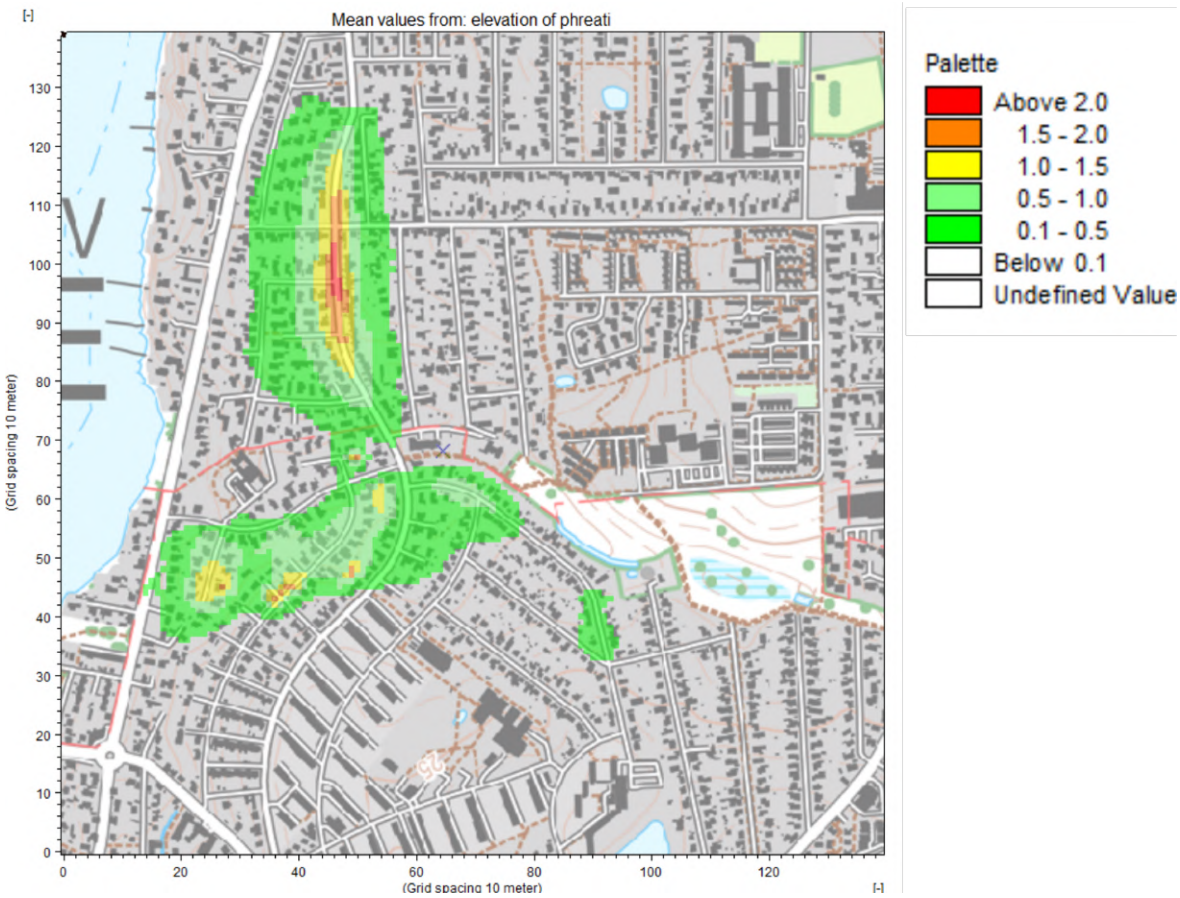

Figure 43: Difference in mean elevation of phreatic surface, with and without the drainage system.

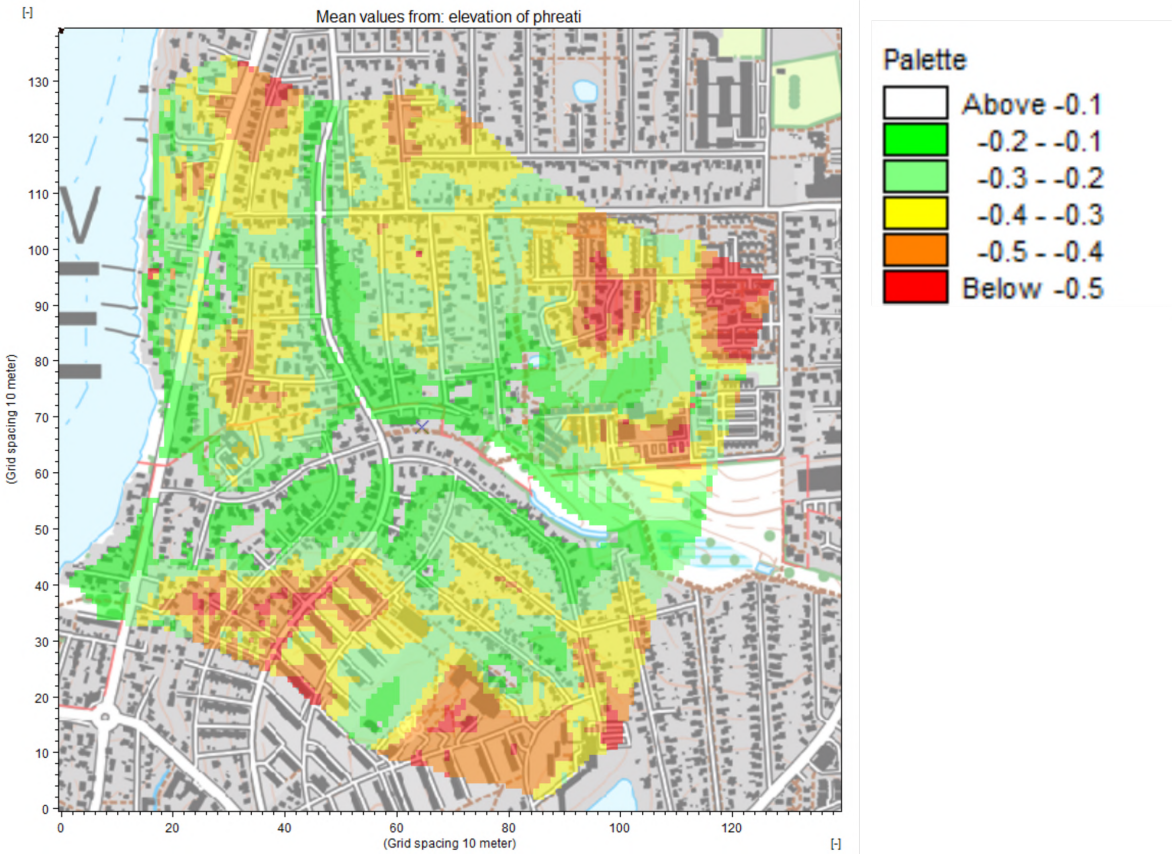

Figure 44: Difference in mean groundwater level after removing urban structures. Note that the negative values are unexpected.

6 Discussion

6.1 Fieldwork

Different methods were used in attempts to resolve an expected sand layer which is seen in multiple wells in the JUPITER database. The sand layer was interesting for a few reasons; firstly, it would have been interesting to monitor the groundwater table, secondly, the assumed sand layer was of interest to the resident in the affected area. The reason was that pumping from the sand layer might counter the assumed influence from closing Haraldsborg. Three methods were used to resolve the sand, but none worked for the purpose. The drilled wells never reached depths deep enough to find the sand. A first assumption was that the sand might fall of the drilling equipment, hence no sand came to the surface. This reasoning was questioned after producing the gamma ray log since this revealed a primarily homogeneous lithology. The ERT profile contains values that fit well with moraine clay in most part of the 2D profile. Yet the data is suspicious due to the shape of the resistivity zones. Using ERT in an urban area is perhaps precariously, since electrical wires in the ground might disturb the signal from the equipment.

6.2 Adding Complexity to The Reference Model

The model setup that differs most from the reference model is the one using the geological interpretated layers. Changing a model consisting of sand to a model primarily of clay is going to change the flow. Adding the geological model decreased the infiltrating water from the boundary and increased the overland drain to river. This is due to the fact that the groundwater table is higher when much is clay and this prohibits water inflow from the boundary and increases the water available for drainage, see figure 33, page 52) The opposite is seen in the model simulating UZ flow using Richards eq. This model effectively removes more water by ET, hence less water is available to infiltrate. This lowers the groundwater table and the result is seen with sligthy lower drain to river and a higher amount of water from the boundary.

The landuse model appears to be close to the reference model in all aspects, while the models using Richards eq., geology- and drainage show much larger differences in various areas of the model. Other differences exist, that are not shown on the waterbalance. E.g. using Richards equation demands a more sophisticated interaction between UZ and SZ, which means that the UZ and SZ timesteps must be similar. The

geological model has more layers than the other models which increases computational time.

6.3 Closing Haraldsborg Waterworks

It is not possible to observe the change in abstraction rate in the near-surface groundwater, using the timeseries from the installed divers. This might be because it does not affect the near-surface groundwater, it might also be because the potential increase is obscured by fluctuations caused by precipitation and barometer effect. The groundwater model also do not show any significant effect on the near-surface groundwater, yet it shows some increase through the soil columns.

The time it takes for the head increase in the limestone to propagate through the entire soil column is dependent on the specific storage, as seen in figure 39, page 60. At 12 m.b.s an increased specific storage of a factor of 10 results in a delay of 1 month, see table 4, page 59. The actual time for scenario 3 (increased specific yield) to reach 12 m.b.s was 54 days in the model. A rough estimate of the time until it reaches 3 m.b.s could be somewhere between 70 - 100 days. Comparing this duration with the duration of different pumping situations, maximum capacity for 4 months and no pumping for 3 months, it is clear that these times are not too far from each other. If the true specific storage is higher than the value used in the model this could explain why the propagation was not seen in the diver data. Another possible explanation is, that because the change on the near-surface groundwater is minor the change in hydraulic head is not possible to distinguish because of the fluctuations caused by precipitation. The lack of affect in the nearsurface water is not only local, around the drainage system, but is seen throughout the model domain. It seems that the parameters in the top fractured clay plays a role in transporting the groundwater out of the model.

Answering what happens to the near-surface groundwater when Haraldsborg waterworks closes, according to the model simulations, is that the affect is minor and the change in maximum increase is in the range of a few centimetres. If this result can be trusted is dependent on if the model can be trusted. There are a few core issues with how trustworthy the model is.

1. The calibrated values for the parameters of the lithologies between the chalk and surface are highly uncertain.

2. The geological interpretation and the boundary conditions are highly uncertain.

3. The average RMSE is of 0.45 m.

If the parameter values and the geological model is trusted then so is the model predictions. In this model the uncertainty between the chalk and the surface is highly uncertain, so predicting the effect on the near-surface groundwater, of a change in the chalk, 50 meters below, is highly uncertain.

The fact that the model uses no flow boundaries actually helps the change in head to propagate upwards with no loss horizontally across the boundaries. With other boundary conditions the change might have been even smaller. An RMSE of 0.45 m is relatively small, but for houseowners an uncertainty of 0.45 m might be a high number to relate to. The fact that model simulations and the pumping experiment both do not show noteworthy affect on the groundwater table during a close of Haraldsborg waterworks adds some thrust to this result.

6.3.1 Drainage

During the model setup and calibration it was apparent that water often occured at terrain. This is something that rarely happens in the natural setting in Roskilde. At the beginning of this project it was assumed that the wastewater/drainage system was responsible for keeping the groundwater away from the surface, but a sewer TV-inspection showed that no drainage occured at Ægirsvej. The TV-inspection was done in the night-time, so no or little input from showers, sinks, washing machines etc. would disturb the result. The pipe at Ægirsvej was dry, exept for the house connections where some water entered. It is not possible to conclude from this single TV-inspection that all the pipes are water-proof, especially since most literature agrees that old pipes drain. But it opens for the idea that something else might also play a role in keeping groundwater well below surface. At a meeting in Vandgruppen, it was brought up that the district heating had pipes laying in gravel castings. Gravel castings in moraine clay might serve as a highway for water and this could transport water away from the area, keeping the groundwater table low. A map of the district heating pipes was obtained from FORS A/S, which can be seen in figure 66, page 100, in appendix. The district heating system covers the area with observation wells quite well.

From the divers installed at the waterworks premises it is also clear that the effect of turning the pumps off and on in the limestone aquifer do not visualize in the head measurements. There are multiple reasons why this might be; first, as just discussed, something might effectively drain whatever water results from turning off the waterworks. Secondly, the potential increase or decrease may be obscured by fluctuations

caused by recharge and barometer effects. Another explanation could be that the sand layer in the model does not represent its actual dimensions. If a thick regional sand layer exists between the limestone aquifer and the terrain, it might transport the additional groundwater away from the model area, in which case it never reaches the surface.

The model setup uses an inner boundary condition to simulate the changing abstraction rate, from the limestone aquifer, using maps of the simulated potential gradient and the cone of depression. The abstraction rate from FORS A/S' pumps are known and this could have been used to construct the model with abstraction instead of an inner boundary condition. The expected result from such a change is unknown.

6.4 Climate

The climate projections used for the simulated scenarios in this thesis, are based on "worst case" predictions. Of the 16 RCP 8.5 predictions the ISPL is the one that anticipates the highest increase in precipitation [Pasten-Zapata et al., 2019]. For this reason, the climate scenarios will tend toward a more extreme situation than an ensemble mean would produce. The ensemble mean for change in precipitation is 133 mm, while the used projection is 215 mm. According to figure 41, page 64 the maximum values will be higher than 0.6 m higher compared to the present measured values, which is significant. The prediction for 2050 is also based on the worst case scenario. The change in mean level of phreatic surface is available in appendix, which shows that the overall groundwater level is falling, see figure 61, page 95. This is the opposite of expectations and the explanation for this is probably found in the way the climate data is used, since the true precipitation data is only used from 1/6-2016 to 20/10-2019 and everything outside this period is looped from this sequence. 2018 points out as an anomalously dry year with only 561 mm rain recorded and this drags the mean value down since evaporation is actually increased comparatively more than precipitation.

6.5 Uncertainty, Model Improvements and Errors

In this section an overview of the sources of uncertainty recognized in this modelling study is presented. Table 7, page 72, summarizes which kinds of uncertainty are present. The table is created with inspiration from Refsgaard et al. [2007] and Sonnenborg and Henriksen [2005]. Uncertainty can occur in the data, in the model setup and in the simulated scenarios.

Source		Uncertainty	Weight	Effect
Data	Head observations	Medium	Medium	Medium
	Climate data	Medium	Medium	Medium
	Geology	High	High	High
Model	Conceptual model	High	High	High
	Parameters	Medium	High	Medium
	Boundary Conditions	High	Medium	Medium
	Code	Low	Low	Low
Scenarios	Abstraction stop	Medium	Medium	Medium
	Climate	High	Medium	Medium

Table 7: Matrix of uncertainty

The head observations made by residents in the model area are measured in many ways, with different methods. After the collection of data some measurements were deleted by the author, either due to seemingly measuring a dry well or measurements that were well above or below reasonable values. For these reasons, the head observations are more uncertain than one might normally expect.

The climate data covers the precipitation and the evaporation. The precipitation is measured by one of DMI's measuring station, that lies inside the model domain, yet it is measuring only in one point, and some spatial variability exist. The evaporation is believed to be a larger source of uncertainty, since the data provided by NOVANA was not up-to-date when needed, therefore some data is repeated from previous years.

Geological data are primarily obtained from the Jupiter database but also supplemented from a few other sources. The amount of data is sparse, especially for the lower part of the model, and much of the data and descriptions from Jupiter are old. E.g. the wells to the limestone were established in 1957. These wells are described using only a few samples to cover more then 50 m of geology. DGU 206.468 is e.g. 66 m deep and only 10 samples are covering this range. Not only is the data limited horizontally but also vertically. It is also worth noting that during the field work an expected sand layer at 10 m.b.s was never detected, yet it is described as a 3 m thick layer in the Jupiter database. With this in mind, it is safe to say that the geology is a key area of uncertainty.

The conceptualization of the system is also an area of high uncertainty. As an example, the data from Richards Equation is extracted from a 500x500 m grid while the actual model is 10x10 m.

Some parameters are calibrated and some are left as originally input in the model. There is some uncertainty with the calibrated parameter values; The true nature is overall heterogenous and therefore setting a fixed value is carrying some uncertainty, during the calibration it was also observed that some parameters regarding the hydraulic conductivity could lie in both ends of the defined band.

The model domain is very small, measuring only ca. 1300x1300 m and can hardly be closed by watersheds. The northern-, eastern- and southern boundary conditions are no flow boundaries in the model but this a highly speculative and probably not true in the actual system. Water will flow across these boundaries and will likely have some effect on the system. Using a hydraulic gradient as a boundary condition was tested in the pre-setup of the model and no effect of the boundary condition visualized but this is still a significant simplification. In the literature the greensand is recognized as a thick, 30 m, regional sandlayer and if this exists between the limstone aquifer and the terrain it might be capable of removing additional water coming from below, before reaching the surface.

Uncertainty regarding the code might exist but probably will have a low impact. If there are any noteworthy effect, these are unknown to the author.

Scenarios of the future are inherently uncertain. The constructed climate scenarios in this thesis contains uncertainty of the hydrological model but also the uncertainty regarding the actual climate projections. Furthermore, the climate scenario is based on the present state with no abstraction. Changes in the urban structures, like paved areas, improvements of drainage systems or new pipes below the surface might all effect the future state of the model. A resident was quoted saying that around his house no one had any issues with near-surface groundwater, until a drainage pipe was restored, at which point the groundwater level rose.

6.5.1 Model improvements

Additional data would naturally improve the model. This data could be head observations, so e.g. the validation could be conducted on a longer period.

Slugtests throughout some of the already established wells would have been ideal to compare the K-value in the upper layer in the model with observations.

A thorough examination of the hydrological model by an expert might have eliminated some of the "unknown-unknowns" or in other words, mistakes that the author do not realize are mistakes, and perhaps to catch other errors and typos in the data etc.

6.5.2 Known Errors

During model simulations with and without roads and rooftops, a remarkable result occured when, adding these urban structures made the overall groundwater level increase. The expected result from urbanization is a decrease in groundwater level due to increased surface runoff. Comparing the water balance for the two models, it was found that the ET from the UZ was about 80 mm for both but the model without urbanization had an overall increase in ET of 72 mm (7% more than with urbanization). The urban structures are only described with a decrease in rootdepth and LAI, not by any overland flow components and this is a mistake. This means that both models effectively removes OL water via the ponded drainage function but the model without urban structures evaporates more. Figure 45, page 75, is created by setting up a new model that includes a description of the paved area. The paved area is roughly 30 %. From this figure a rather large overall effect is seen. In the upper right corner the effect of paved areas turns out to be an increase of more than 0.9 m on the mean phreatic surface. In the area close to Haraldsborg waterworks the effect is smaller, around 0.2 - 0.9 m. The effect is smallest at and around the drainage system. These numbers reflect a model where there is no infiltration from the water precipitated on the paved areas. This is an exaggeration since some water will infiltrate, hence the actual difference is somewhat lower. Besides, the model is calibrated without the paved area, which might partly compensate for this lack e.g. by increasing the hydraulic conductivity in the upper geological layers and thus lower the groundwater table.

The sensitivity analysis was performed using a model quite different from the final model. The subsequent changes include a new upper layer of 4 m, which is assumed to be fractured clay and a fundamental change in the MIKE11 setup. The river network in MIKE11 was first build to mimic the actual drainage system, with pipes as small as 0.3 m in diameter and with a Manning number of just 1. The low Manning number was selected to simulate gravel castings where groundwater can easily drain to but hardly flow in. This means that a lot of the water drains into small pipes where flow is constrained. This setup lead to many errors due to water level in the pipes exceeding allowable values. Changing the diameter of the pipes to above 3 m and raising Manning's number to 10 removed all of these errors. In hindsight it might have been a better solution to use the drainage component in MIKESHE, instead of the more complicated MIKE11.

The Van Genuchten parameter was not included in the sensitivty analysis, yet it

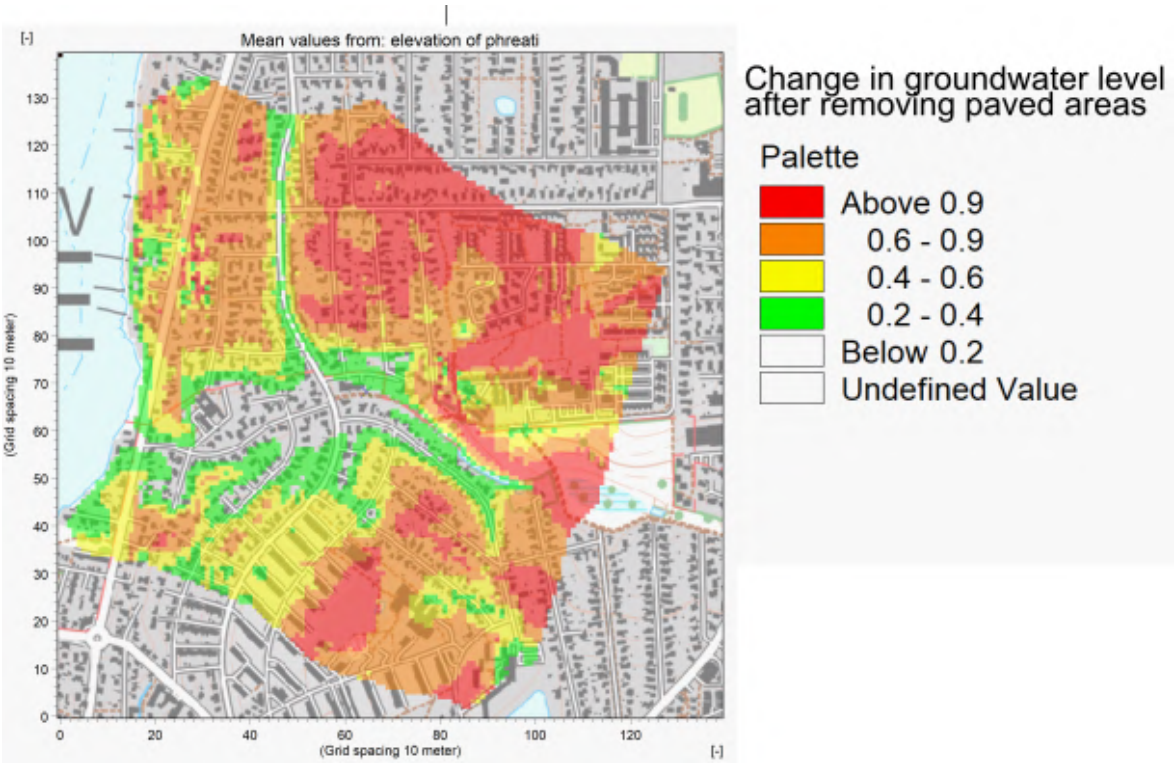

Figure 45: Effect of Paved Areas

was found to have quite an effect on the dynamics of the groundwater table.

Because of these changes in the model, some parameters are not included in the sensitivity analysis and the sensitivity of others might have been altered.

7 Conclussion

In this study, hydrological modelling was utilized as a tool to make predictions regarding the effects of closing Haraldsborg waterworks in Roskilde. Furthermore, the model was configured to incorporate climate change predictions, the RCP 8.5, to estimate the effect hereof. A handful of fieldwork methods were carried out to improve the geological knowledge and to monitor effects of an abstraction change at the waterworks.

A network of divers were installed at the waterworks premises, monitoring the hydraulic head during increased and decreased pumping rate. No clear outcome was observed. It is inconclusive whether the lack of response is because the effect is minor, hence being hidden because of precipitation events or if the propagation of the pressure change is slower than the duration with a changed abstraction rate.

According to the hydrological model, the effect of an abstraction stop is between 0 to 0.1 m. This is true for both abstraction stop scenarios. For concerned houseowners, nothing indicates associated problems regarding a potential closing of Haraldsborg waterworks, though this conclusion is preliminary and uncertainies remain.

Future climate impacts are vitiated by uncertainty from the hydrological model but also from the climate projections themselves. This thesis investigated the worst-case climate scenarios and found that the maximum recorded phreatic surface, by year 2050, increases from 0 to approximately more than 0.45 m in few areas. The area adjacent to Haraldsborg waterworks can, according to the model, expect a significant rise during times of heavy rainfall. By year 2100 this increase reaches more than 0.6 m, while the mean groundwater level rises with 0 to 0.3 m. These numbers are significant and since multiple head observations are well below 0.45 m.b.s, probably will cause flooding. Since this is a worst-case scenario, the actual impact of projected climate change will probably be somewhat lower.

The effects of urbanization are also investigated using the hydrological model, this time removing the drainage system and converting roads and rooftops into gardens. The drainage system lowers the groundwater table locally, mainly with values between 0.1 to 1.0 m, but at extreme locations by more than 2 m. During this process, an incorrect description of the model was discovered regarding the paved areas. This effect was tested, and it was concluded that the impervious surfaces causes a significant lowering of the groundwater table.

References

Peter Allerup, Henning Madsen, and Flemming Vejen. Standardværdier (1961-90) af nedbørkorrektioner. *DMI*, 1998.

Karsten Arnbjerg-Nielsen and HS Fleischer. Feasible adaptation strategies for increased risk of flooding in cities due to climate change. *Water Science and Technology*, 60 (2):273–281, 2009.

Guillaume Attard, Thierry Winiarski, Yvan Rossier, and Laurent Eisenlohr. Impact of underground structures on the flow of urban groundwater. *Hydrogeology journal*, 24 (1):5–19, 2016.

Thor Danielsen. Integrated hydrological modelling of an urban catchment - a case study for the city of kolding. *Master Thesis of University of Copenhagen*, 2018.

DHI. Mikeshe user manual volume 1. *MIKESHE*, 2017a.

DHI. Mikeshe user manual volume 2. *MIKESHE*, 2017b.

DHI. Autocal. *Danish Hydrology Institution*, 2017c.

DHI. A modelling system for rivers and channels user guide. *MIKESHE*, 2017d.

Claus Ditlefsen, Jette Sørensen, Tom Martlev Pallesen, Dorthe Pedersen, Ole Bjørslev Nielsen, Christian Christiansen, Birgitte Hansen, and Peter Graversen. Jordprøver fra grundvandsboringer. *GEUS*, 2008.

Charles R Fitts. *Groundwater science*. Elsevier, 2002.

Tim D Fletcher, Herve Andrieu, and Perrine Hamel. Understanding, management and modelling of urban hydrology and its consequences for receiving waters: A state of the art. *Advances in water resources*, 51:261–279, 2013.

Claus Heilman-Clausen. Palæogene aflejringer over danskekalken. *GEUS*, 1995.

Hans Jørgen Henriksen, Lars Troldborg, Per Nyegaard, Torben Obel Sonnenborg, Jens Christian Refsgaard, and Bjarne Madsen. Methodology for construction, calibration and validation of a national hydrological model for denmark. *Journal of Hydrology*, 280(1-4):52–71, 2003.

Philip Kearey, Michael Brooks, and Ian Hill. *An introduction to geophysical exploration*. John Wiley & Sons, 2013.

David N Lerner. Groundwater recharge in urban areas. *Atmospheric Environment. Part B. Urban Atmosphere*, 24(1):29–33, 1990.

Ole Mark, Sutat Weesakul, Chusit Apirumanekul, Surajate Boonya Aroonnet, and Slobodan Djordjević. Potential and limitations of 1d modelling of urban flooding. *Journal of hydrology*, 299(3-4):284–299, 2004.

Scott J McGrane. Impacts of urbanisation on hydrological and water quality dynamics, and urban water management: a review. *Hydrological Sciences Journal*, 61(13):2295–2311, 2016.

V Grace Mitchell, Russell G Mein, and Thomas A McMahon. Modelling the urban water cycle. *Environmental modelling & software*, 16(7):615–629, 2001.

Ernesto Pasten-Zapata, Torben O Sonnenborg, and Jens Christian Refsgaard. Climate change: Sources of uncertainty in precipitation and temperature projections for denmark. *GEOLOGICAL SURVEY OF DENMARK AND GREENLAND BULLETIN*, 43, 2019.

Rambøll. Nedlukning af haraldsborg vandværk, roskilde. 2017.

D Ramier, E Berthier, and H Andrieu. The hydrological behaviour of urban streets: long-term observations and modelling of runoff losses and rainfall–runoff transformation. *Hydrological Processes*, 25(14):2161–2178, 2011.

Jens Christian Refsgaard. Parameterisation, calibration and validation of distributed hydrological models. *Journal of hydrology*, 198(1-4):69–97, 1997.

Jens Christian Refsgaard, Jeroen P van der Sluijs, Anker Lajer Højberg, and Peter A Vanrolleghem. Uncertainty in the environmental modelling process–a framework and guidance. *Environmental modelling & software*, 22(11):1543–1556, 2007.

Jens Christian Refsgaard, Karsten Arnbjerg-Nielsen, Martin Drews, Kirsten Halsnæs, Erik Jeppesen, Henrik Madsen, Anil Markandya, Jørgen E Olesen, John R Porter, and Jens H Christensen. The role of uncertainty in climate change adaptation strategies—a danish water management example. *Mitigation and Adaptation Strategies for Global Change*, 18(3):337–359, 2013.

Rider Rider, Malcolm & Kennedy. The geological interpretation of well logs, 2011.

Dan Rosbjerg and Torben Obel Sonnenborg. Grundvandsstrømninger. *Unknown*, 1999.

Elga Salvadore, Jan Bronders, and Okke Batelaan. Hydrological modelling of urbanized catchments: A review and future directions. *Journal of hydrology*, 529:62–81, 2015.

Mario Schirmer, Sebastian Leschik, and Andreas Musolff. Current research in urban hydrogeology–a review. *Advances in Water Resources*, 51:280–291, 2013.

TO Sonnenborg and HJ Henriksen. Håndbog i grundvandsmodellering. *GEUS, København*, 2005.

Torben O. Sonnenborg and Kidmose Jacob. Klimabetingede grundvandsstigninger i urbant område - pilotområde odense. *Region syddanmark*, 2016.

Torben O Sonnenborg, Britt SB Christensen, Per Nyegaard, Hans Jørgen Henriksen, and Jens Christian Refsgaard. Transient modeling of regional groundwater flow using parameter estimates from steady-state automatic calibration. *Journal of Hydrology*, 273(1-4):188–204, 2003.

Richard G Taylor, Bridget Scanlon, Petra Döll, Matt Rodell, Rens Van Beek, Yoshihide Wada, Laurent Longuevergne, Marc Leblanc, James S Famiglietti, Mike Edmunds, et al. Ground water and climate change. *Nature climate change*, 3(4):322, 2013.

Jesper Waagepetersen, Ruth Grant, Christen Duus Børgesen, and Torben Moth Iversen. Midtvejsevaluering af vandmiljøplan iii. *GEUS*, 2008.

8 Appendix

8.1 Fieldwork

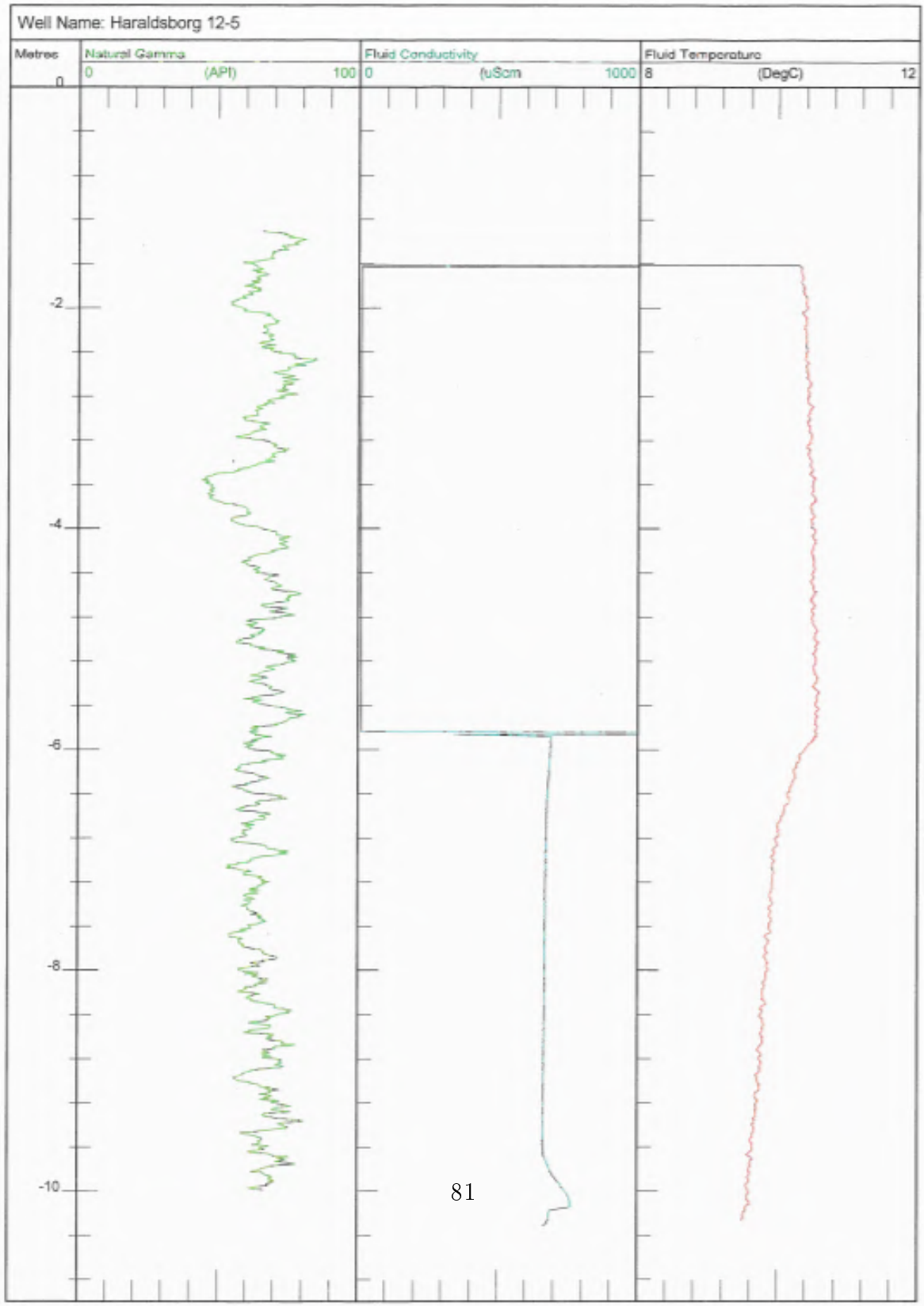

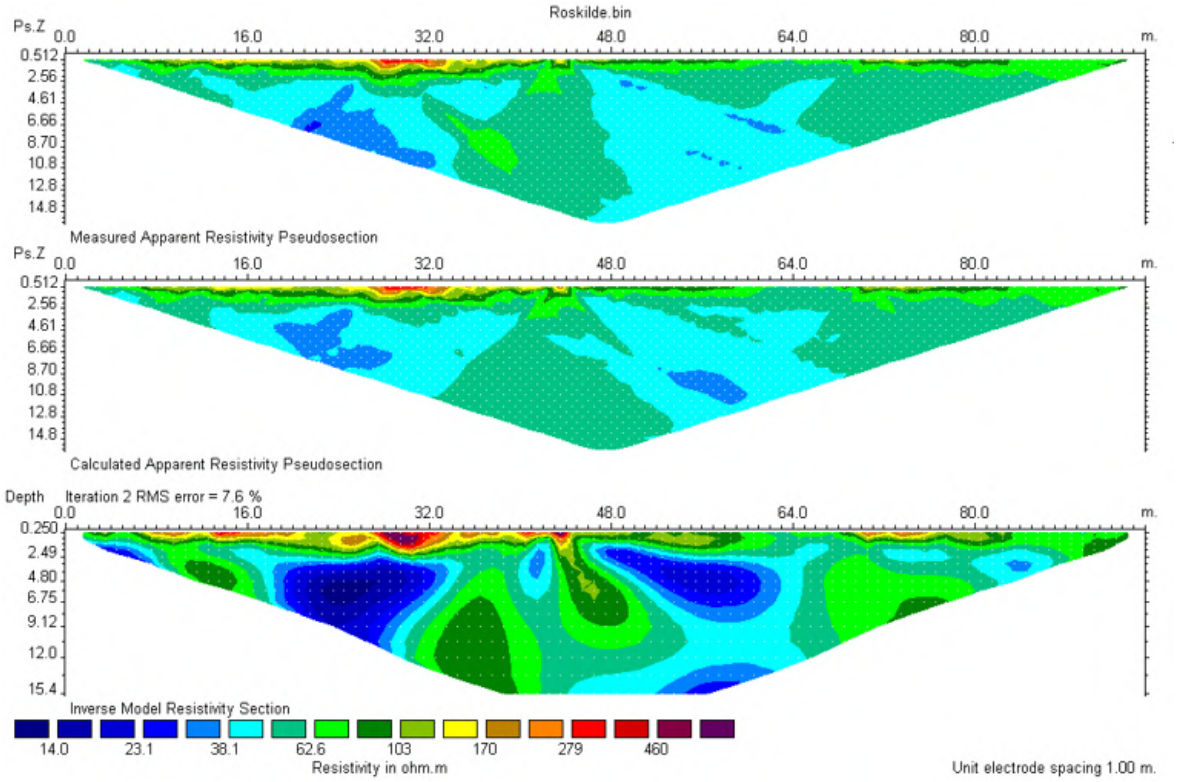

Figure 47: Second iteration of the ERT profile gives and RMS error of 7.6 %. The profile looks as disturbed.

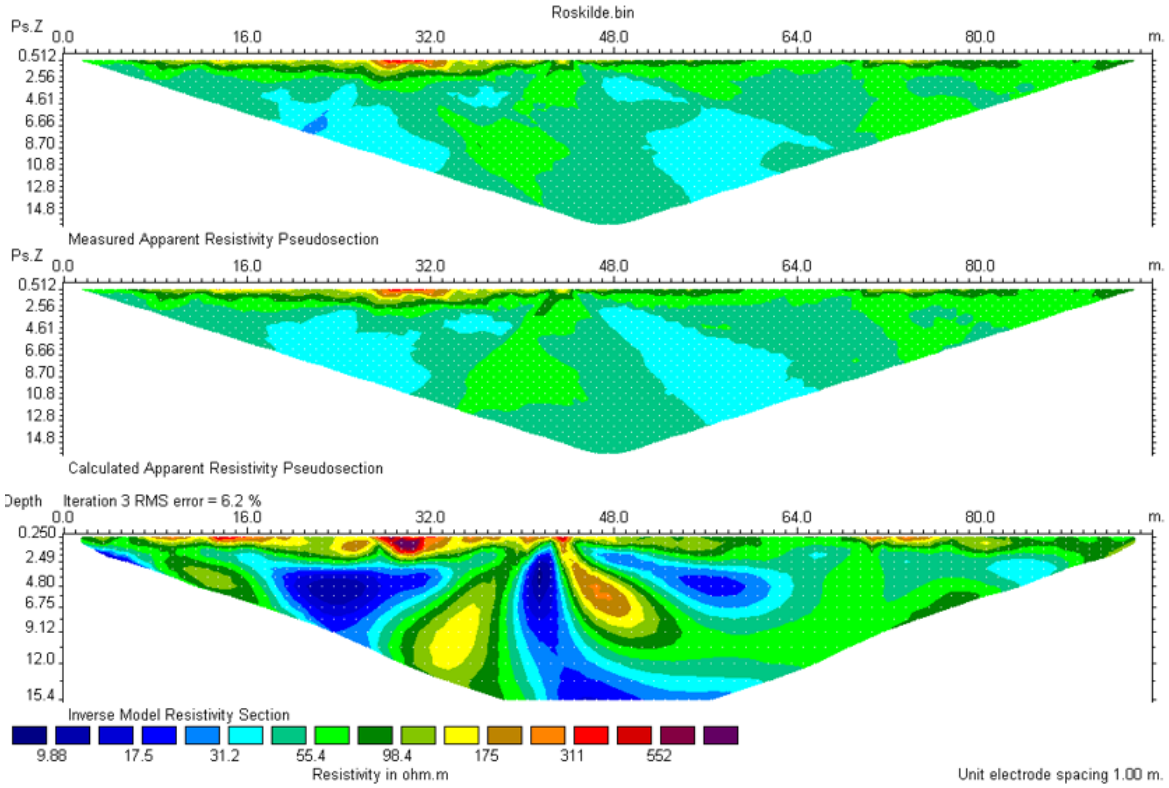

Figure 48: Third iteration and the profile with the lowest RMS error of 6.2 %. The profile looks highly disturbed.

8.2 Calibration

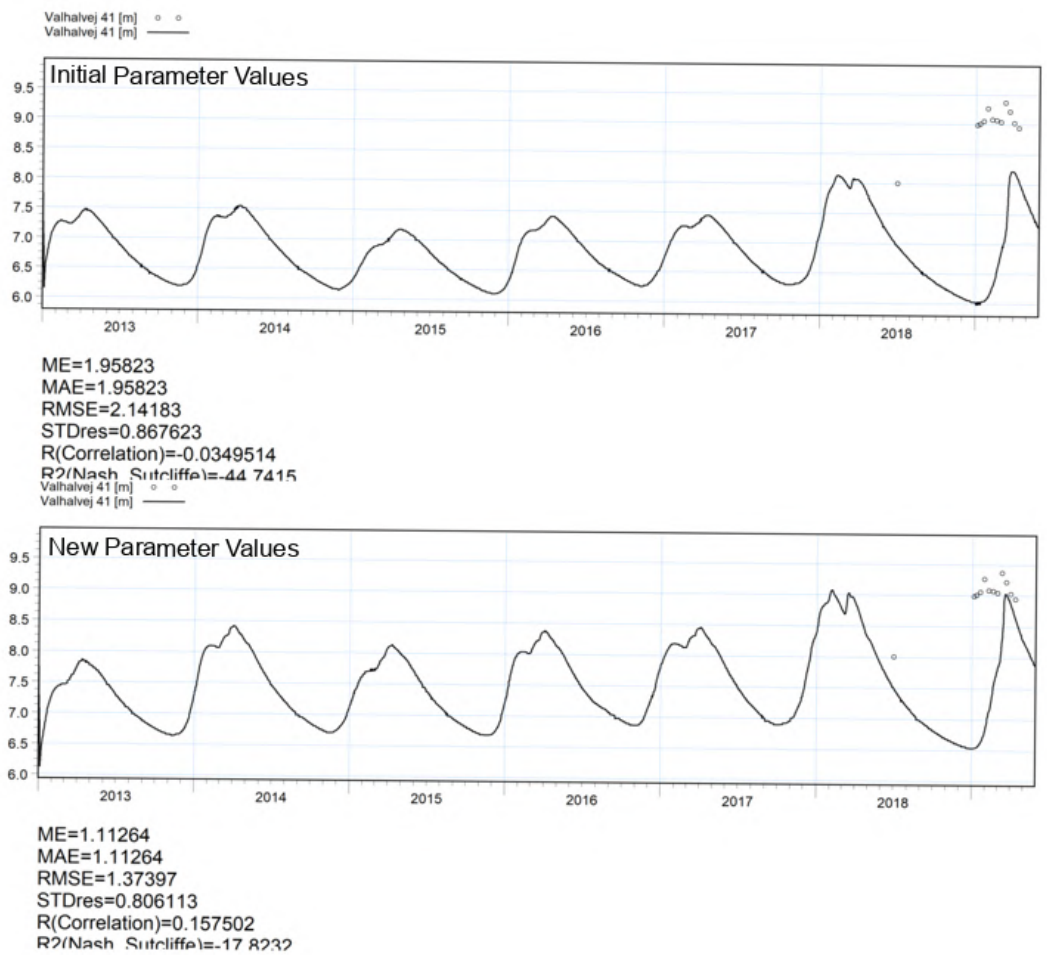

Figure 49: Comparison of head simulations and observations with initial and new parameter values.

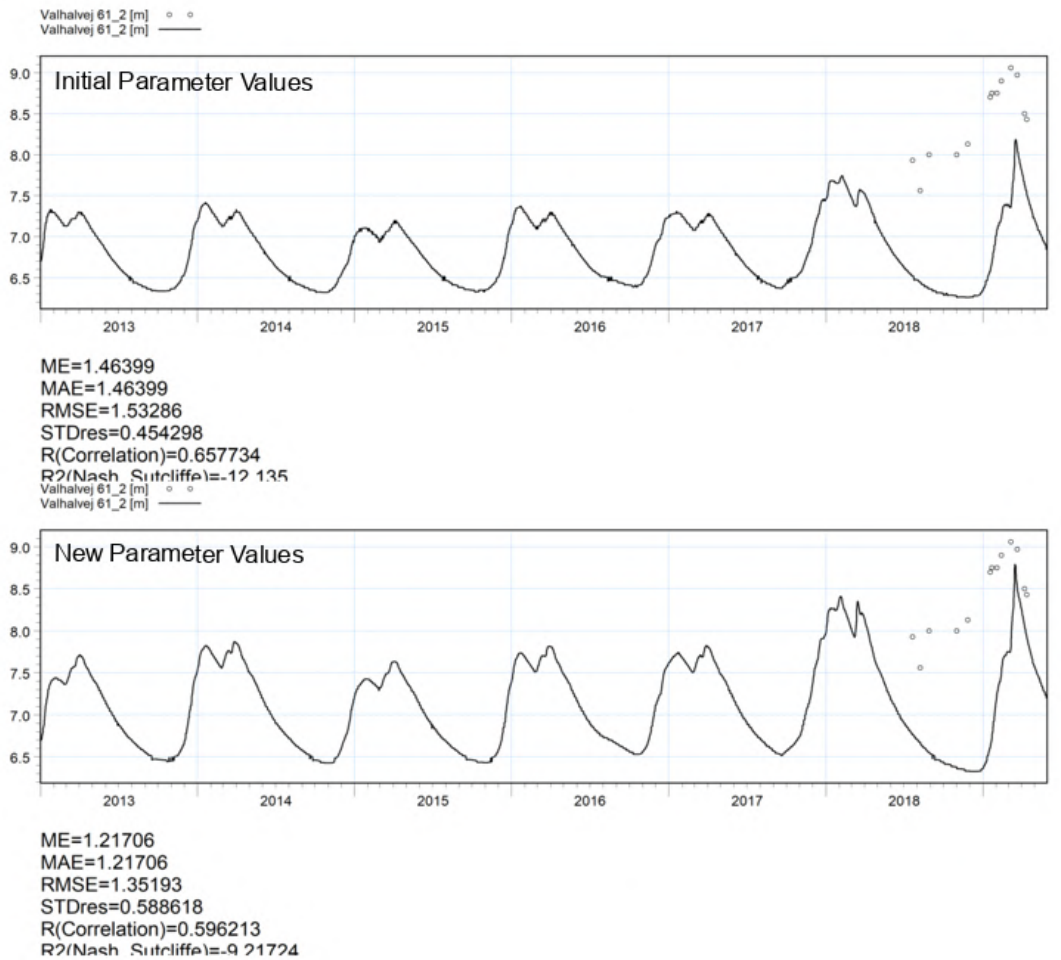

Figure 50: Comparison of head simulations and observations with initial and new parameter values.

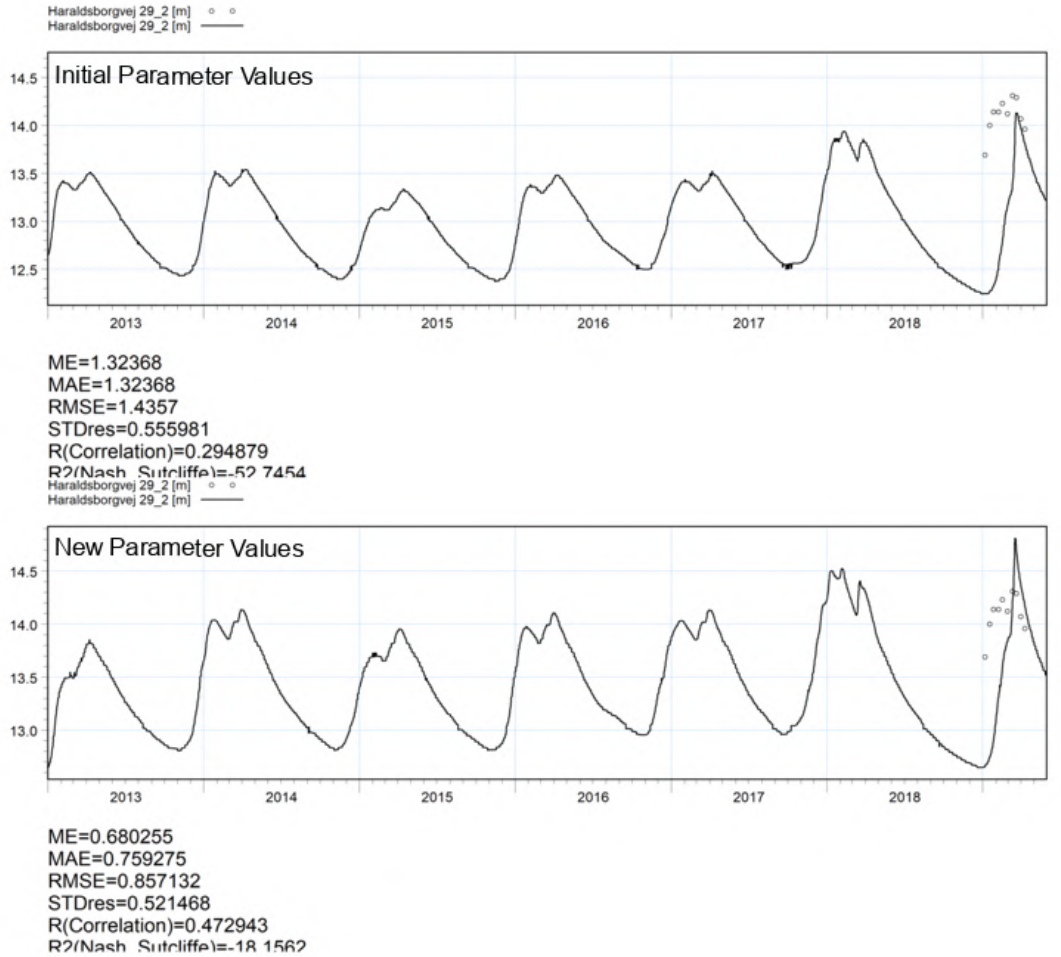

Figure 51: Comparison of head simulations and observations with initial and new parameter values.

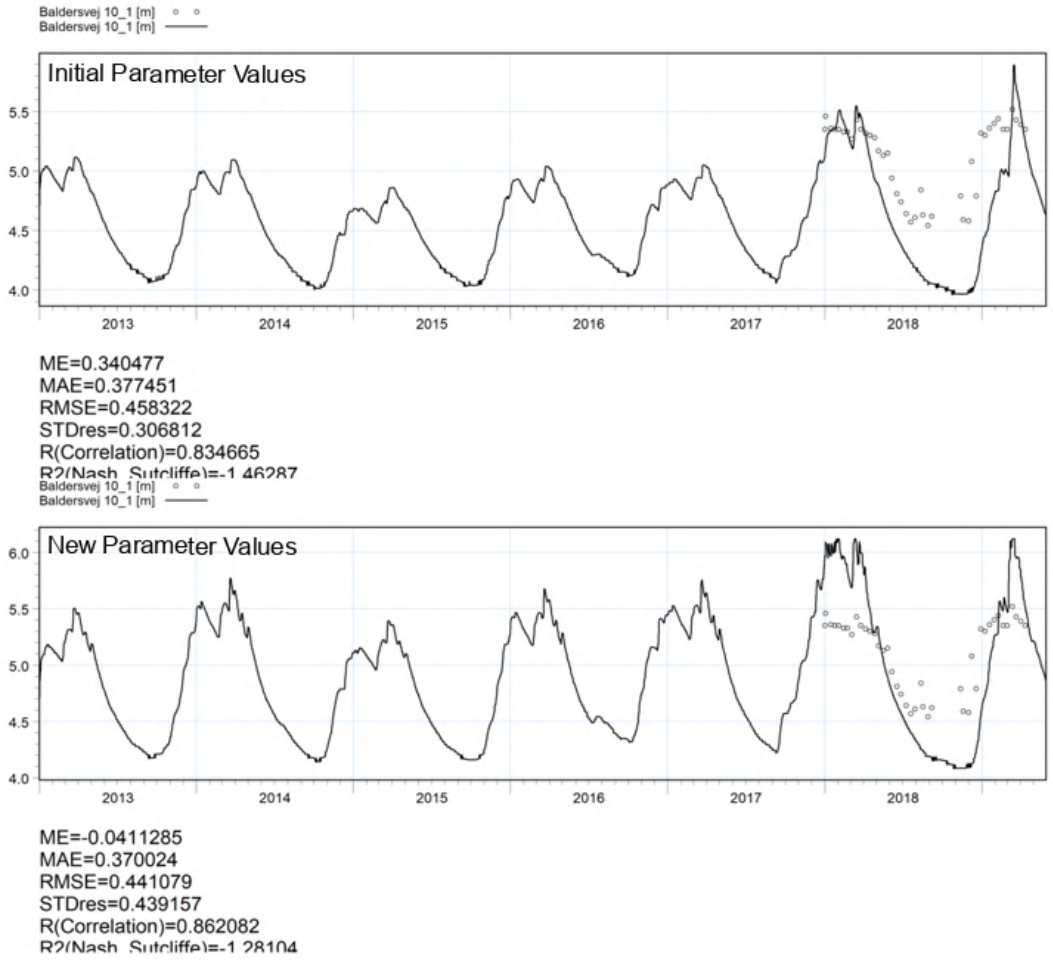

Figure 52: Comparison of head simulations and observations with initial and new parameter values.

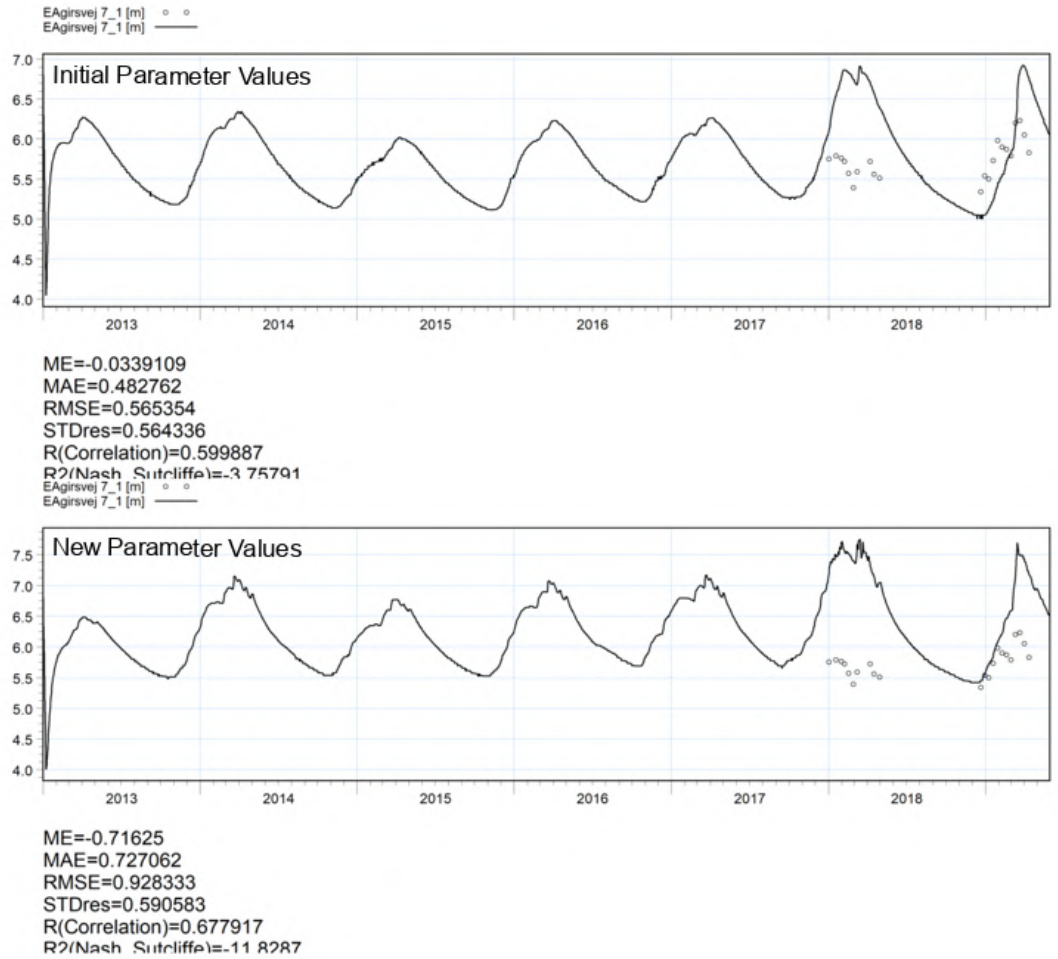

Figure 53: Comparison of head simulations and observations with initial and new parameter values.

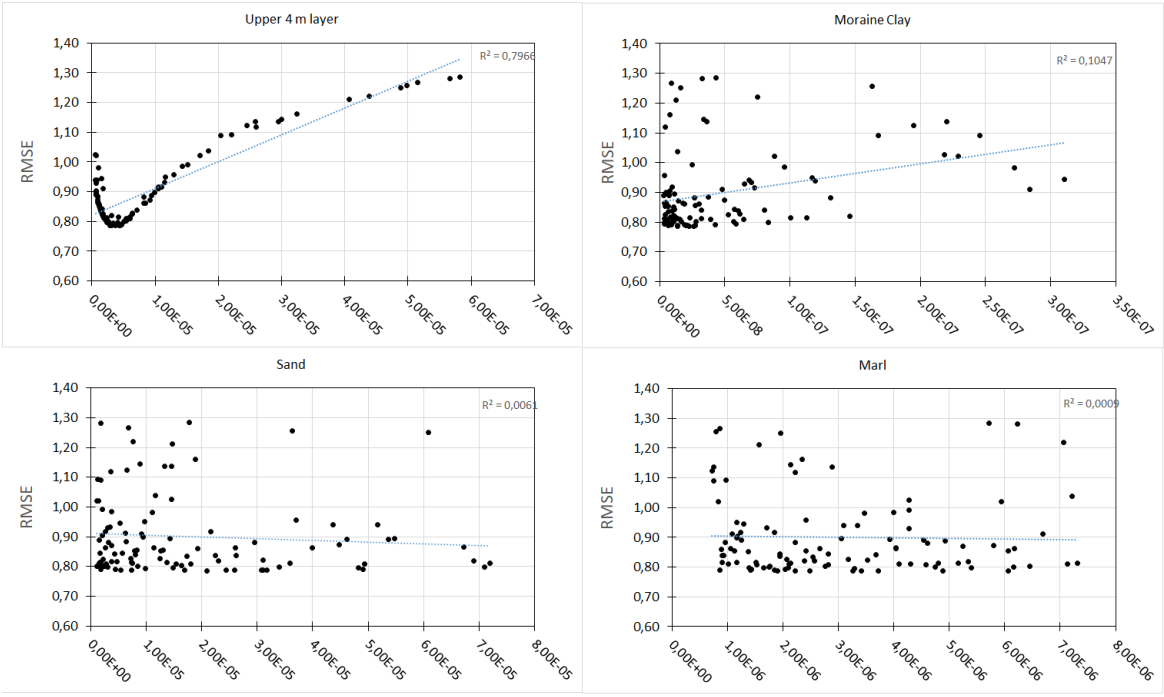

Figure 54: The 10 best simulations from the calibration. The dashed line represents the upper and lower limit.

8.3 Timeseries from Divers

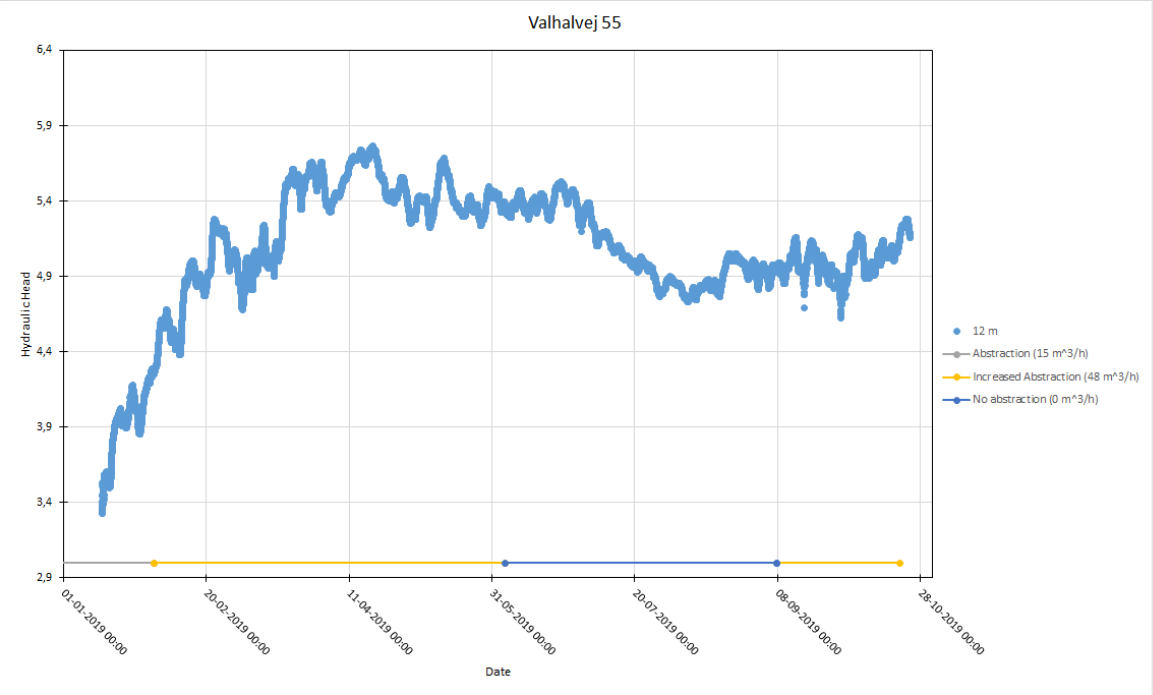

Figure 55: The hydraulic head in 12 m below surface on Valhalvej 12. The hydraulic head starts at 3.4 m and increases with more than 2 m over the next 3 month. It was discussed that the filter in the well might have been effected so the well is not connected to the respectively layer.

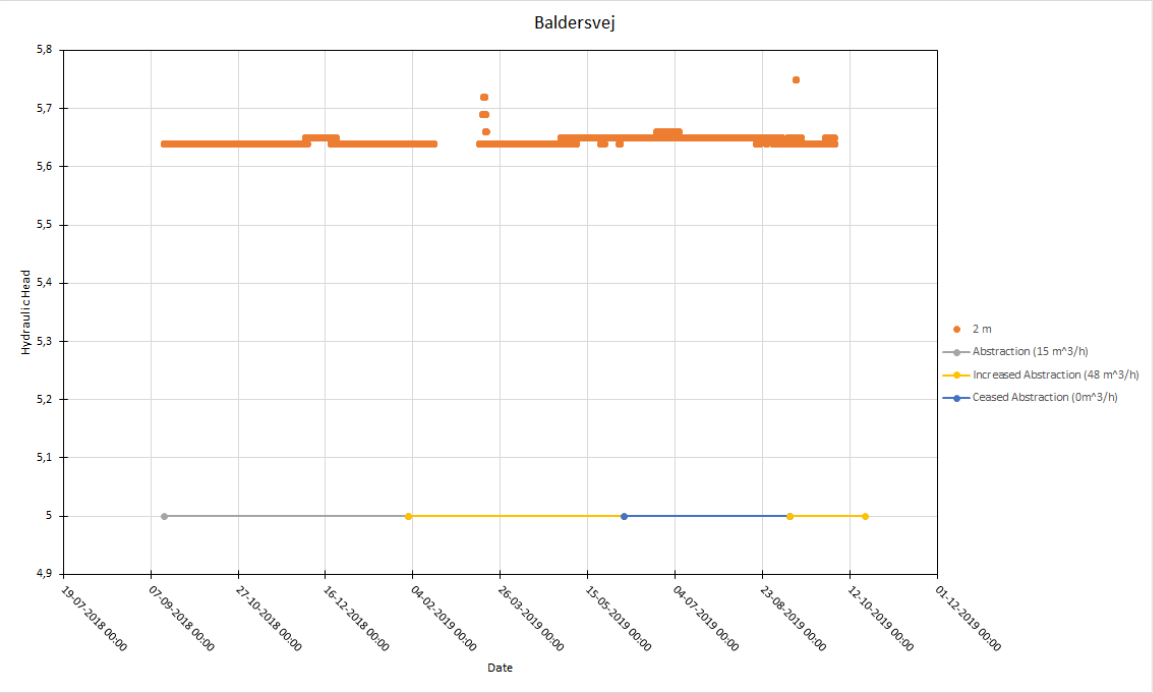

Figure 56: The hydraulic head at Baldersvej in 2 m. Basically just a straigt line at 5.65 m. This indicates that either the well is dry or the diver is broken.

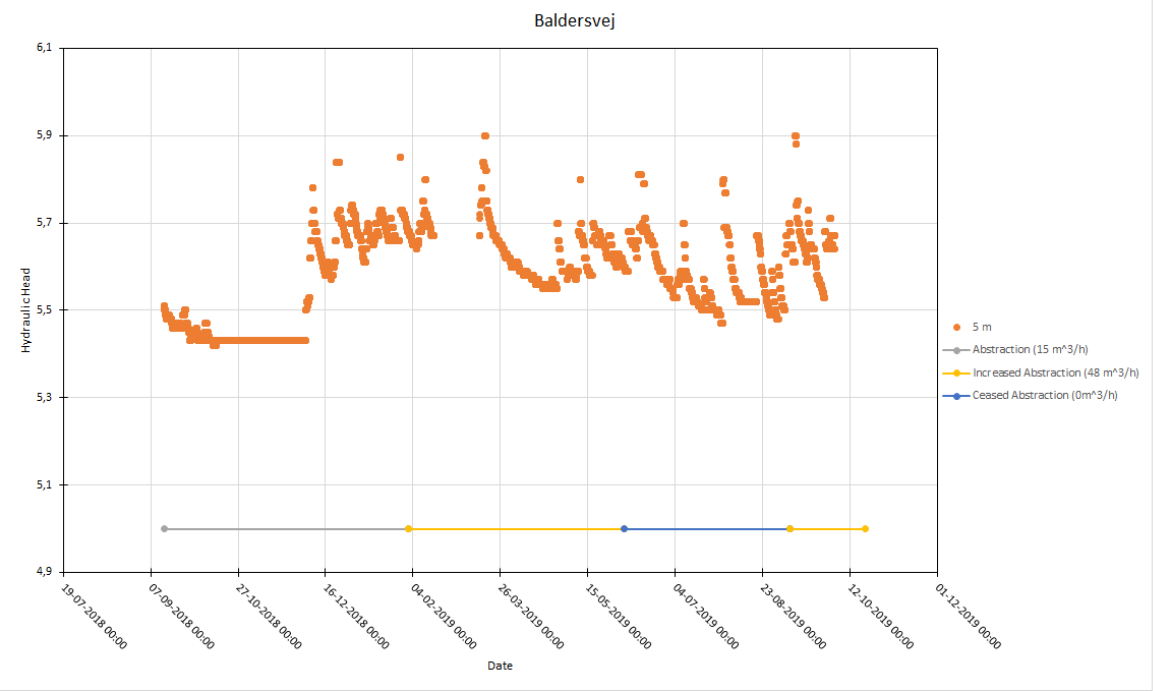

Figure 57: The well at Baldersvej in 5 m.b.s seems to be controlled by climate.

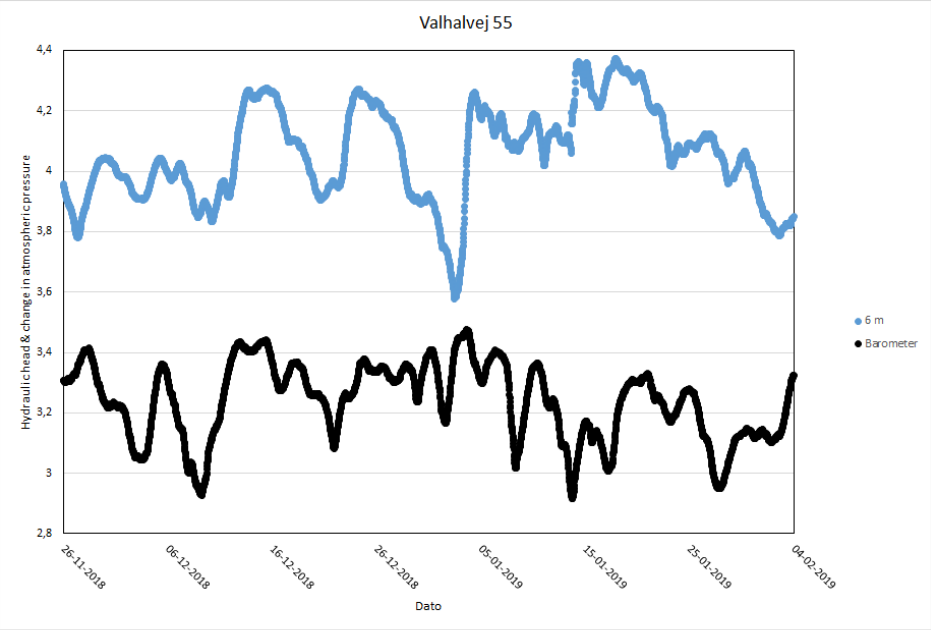

Figure 58: The blue line represent the hydraulic head in Valhalvej 55 6 m below surface. The black line represents the change in air pressure. Peaks on the blue line should correlate with throughs on the blakc line for the barometer effect to dominate.

8.4 Climate

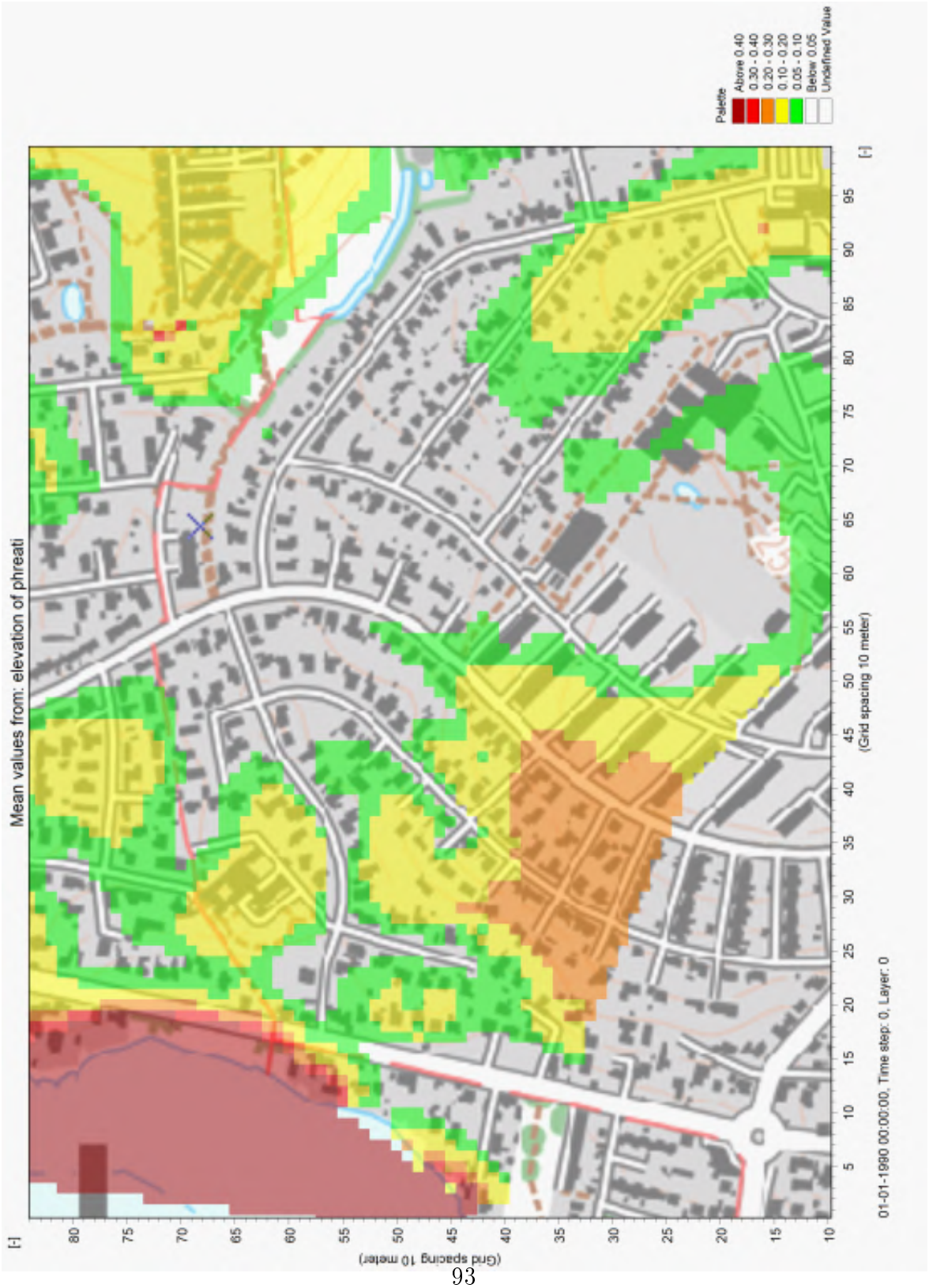

Figure 59: This map shows the change in mean groundwater level in a new climate condition of the area adjacent to Haraldsborg waterworks.

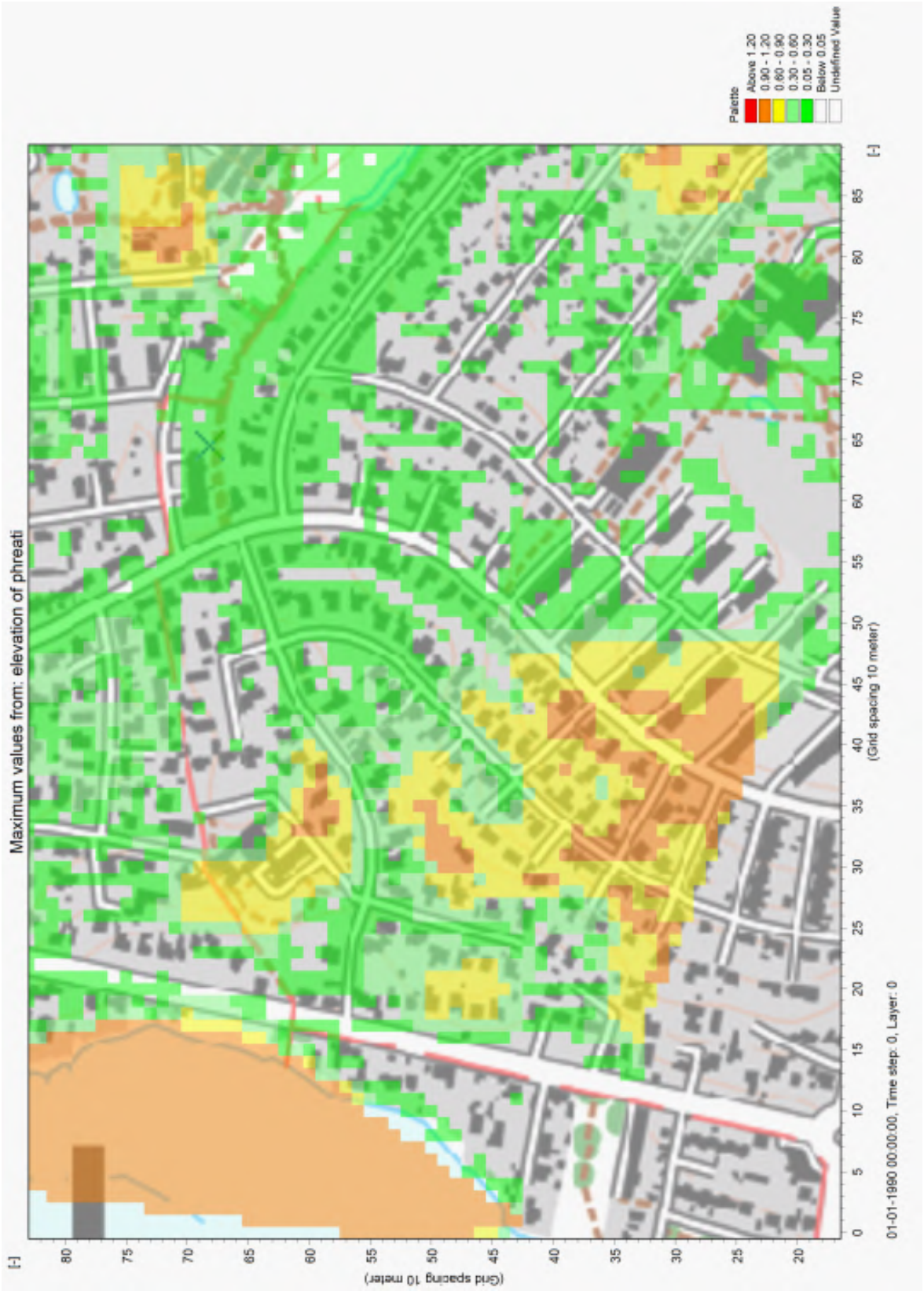

Figure 60: This map shows the change in maximum groundwater level in a new climate condition of the area adjacent to Haraldsborg waterworks.

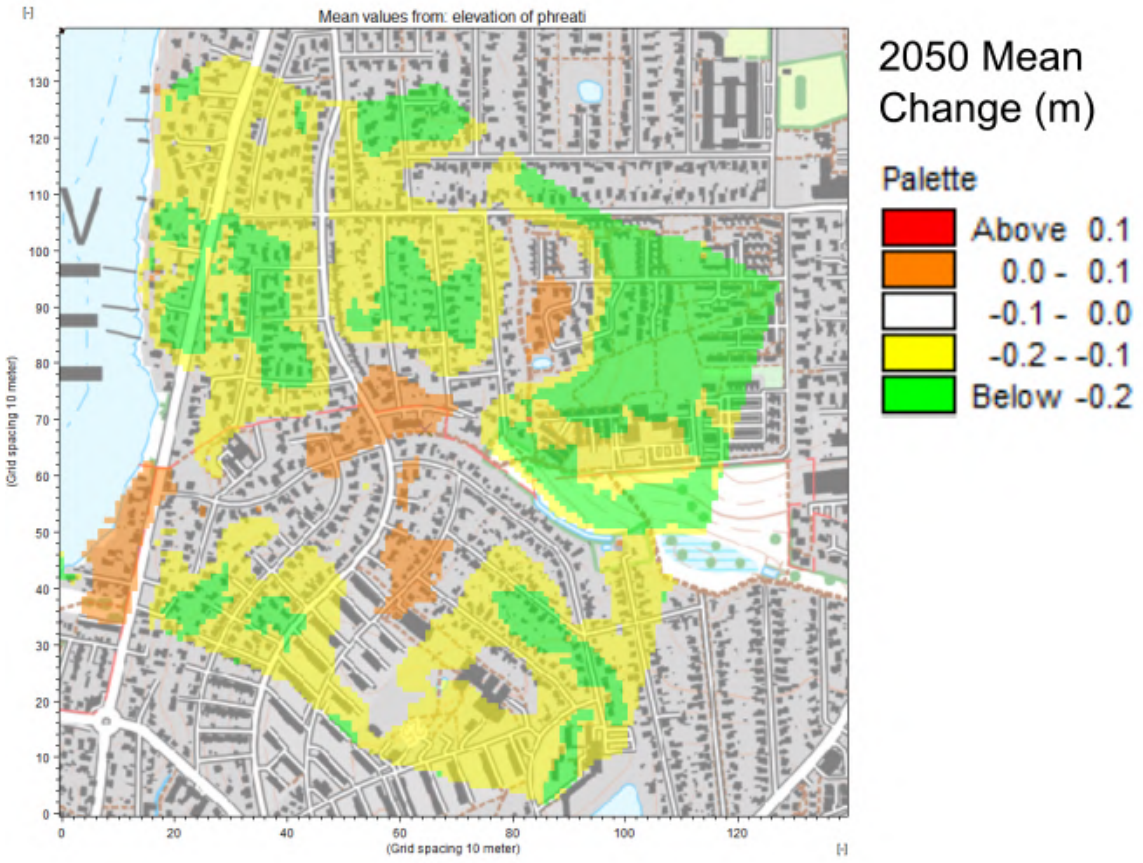

Figure 61: Change in mean level of phreatic surface from present to 2050. Note that most value shows a decline in groundwater level.

8.5 Effect of urbanization

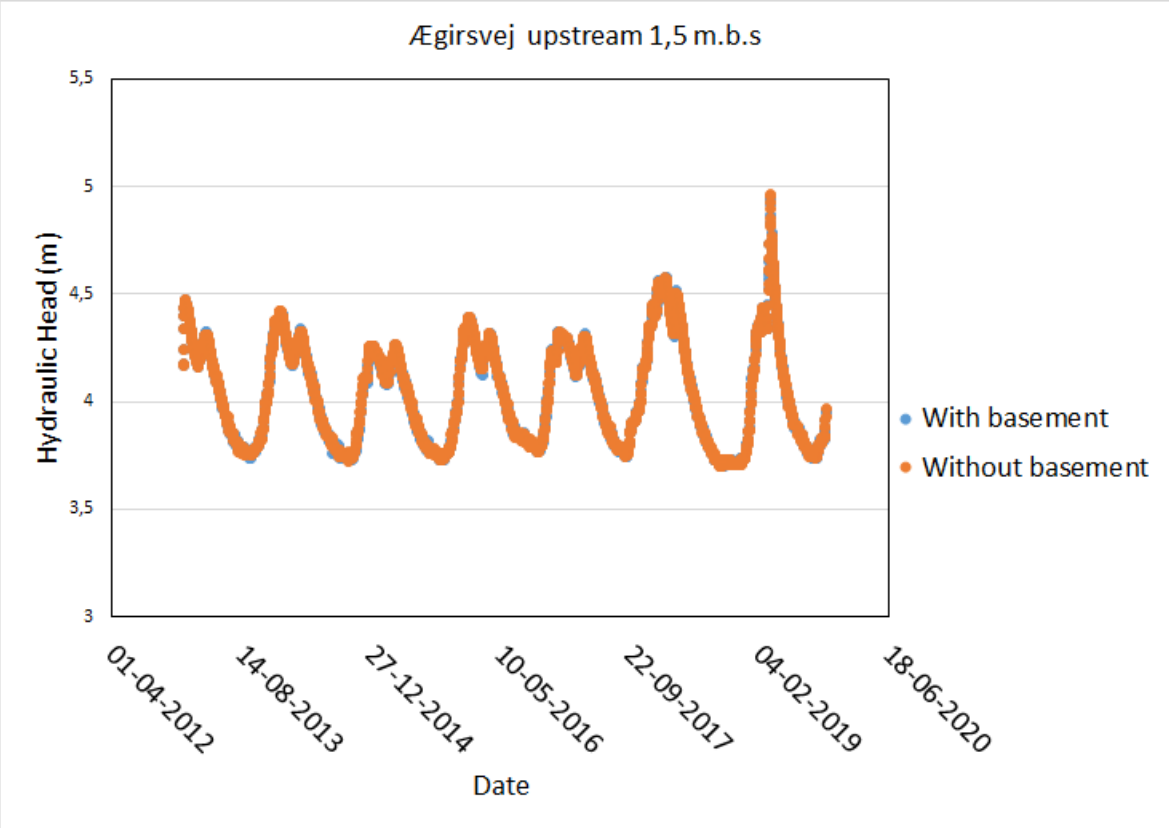

Figure 62: Effect of basement 1.5 m.b.s, upstream.

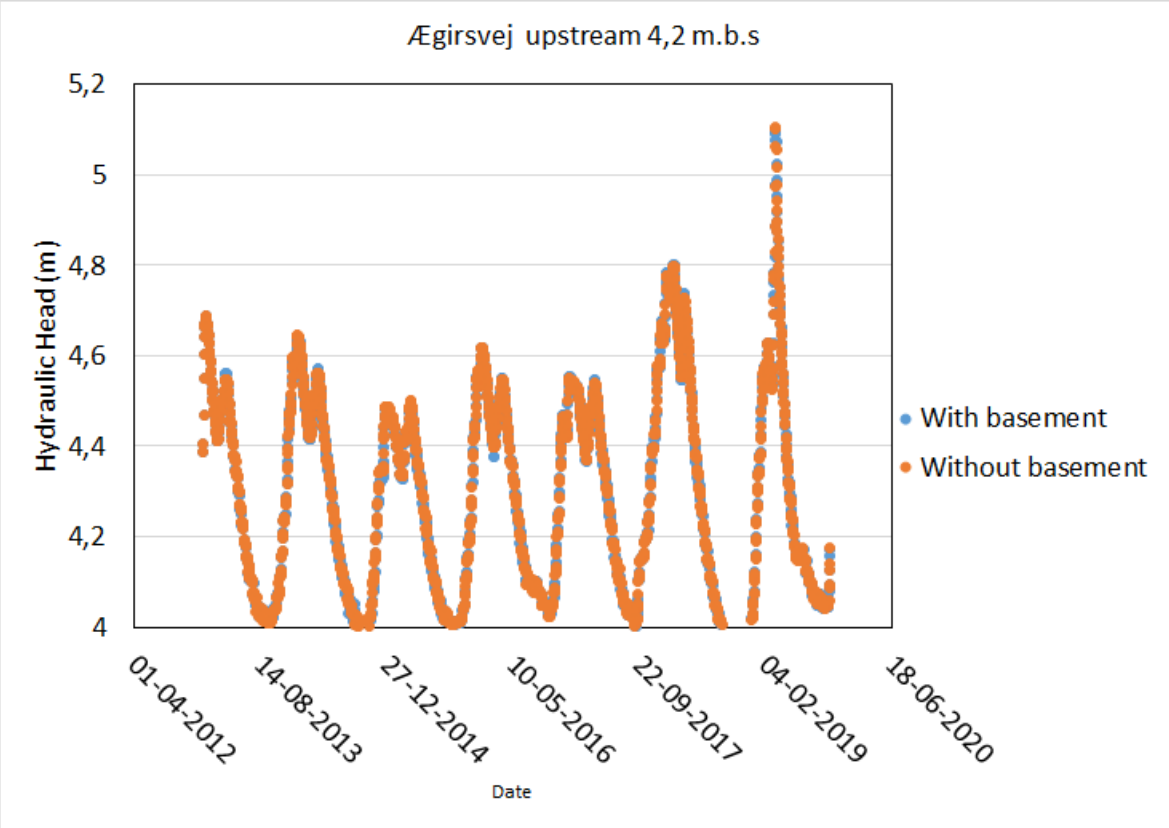

Figure 63: Effect of basement 4.2 m.b.s, upstream.

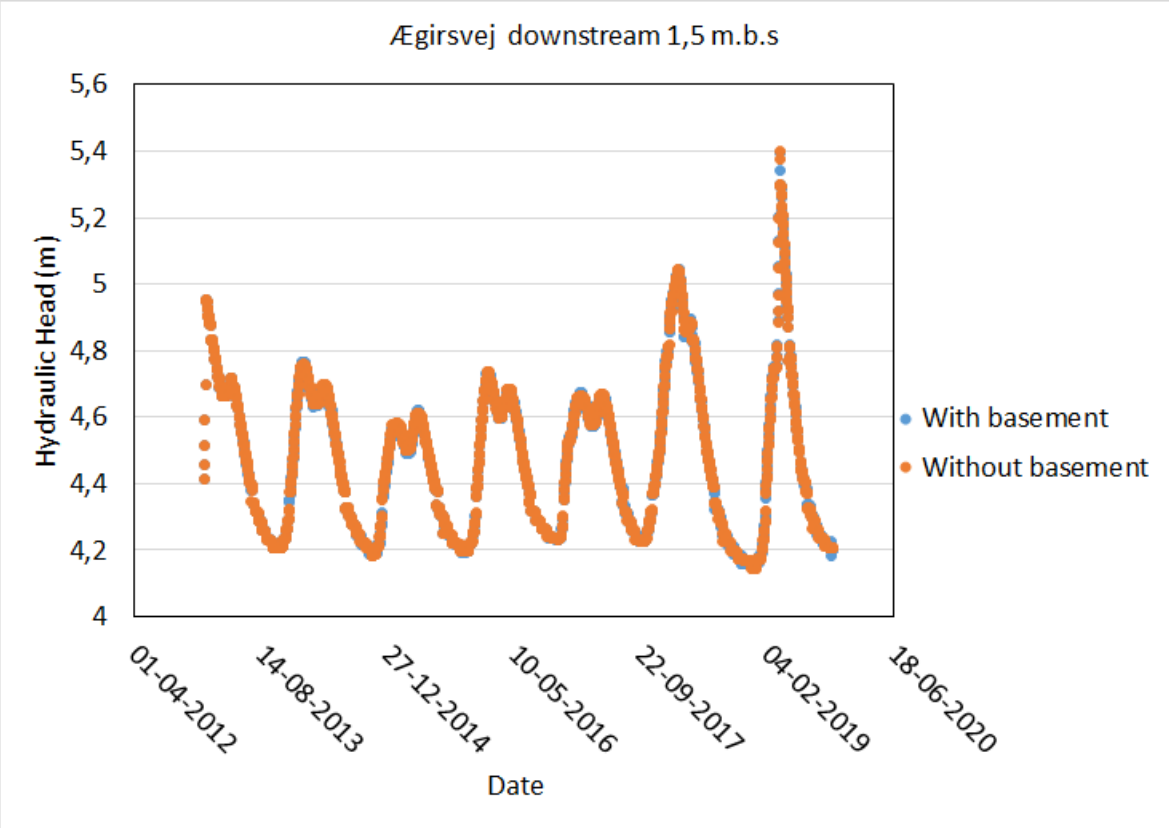

Figure 64: Effect of basement 1.5 m.b.s, downstream.

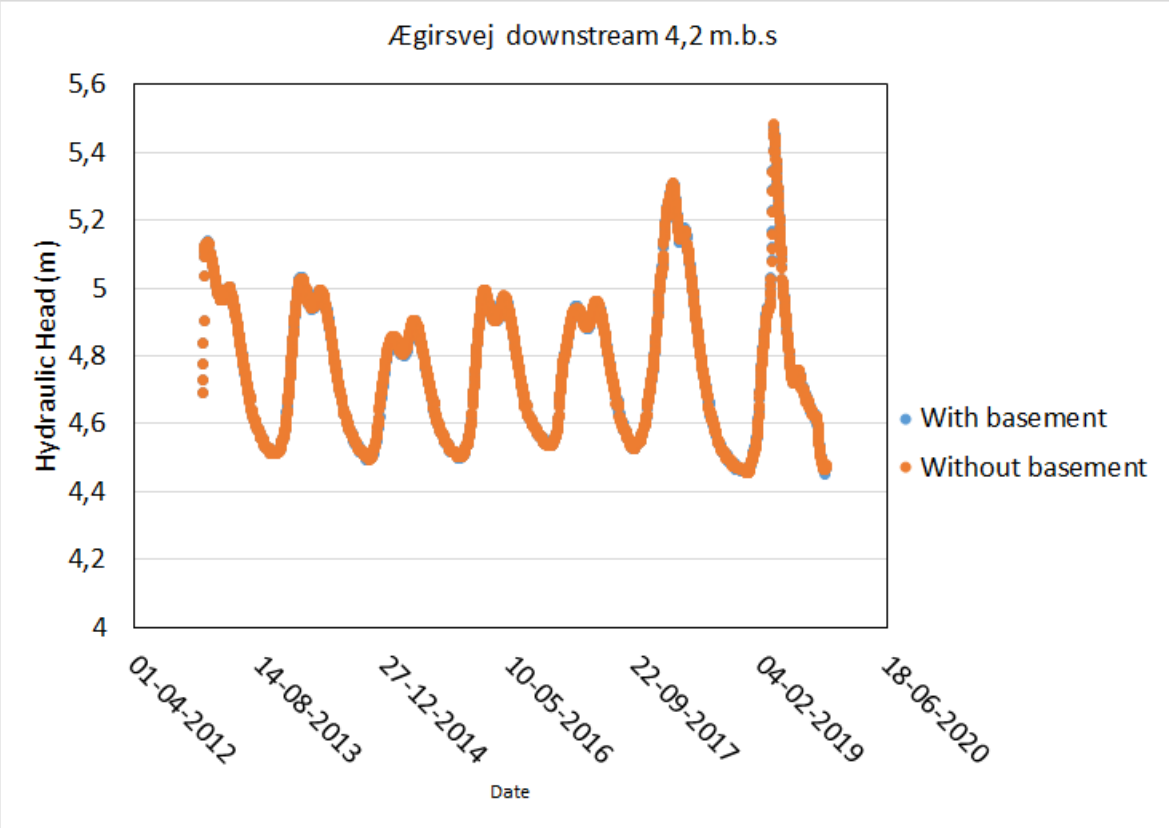

Figure 65: Effect of basement 4.2 m.b.s, downstream.

8.6 Discussion

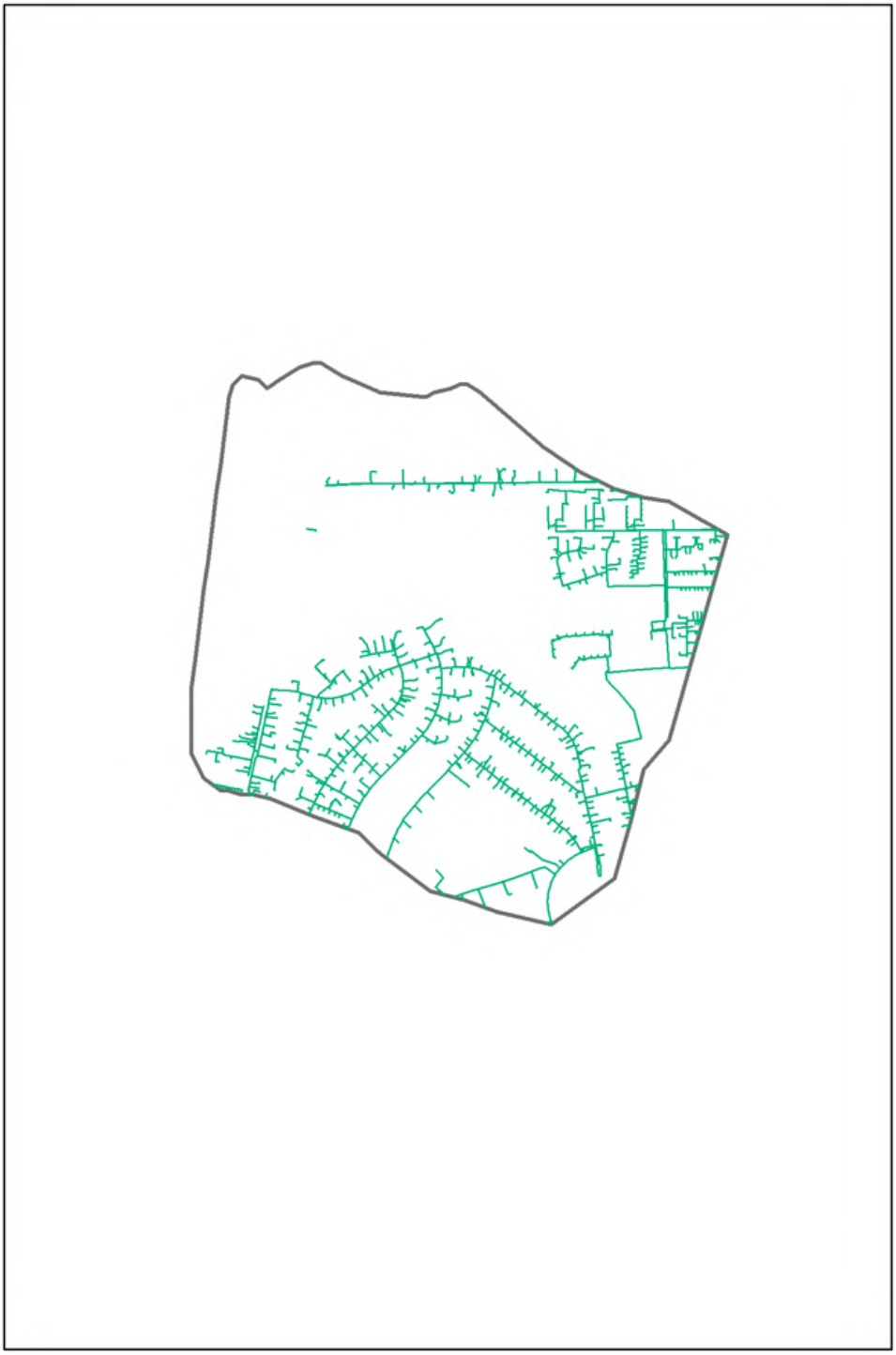

Figure 66: The model domain is seen with a green ouline and the central heating gravel castings is seen with green lines.

8.7 Timeseries from the Calibration and the Validation period

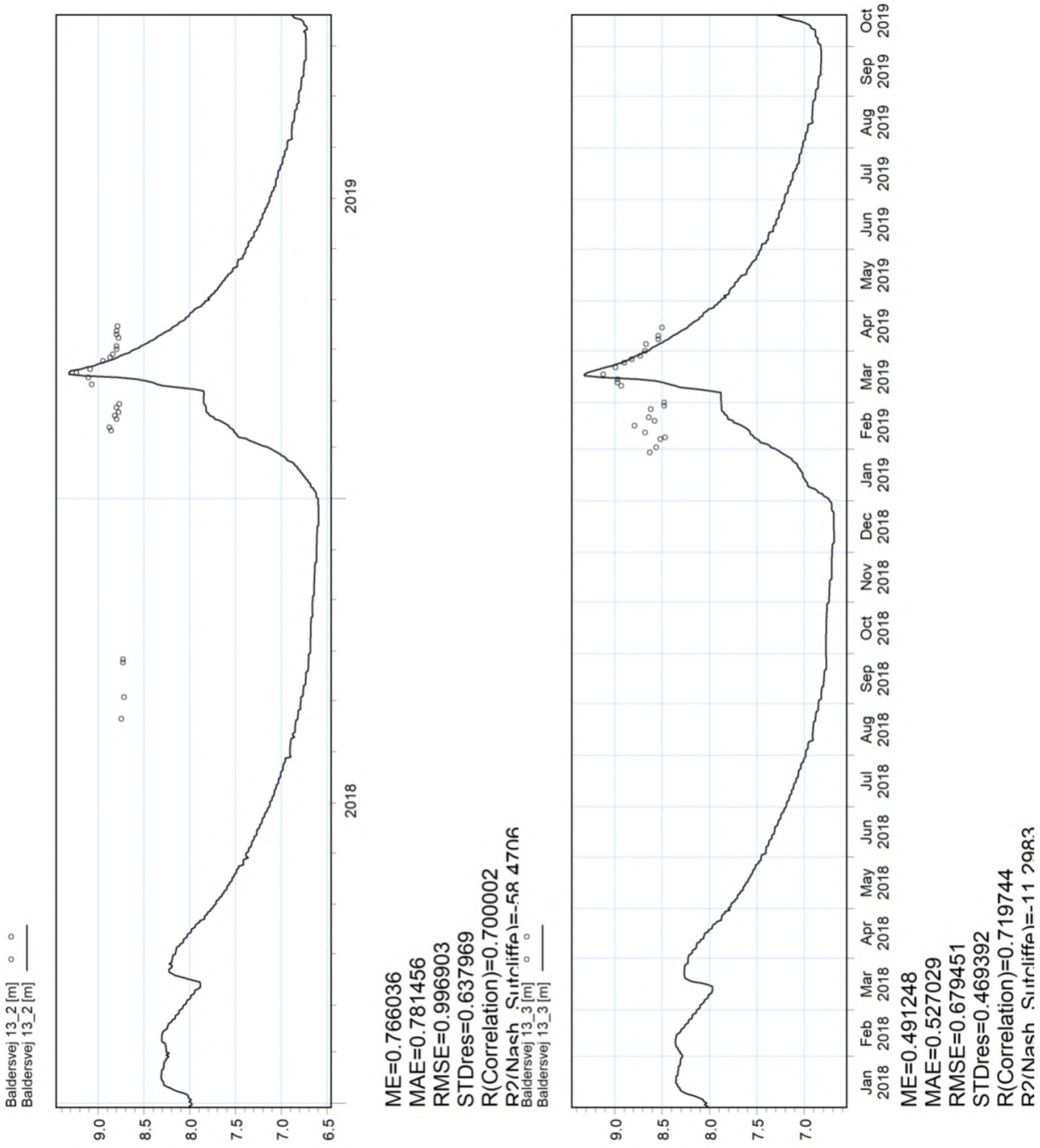

Figure 67: Baldersvej 13 (2-3

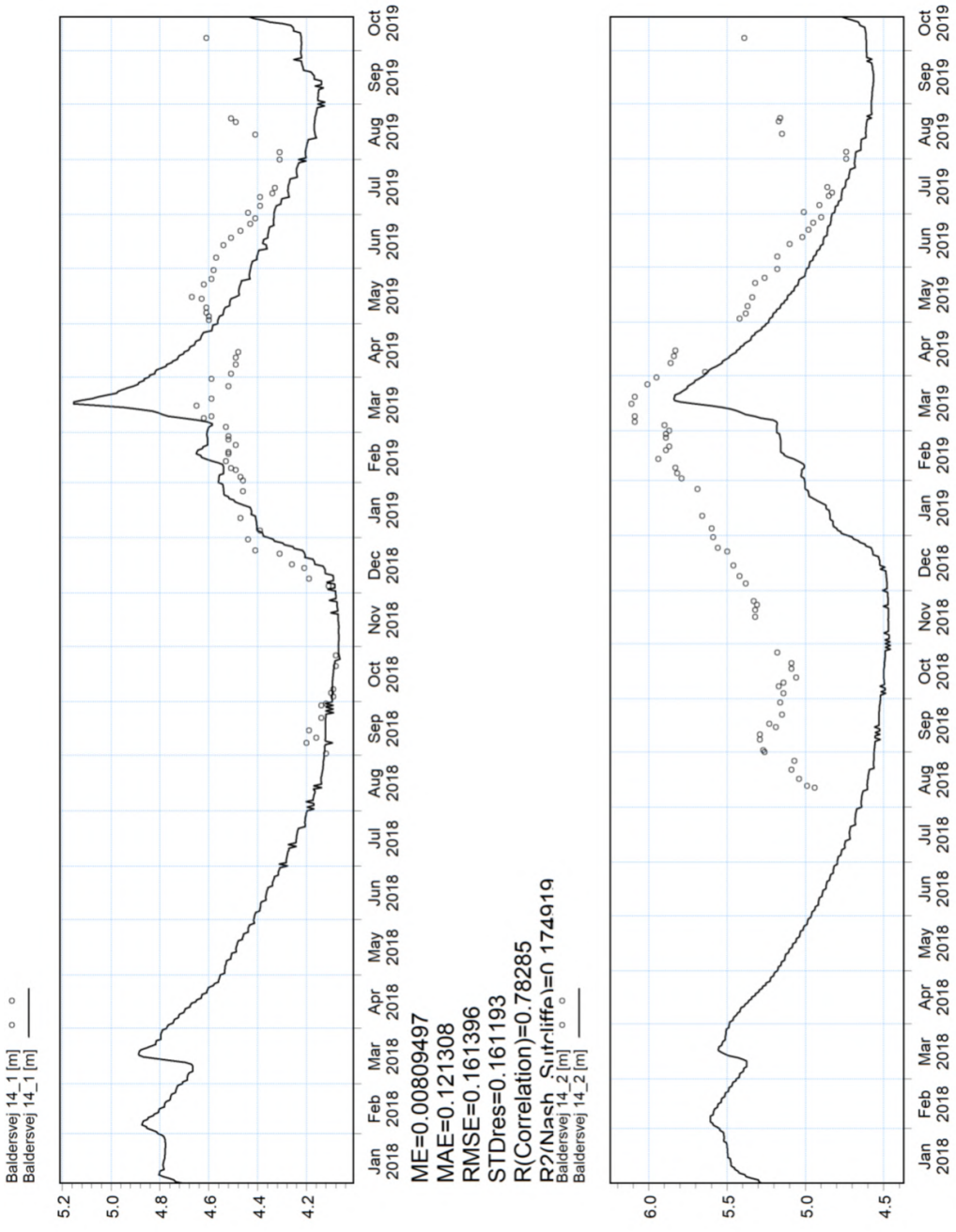

Figure 68: Baldersvej 14 (1-2)

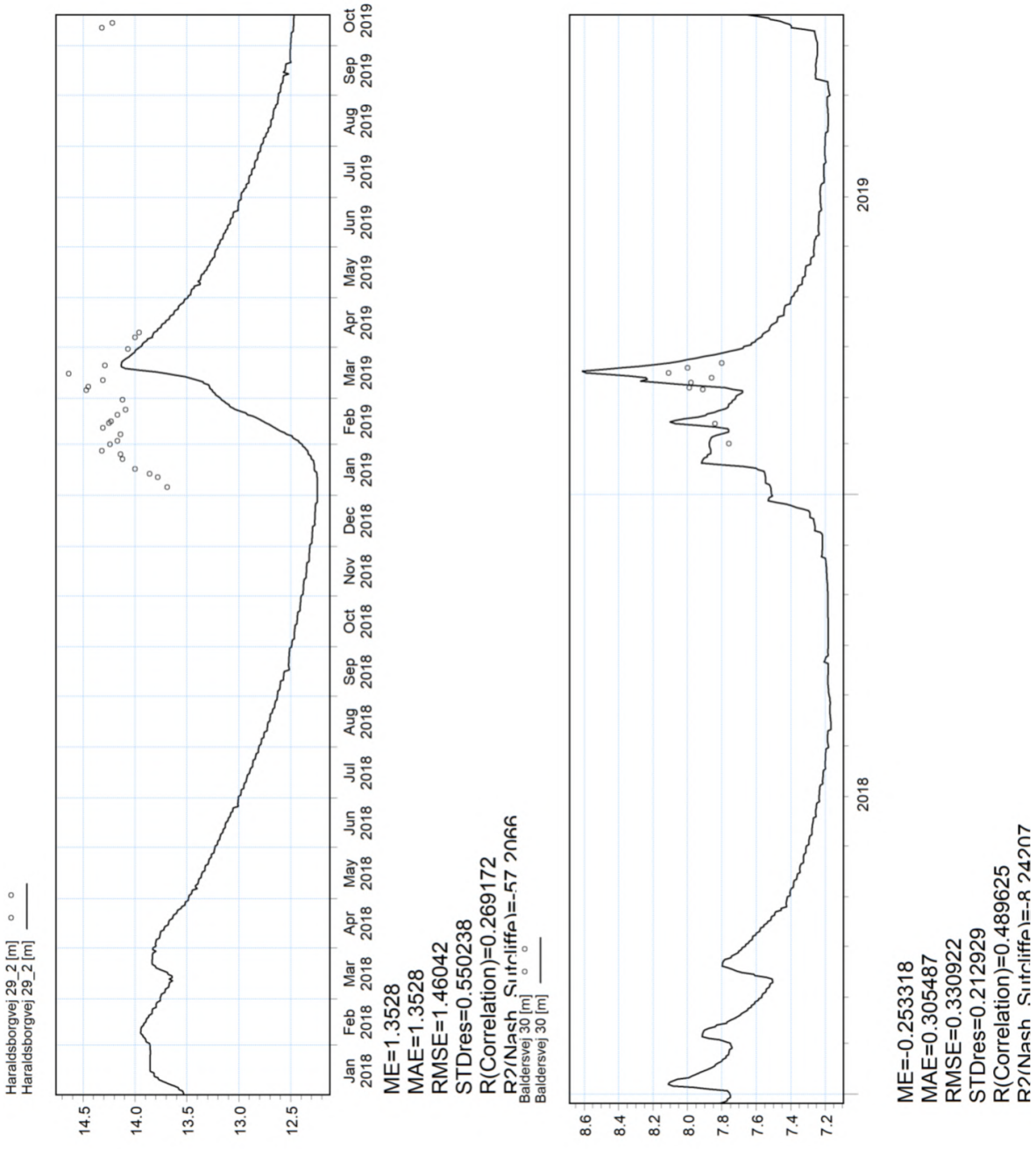

Figure 69: Haraldsborgvej 30 & Baldersvej 30

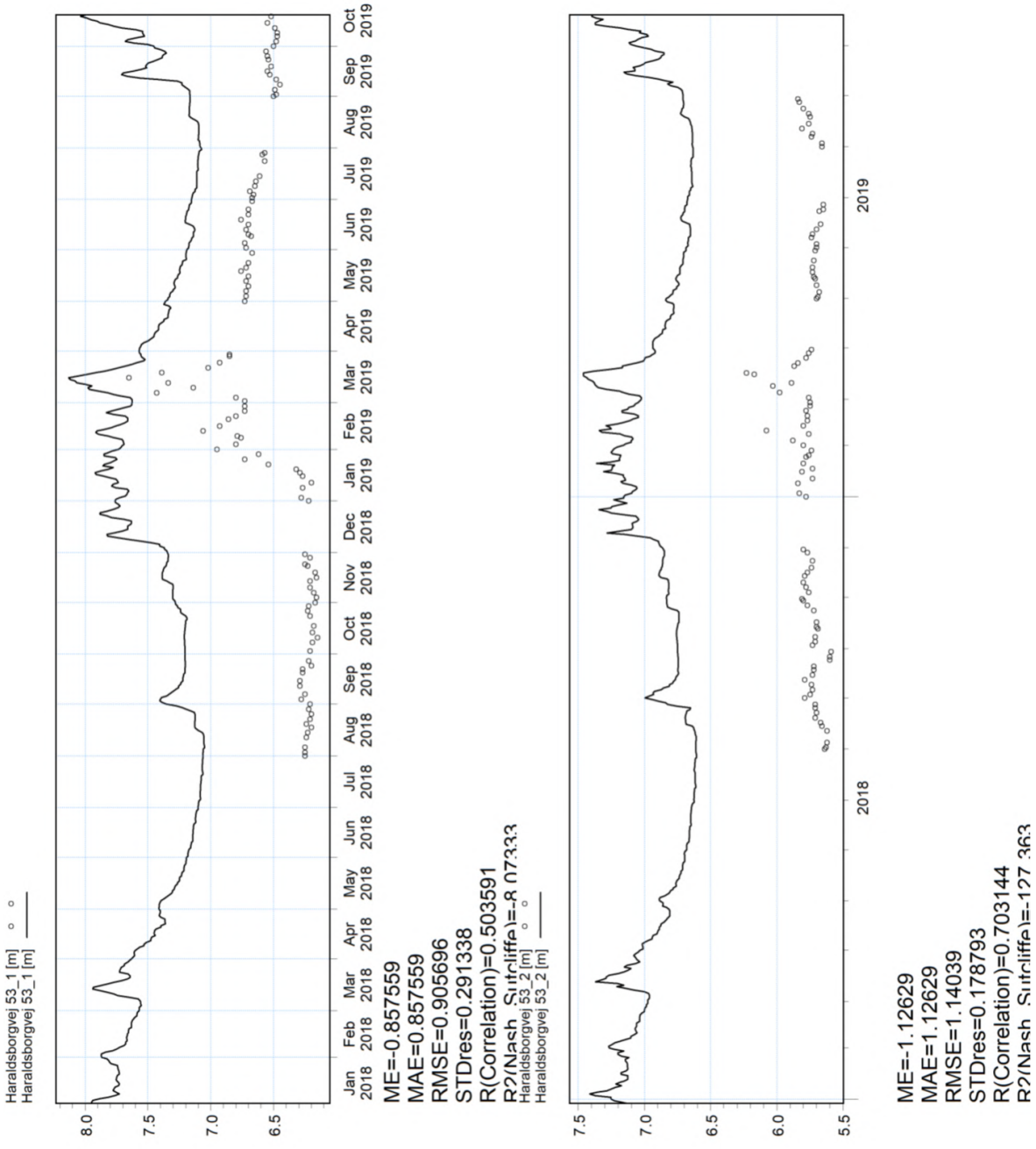

Figure 70: Haraldsborgvej 53 (1+2)

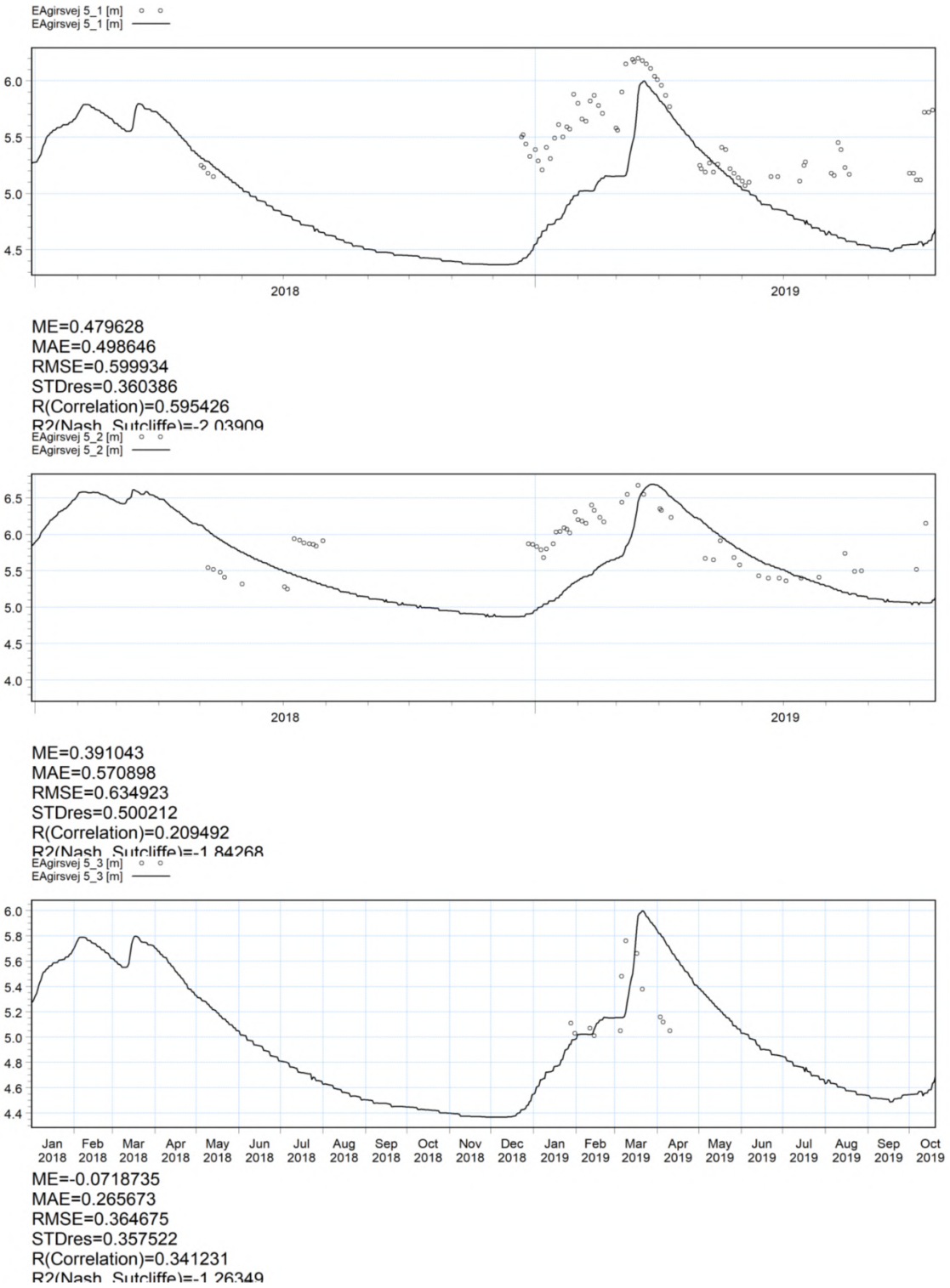

Figure 71: Ægirsvej 5 (1+2+3)

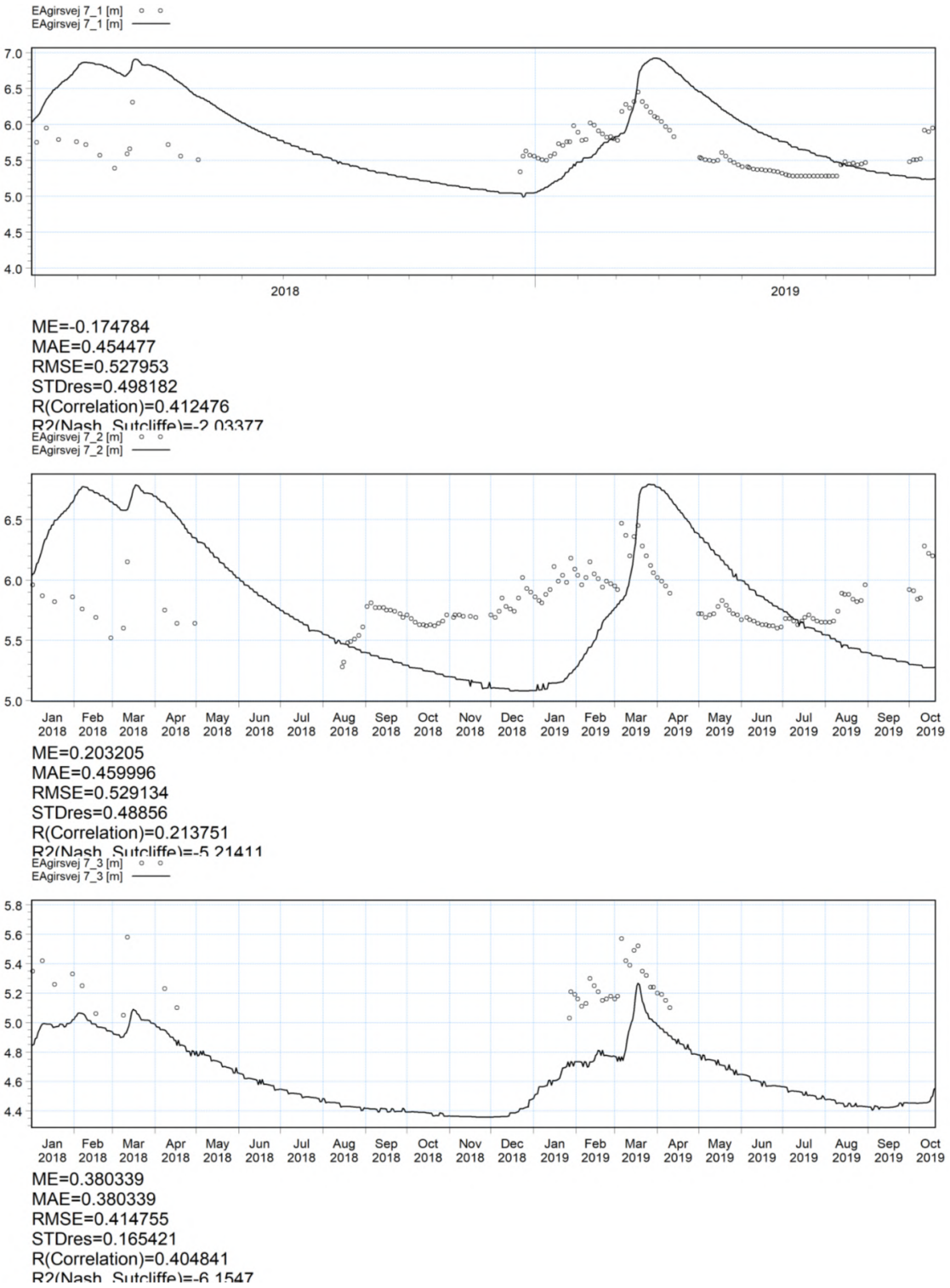

Figure 72: Ægirsvej 7 (1+2+3)

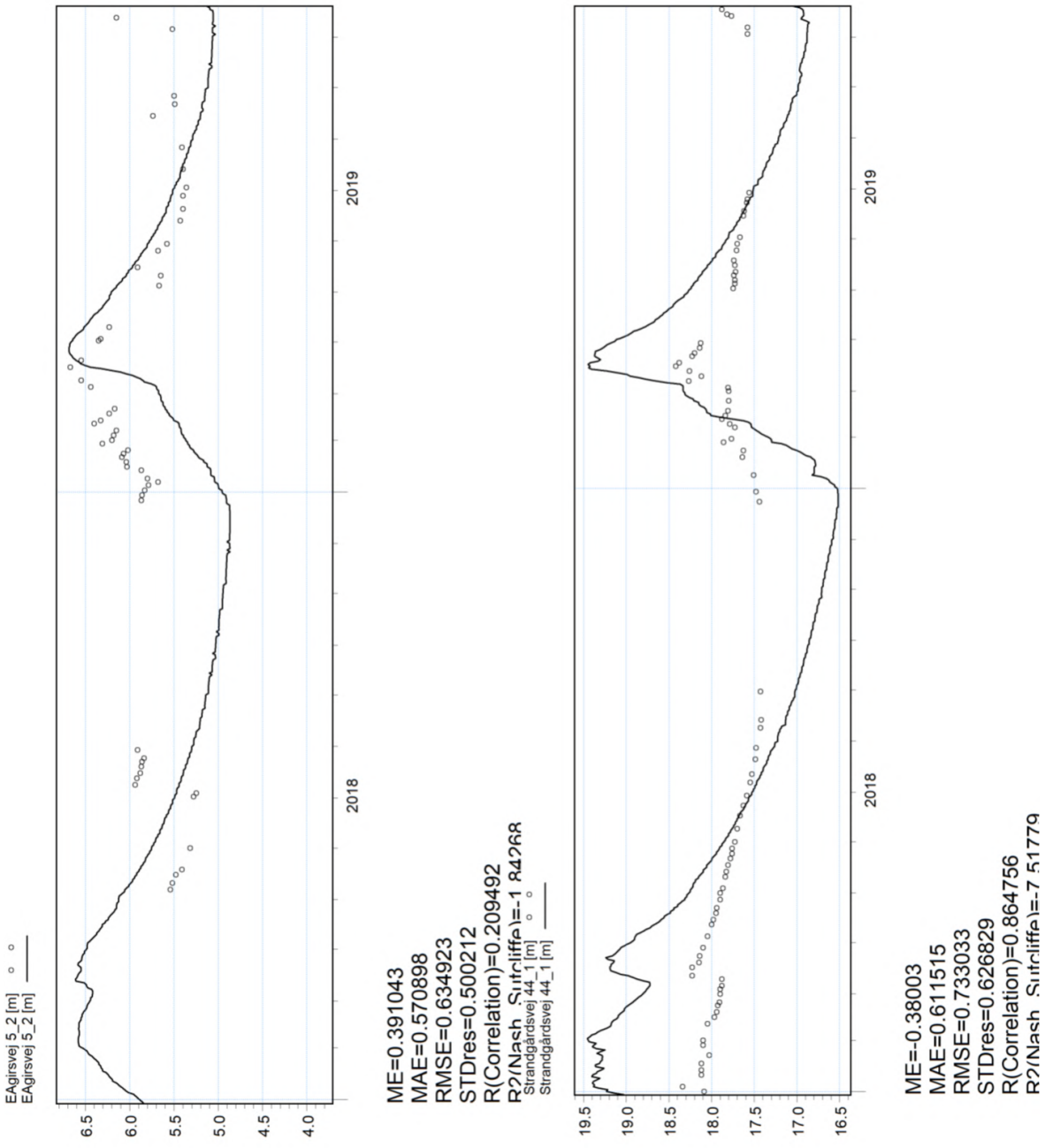

Figure 73: Strandgårdsvej 44 & Ægirsvej 2

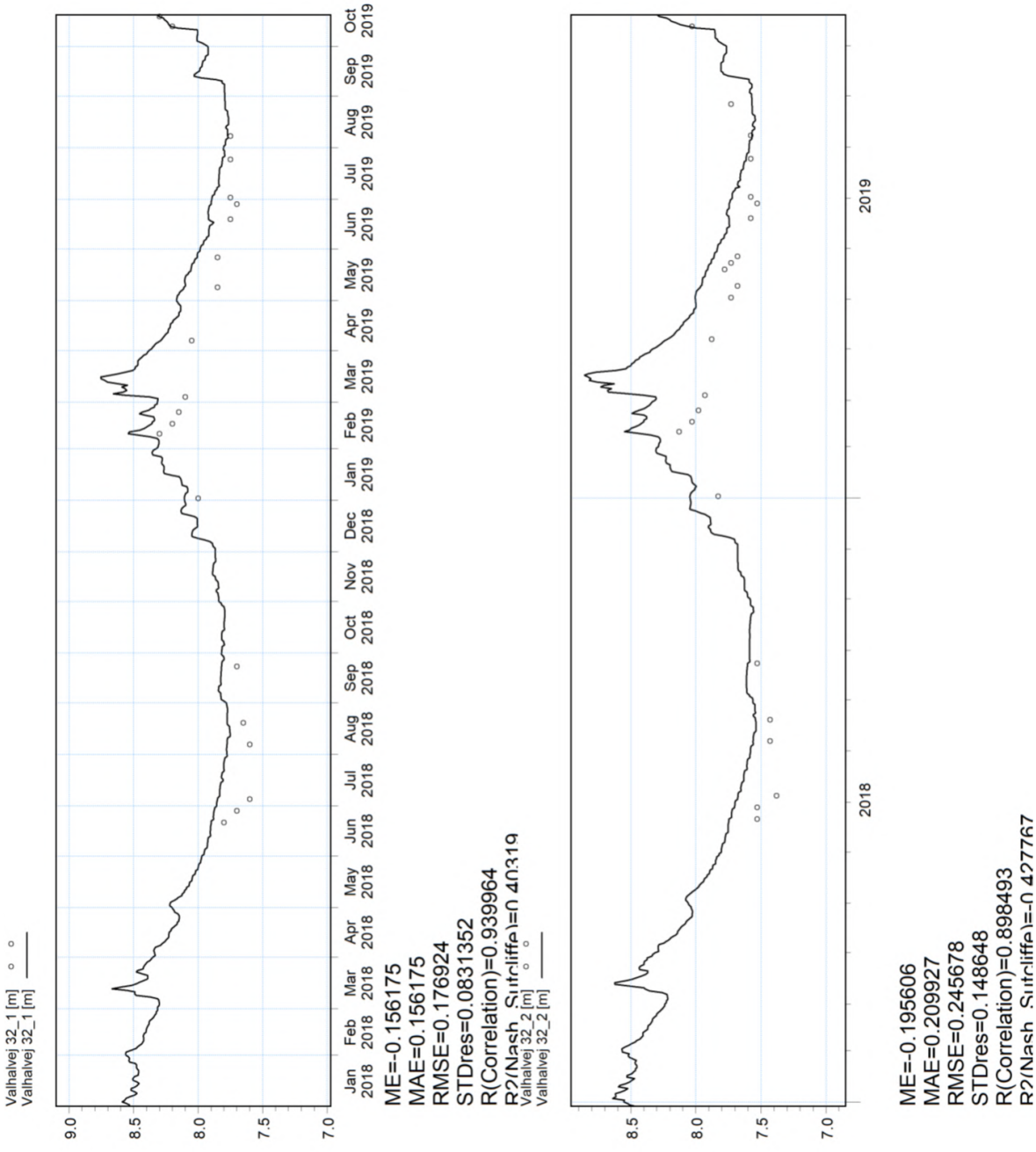

Figure 74: Valhalvej 32 (1+2)

Figure 75: Valhalvej 41 & Valhalvej 49

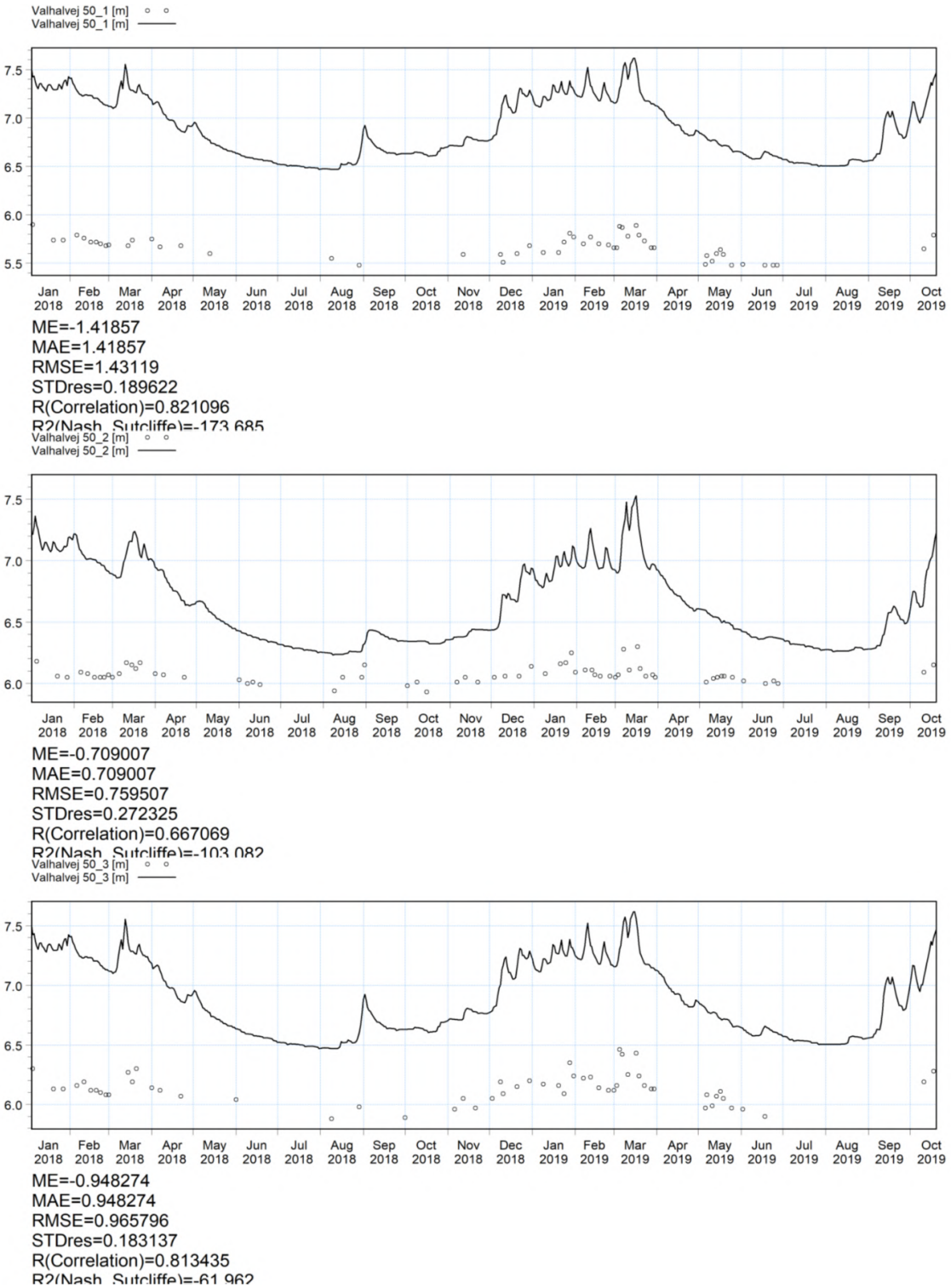

Figure 76: Valhalvej 50 (1+2+3)